SEISMIC MONITORING OF DYNAMIC BRIDGE DEFORMATIONS USING STRAIN MEASUREMENTS

Stephanie S. Y. Fung

Ian N. Robertson

Research Report UHM/CEE/03-02

MAY 2003

ABSTRACT

In recent years, civil engineers have become very interested in developing systems to monitor the health of the structures that they have designed and built. There are many systems that can monitor the vertical deflections of structures, but there are few that can effectively measure deflections due to dynamic loads. This report investigates the use of a mathematical model proposed by Swiss engineers, Vurpillot *et al* [1998], and the selection of innovative fiber optic strain gauges along with a high-speed data acquisition system for future verification tests.

Various laboratory static and dynamic verification tests using traditional electrical resistance strain gauges were performed on three beam specimens in the Structures Laboratory at the University of Hawai`i at Manoa. The results produced by the mathematical model agreed well with the measured results and the theoretical results from the SAP2000 model. Further tests will be performed using the Fabry-Perot fiber optic strain gauges and data acquisition system that has been selected in this report.

ACKNOWLEDGEMENTS

This report is based on a Masters Thesis prepared by Stephanie Fung under the direction of Ian Robertson. The authors wish to express their gratitude to Drs. Si-Hwan Park and H. Ronald Riggs for their effort in reviewing this report.

The authors would also like to extend their gratitude to Dr. Marcus Aberle, Dr. Si-Hwan Park, Kainoa D. Aki, Alison A. Agapay, Jennifer B. J. Chang, Miles Wagner, and Andy Oshita. Dr. Marcus Aberle helped construct the test set-up for Beam II, created a Microsoft Visual Basic 6.0/Excel 2000 program spreadsheet that implements the mathematical model presented in this report, and also assisted in many of the laboratory verification tests performed on Beam II. Dr. Si-Hwan Park assisted in the animation of the deflected shapes using Digital Visual Fortran code and Tecplot 8.0. Kainoa D. Aki programmed the LabVIEW data acquisition system and also assisted in the testing of Beam II. Alison A. Agapay provided the concrete beam application and Jennifer B. J. Chang modeled Beam II and the Kealakaha Stream Bridge using SAP2000. Miles Wagner and Andy Oshita provided assistance in the Structures Laboratory at the University of Hawai`i at Manoa. The authors sincerely appreciate the time and effort contributed by all of these individuals.

This project was funded by the Hawai`i Department of Transportation (HDOT) and the Federal Highway Administration (FHWA) program for Innovative Bridge Research and Construction (IBRC) as a part of the seismic instrumentation of the Kealakaha Stream Bridge. This support is gratefully acknowledged and appreciated.

TABLE OF CONTENTS

LIST OF TABLES

LIST OF FIGURES

Figure Page

CHAPTER 1
INTRODUCTION

1.1 Introductory Remarks

The existing Kealakaha Stream Bridge on the island of Hawai`i will soon be replaced with a new pre-stressed concrete structure, which will span approximately 722 feet (220 m). In the 1997 Uniform Building Code (UBC), the island of Hawai`i is classified as Zone 4, the zone with the highest level of seismic activity. Therefore, being situated in an area of high seismic activity, this bridge provides an ideal environment to investigate the effects of seismic loads on structures, particularly on elements of the transportation infrastructure. Accurate deformation measurements during a seismic event or other dynamic loading can be used to determine bending moments and shears in the member. In addition, comparison of the measured deformations with those predicted by analytical models of the structure can be used to improve modeling techniques. To effectively measure these deformations, research must be carried out to select the instrumentation and to design the instrumentation layout that will be installed in the bridge.

1.2 Statement of the Problem

Numerous instrumentation systems have been used to measure and monitor the vertical deflection of structures due to various loading conditions. However, these systems are not adequate for earthquake-induced displacements because there are no stable points of reference during seismic events and high-frequency monitoring is required to adequately capture the structural response. In the past, accelerometers have been used to obtain deflections by double numerical integration of the acceleration

record. Inaccuracies in the numerical integration of the acceleration record and the need for adjustment to compensate for residual deformation reduce the accuracy of the resulting deformation record.

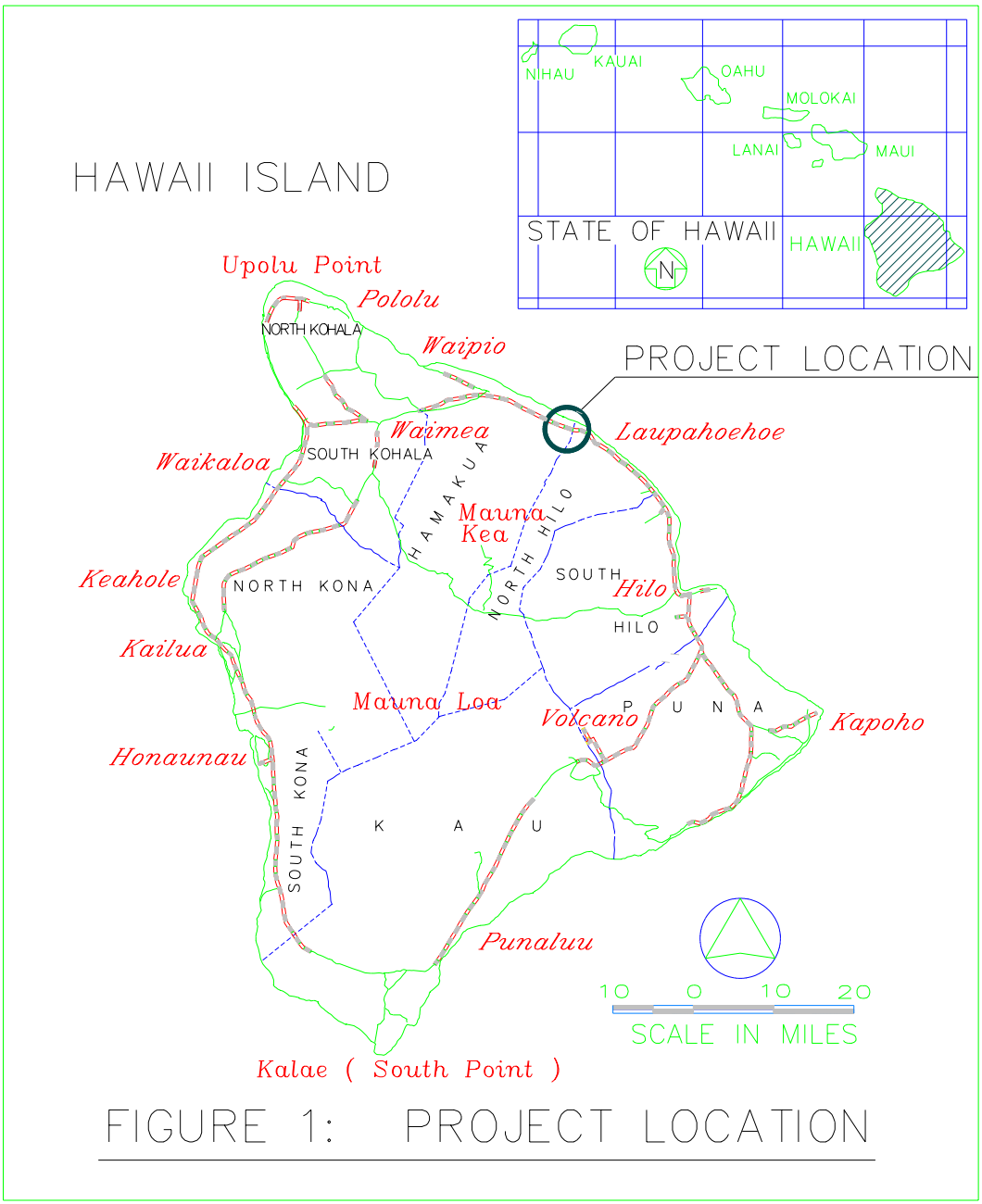

Figure 1.1. Project Location.

This project investigates the use of an innovative fiber optic strain gauge monitoring system. This strain gauge-based deformation monitoring system can be used in structures such as the new box-girder Kealakaha Stream Bridge. This type of monitoring system will be extremely beneficial to future structural engineers because it can provide a real-time deformation system, which illustrates how structures respond to earthquakes and other dynamic loads.

1.3 Objectives and Scope

The overall objective of the current phase of this project is to develop a dynamic deflection monitoring system using fiber optic strain gauges for the Kealakaha Stream Bridge. The specific objectives that need to be fulfilled to achieve the overall objective are as follows:

(1) Verify the mathematical model based on research done at the Federal Polytechnic College of Lausanne (EPFL) [Vurpillot, 1998], which will be discussed in Chapter 3, in the laboratory through static and dynamic tests using electrical resistance strain gauges.

(2) Select a fiber optic strain gauge system to use in the laboratory and field verification tests.

(3) Verify the model in the laboratory using fiber optic strain gauges.

(4) Verify the model in the field on the H-3 Highway using fiber optic strain gauges.

The scope of this report is to verify the mathematical model using electrical resistance strain gauges and to select the fiber optic strain gauge system to be used in future verification tests. The laboratory verification using the fiber optic strain gauges and the

field verification tests on the H-3 Highway North Halawa Valley Viaduct will be performed in the future as a separate project.

The basic concept behind the deflection monitoring system is that strain measurements from gauges placed along the bridge will be used to obtain the girder curvature, which will then be used to mathematically determine the deformed shape of the bridge. Several laboratory experiments, both static and dynamic, were performed on three different beam specimens, two tube steel specimens and one pre-stressed concrete girder.

Here is a brief overview of the contents of this report. A review of current deflection monitoring systems available is presented in Chapter 2. Chapter 3 introduces the mathematical model used in the proposed strain gauge-based system. Fiber optic strain gauges are then introduced in Chapter 4 and a selection is made for the fiber optic strain gauges to be used in the laboratory verification tests. Chapter 5 describes the various laboratory experiments used to verify the mathematical model using electrical resistance strain gauges. The results of these tests are presented and discussed in Chapter 6. Chapter 7 presents the resulting strain gauge system proposed for the Kealakaha Stream Bridge while Chapter 8 provides a summary and conclusions for this study.

CHAPTER 2
LITERATURE REVIEW

Currently, there are many different systems that can be used to monitor the vertical deflections of structures, such as bridges. Some of these systems include base-line systems, strain gauge-based systems, Global Positioning Systems (GPS), Linear Variable Displacement Transducers (LVDTs), and accelerometers. Most of these systems provide accurate information on how a structure deforms in static loading conditions, but are limited when it comes to measuring dynamic deformations caused by seismic activity.

2.1 Base-line Systems

Base-line systems are typically used for static measurements. A taut-wire base-line system was used as the deflection monitoring system for the instrumentation of the H-3 North Halawa Valley Viaduct [Lee, 1995]. This system consists of a high-strength piano wire strung at a constant tension between two end brackets inside the box girder (Fig. 2.1). A weight and pulley system at the "live end" maintains a constant tension in the piano wire regardless of axial deformations in the span. The wire spans from one pier to the next, acting as a reference line. Precision measurements between this base-line and plates attached to the underside of the top slab are measured using a digital caliper, providing accurate vertical deflection measurements.

This base-line system proved to be sufficient for monitoring static deflection measurements, but the current system does not allow for dynamic deformation measurements because the caliper is read manually. Linear Variable Displacement Transducers (LVDTs) can be installed to monitor deflections relative to the piano wire

more rapidly. However, during a seismic event, the vibration of the piano-wire and constant tension weight will distort these deflection measurements.

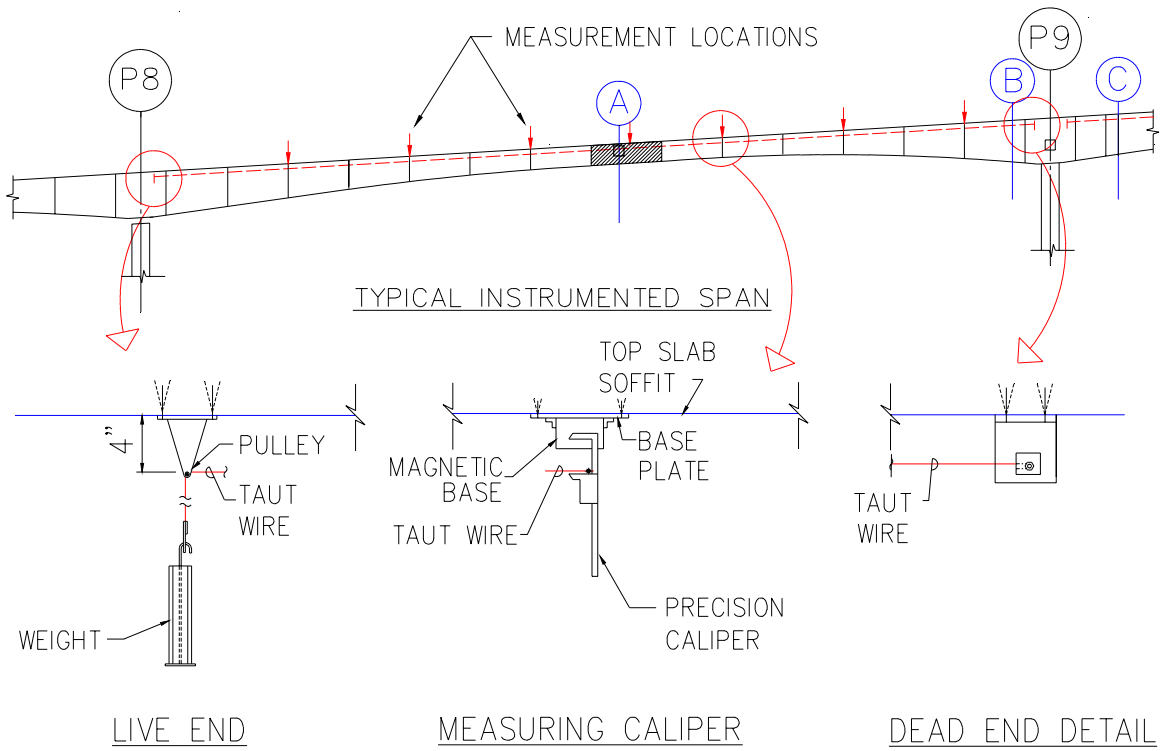

Figure 2.1. Base-line Deflection Measurement System.

2.2 Strain gauge-based Systems

Strain gauge-based systems have been used to measure deformations produced by static loads. Bridge deformations have been and are still being monitored using strain sensors, including fiber optic strain sensors, by researchers at SMARTEC, a Swiss company involved with civil structural monitoring. Their SOFO (Surveillance d'Ouvrages par Fibres Optiques) system has been used in many bridges, such as the Lutrive Highway Bridge, a box girder bridge in Switzerland, which has 30 six-meter-long sensors installed along the length of the fourth span [Inaudi, 1999]. The strains from these sensors are used to monitor how the curvature is affected due to variations in daily

temperature. The method can also be used for static and dynamic loads as well. The vertical displacements are obtained from these curvature measurements by double integration. This mathematical model is described in more detail in Chapter 3 and is also implemented in this project. For end support settlements, a reference point is also needed to acquire absolute dimensions since the model only shows the beam deformation and not its rigid body displacements in space [Vurpillot, 1998]. The SOFO gauges are not capable of high frequency strain monitoring and so this system is not suitable for seismic monitoring.

2.3 Global Positioning Systems (GPS)

Global Positioning Systems (GPS) are often used for displacement measurements. Sensors are placed on the structure to be monitored and also on a known fixed reference site, or benchmark, adjacent to the structure. To ensure accurate results, all of the sensor antennas must be able to communicate clearly with four or more GPS satellites. Using this system, one can obtain the absolute location of each sensor in three dimensions within millimeters of the true location. Figure 2.2 depicts a sample GPS with real-time web dissemination of the deformation data [www.mezure.com].

The GPS sensors currently available from Mezure, Inc. can only process one reading every ten seconds. This system is therefore only suitable for static loading or thermal and long-term effects. Faster reading rates, up to 10-20 Hz, are being developed and have been used in some experiments to monitor the response of long-period structures to wind and other low frequency excitation [Çelebi, 2002]. For this system to work, there must be a stable reference station nearby, however, in the event of an

earthquake, there is no stable reference point. This resulting position coordinates would be inaccurate.

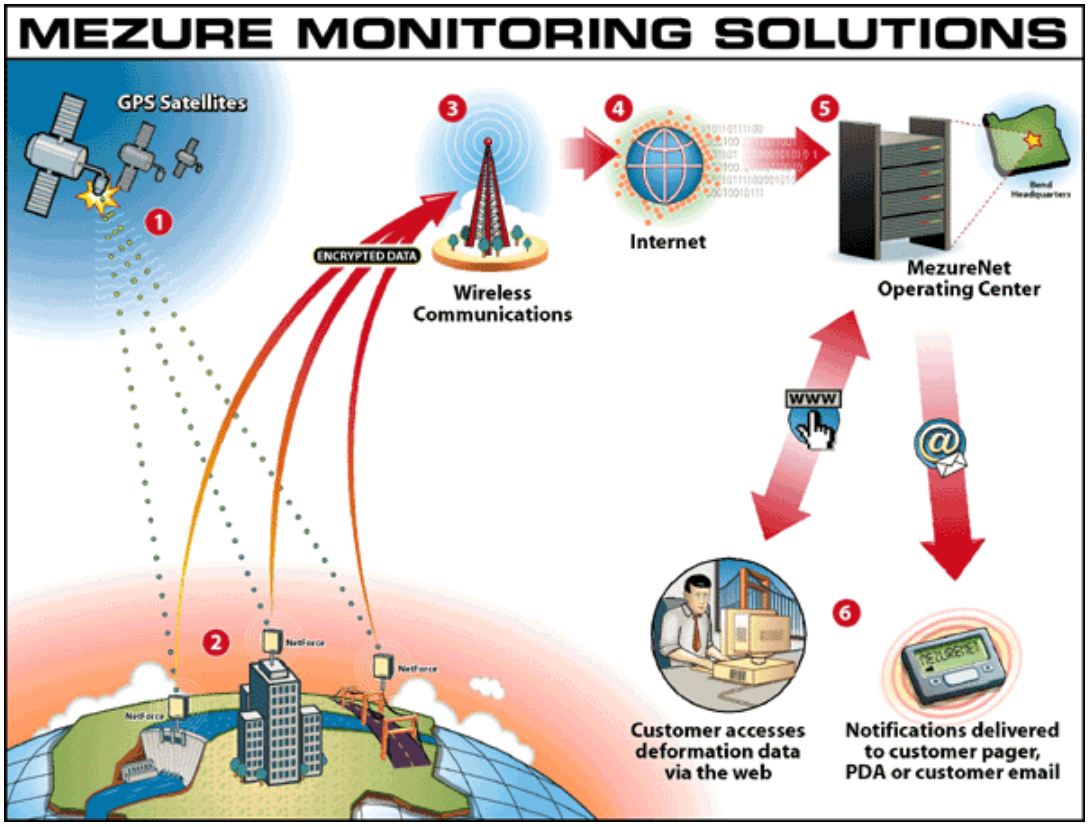

Figure 2.2. Mezure GPS Sensor System [www.mezure.com].

2.4 Linear Variable Displacement Transducers (LVDTs)

Linear Variable Displacement Transducers (LVDTs) can provide high frequency measurements of relative displacement between two points. They can be used at bridge expansion joints, for example, to monitor relative displacement during an earthquake. However, to monitor vertical deflection of a bridge girder during an earthquake, it would require a fixed reference point on the ground below the girder. Since the ground will also be moving, this measurement will not record the true structural deformation.

2.5 Accelerometers

Accelerometers are currently being used to measure dynamic deflections in structures. Numerical integration of the acceleration record results in a velocity trace. Numerical integration of the velocity trace yields the deflection. According to Çelebi [Çelebi, 2002], the integration process is not readily automated because of the nature of the signal processing, which requires (a) selection of filters and baseline correction (the constants of integration), and (b) use of judgment when anomalies exist in the records. Therefore, double numerical integration of the accelerometer record generally introduces a number of errors into the resulting deflection record. Furthermore, the errors are more apparent for permanent displacements, which accelerometer measurements most likely cannot recover at the centimeter level [Çelebi, 2002]. Usually, the permanent displacements are assumed to be zero, therefore, there is error in the resulting relative displacements. For these reasons, comparison of deflection records at various locations along the bridge span to determine the deformed shape is an unreliable measure of bridge deformation.

Since all of these previously used deflection monitoring systems have drawbacks for seismic monitoring, a new system is investigated that can provide more accurate deformation measurements during seismic and other dynamic events.

CHAPTER 3
MATHEMATICAL THEORY

3.1 The Mathematical Model

The mathematical model used in the proposed deflection system is based on research done at the Federal Polytechnic College of Lausanne (EPFL) [Vurpillot 1998]. It is based on strain measurements from gauges placed at strategic locations along the span of a beam, aligned parallel to the beam axis. The strain values are used to obtain the beam curvature at discrete locations along the beam. Curve fitting is used to develop a set of equations for the beam curvature, which is then used to determine deflection equations by double integration. Boundary conditions, which are known or assumed, are used to solve the constants of integration. Since the integration is exact, the only approximations are the determination of beam curvature equations from the strain measurements and inaccuracies in the strain measurements themselves.

To develop polynomial expressions for the curvature, strain readings are required at predefined locations along the bridge span. Vurpillot *et al.*[1998] provide specific guidelines on how a beam or structure should be sub-divided into sections and cells. The beam must first be divided into sections. There should be at least one section between supports or points where boundary conditions are known. Each section is then subdivided into cells. If the deformations can be approximated by a degree N polynomial, then each section should be divided into N-1 cells. Note that the mathematical model does not need the locations or magnitudes of the applied loads or the locations of the interior supports, if any.

For the laboratory tests described in the following chapters, since the beams tested were prismatic, deformations could be approximated by a fourth degree polynomial. Therefore, each section is divided into three cells. Strain gauges are then placed at, or close to, the center of each cell, and are assumed to provide the mean strain for that particular cell. To ensure that the strain gauge provides the mean strain for a particular cell, the gauge length should ideally approach the length of the cell. This could be unreasonable if the cell lengths are extremely long. Therefore, the use of shorter gauge lengths was investigated in the laboratory verification tests.

If the location of the neutral axis is known precisely for the member cross-section, then a single strain gauge either at the top or bottom of the section is sufficient to define the curvature. In the steel tube laboratory test specimens, the neutral axis location is well defined. However, if the member cross-section is not known exactly or if the neutral axis varies along the span, as in the case of the pre-stressed concrete laboratory test specimen or the pre-stressed concrete box girder bridge, strain gauges should be located at both the top and bottom of the section to define the curvature regardless of the location of the neutral axis.

According to Bernoulli beam theory, the following relationship exists between curvature and the longitudinal strains in an elastic beam where the neutral axis location is known (Fig. 3.1):

$$\frac{1}{r(x)} = \frac{\varepsilon(x)}{y} \tag{3.1}$$

where

r = radius of curvature
x = curvilinear abscissa along the beam
ε = elongational strain

y = distance from the neutral axis to the strain measurement

If the neutral axis location is not known or varies due to cracking or other non-linear behavior, then the curvature can be found using the following equation:

$$\frac{1}{r(x)} = \frac{\varepsilon_t(x) - \varepsilon_b(x)}{d} \tag{3.2}$$

where

ε_t = top fiber elongational strain
ε_b = bottom fiber elongational strain
d = distance between top and bottom strain measurements

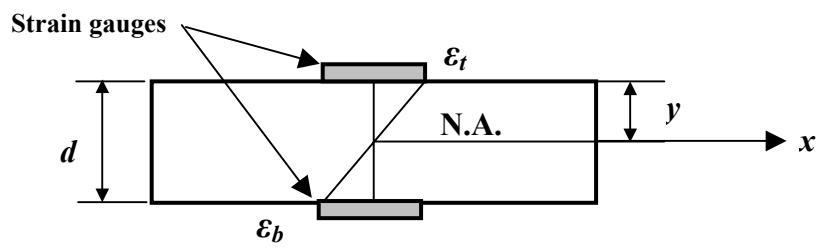

Figure 3.1. Schematic of Strain Measurement in a Beam Cell.

Equations (3.1) and (3.2) are used to calculate the local curvatures of each cell. From these local curvatures, a curvature equation for the beam section is then derived by fitting a polynomial through the values produced in each cell. A beam section is defined as a segment of a whole beam with a constant or continuously varying inertia, a constant uniform load and an additional introduction of concentrated load (force, moment, support reaction, etc.) only at its extremes [Vurpillot, 1998; Inaudi, 2000]. For a simple beam, each section is divided into three cells (Fig. 3.2) and the curvature, Ψ, is represented by the quadratic equation:

$$\Psi = P_2(x) = a \cdot x^2 + b \cdot x + c \tag{3.3}$$

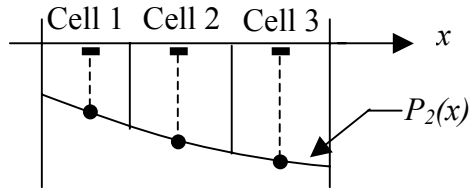

Figure 3.2. Typical Section Division into 3 Cells

The quadratic equation has three unknowns and thus, three independent measurements, or values taken from three cells, are needed to find these constants. The following equation can be used to express the mean curvature for a single cell:

$$\frac{1}{r_i} = \frac{\int_{x_A^i}^{x_B^i} (a \cdot x^2 + b \cdot x + c)dx}{x_B^{\,i} - x_A^{\,i}} \tag{3.3}$$

where $1/r_i$ is the mean curvature of the ith cell and x_A^i and x_B^i are the start and end points of the ith cell. Integration of equation (3.3) yields the following equation:

$$a \cdot \frac{(x_B^{\,i3} - x_A^{\,i3})}{3} + b \cdot \frac{(x_B^{\,i2} - x_A^{\,i2})}{2} + c \cdot (x_B^{\,i} - x_A^{\,i}) = \frac{x_B^{\,i} - x_A^{\,i}}{r_i} \tag{3.4}$$

Equation (3.4) is applied to each of the three cells producing three equations that can be solved simultaneously to find the constants, a, b, and c, thus producing a quadratic expression for the curvature of the section. This is repeated for each section along the beam. Finally, the curvature expression for each section is integrated twice to produce the deformed shape, D, such as the following expression for the ith section:

$$D = P_4^{\,i} = \frac{a^i}{12} \cdot x^4 + \frac{b^i}{6} \cdot x^3 + \frac{c^i}{2} \cdot x^2 + \alpha^i \cdot x + \beta^i \tag{3.5}$$

where α^i and β^i are the constants of the double integration for the ith section. The subscript "4" is used to denote the order of the polynomial. The α and β constants for

each section are determined so as to maintain continuity of displacement and slope between adjacent sections and to satisfy the boundary conditions at the ends of the beam. The following expressions must be satisfied at each section boundary to maintain continuity:

$$P_4^{\,i}(x_B^{\,i}) = P_4^{\,i+1}(x_A^{\,i+1}) \tag{3.6}$$

$$\frac{dP_4^{\,i}}{dx}(x_B^{\,i}) = \frac{dP_4^{\,i+1}}{dx}(x_A^{\,i+1}) \tag{3.7}$$

Equation (3.6) guarantees the continuity of displacements and equation (3.7) guarantees the continuity of the slopes at each section boundary. At the ends of the beam, the following boundary conditions are assumed:

$$P_4^{\,1}(x_A^{\,1}) = 0 \qquad and \quad P_4^{\,n}(x_B^{\,n}) = 0 \tag{3.8}$$

where n is the number of sections in the beam. The resulting fourth-order polynomials for each section now represent a continuous function for the full beam deformed shape. This approach to deflection monitoring will not detect overall beam translation or movement of the beam ends, but will provide the deformed shape of the beam between end points assumed to remain in place. This is sufficient to determine bending moment and shear force distributions along the beam. The bending moment can be calculated directly from the curvature using equation (3.9) and then the shear can be calculated from the bending moment by using equation (3.10).

$$M = EI\Psi \tag{3.9}$$

where

M = bending moment
E = modulus of elasticity

I = moment of inertia
Ψ = curvature

$$V = \frac{dM}{dx} \tag{3.10}$$

where
V = shear
x = horizontal distance along the beam

The vertical displacements are calculated for comparison with the measured displacements in order to verify that the curvatures are accurate.

3.2 The Microsoft Visual Basic 6.0/Excel 2000 Program

A Microsoft Visual Basic 6.0/Excel 2000 program (see Appendix B) was created using the mathematical model described in the previous section. The program required certain parameters. They include the number of sections, the locations of the cells, the strain measurements, and the vertical distance between the strain measurements or the distance to the neutral axis, if known. The number of cells in each section was assumed to be three. Once those parameters are inputted, the program implements the mathematical model. The output includes the constants a, b, c, α, and β and a plot of the deflected shape.

CHAPTER 4
SELECTION OF FIBER OPTIC STRAIN GAUGES

4.1 Fiber Optic Sensors Versus Conventional Sensors

Fiber optic sensors (FOS) are innovative sensing devices for structural monitoring. FOS have numerous advantages over conventional electrical-based sensors. First of all, FOS are very light in weight and extremely small in diameter. Thus, if they are embedded in a structure, they are not obtrusive and do not degrade the integrity of the structure. Second, FOS are all passive. The fibers are dielectric in nature; therefore, conductive paths are eliminated. As a result of the size and passive nature, they are safer to use because they are not likely to cause fires or explosions and they are also immune to electromagnetic interference. Third, FOS are sensitive to a wide range of strains and temperatures, but also resistant to corrosion and fatigue. Fourth, FOS are capable of wide bandwidth operation. Last, FOS can be multiplexed, meaning data from many channels can be merged into one channel. This can be accomplished by having a string of sensors along a single optical fiber, also known as single multiplexing, or an array of FOS excited with a single source, also known as parallel multiplexing. The frequency of monitoring is dependant only on the speed of the data acquisition system.

4.2 Considerations in Selecting Fiber Optic Structural Sensors

There are many factors that must be considered in order to select the ideal fiber optic sensor for a particular application. One must determine:

- What parameters are to be measured, whether it is strain, temperature, pressure, or vibration frequencies.
- How long the gauge length needs to be in order to measure the selected parameter effectively.
- The number of fiber sensors to be multiplexed.
- The diameter of the fiber sensor.

- The dynamic range and the sensitivity of the sensor.

Although the issues mentioned above are very important, sometimes overall costs or concerns of how the fiber sensor will affect the structural integrity of the project govern the selection of a sensing system.

4.3 Types of Fiber Optic Strain Gauges

There are many specific criteria that a fiber optic sensor should meet in order to ideally measure parameters for an instrumented structure. Raymond M. Measures [1995], the author of "Fiber Optic Strain Sensing" and "Structural Monitoring with Fiber Optic Technology", specifies fourteen standards that make a fiber optic sensor ideal. There were only four types of sensors that met a majority of these requirements: polarimetric, two-mode, Fabry-Perot, and Bragg grating. These sensors met the following criteria specified by Measures [1995]:

1. Localized
2. Intrinsic in nature for minimum perturbation and stability
3. Well-behaved with reproducible response
4. All fiber for operational stability
5. Insensitive to phase interruption at the structural interface
6. A single optical fiber for minimal perturbation and common-mode rejection .

Measures [1995] goes on to compare the following characteristics for these fiber optic sensors:

1. Localized
2. Responds only to strain
3. Direction change response
4. Linear response
5. Single-ended
6. Adequate sensitivity and range
7. Absolute measurement
8. Multiplexing within structure
9. Potential for mass production.

Of these specifications, only two types of fiber optic sensors measured up, fully meeting three to six of the specifications. They were the Fabry-Perot and the Bragg grating fiber optic sensors. The Fabry-Perot sensors are localized, single-ended, and have adequate sensitivity and range. The Bragg grating sensors are localized, have a direction change response, have a linear response, take absolute measurements, can have multiplexing within a structure, and have the potential for mass production. According to Measures [2001], the Fabry-Perot and Bragg grating sensors best meet the criteria for structural sensing and thus, they will be discussed in further detail in the next section.

4.4 Types of Fiber Optic Strain Gauges Considered

The Fabry-Perot and the Bragg grating fiber optic sensors were considered as possible fiber optic strain gauges to use in the Kealakaha Stream Bridge project.

4.4.1 Fabry-Perot Fiber Optic Strain Gauge

Fabry-Perot fiber optic strain gauges have a cavity, which is defined by two mirrors (Fig. 4.1). These mirrors are parallel to each other and lie perpendicular to the axis of the optical fiber. There is a pre-defined distance, nL, between the two mirrors, which corresponds to a certain light frequency, where n is the core index of refraction and L is the physical length (measured from the coupler to each of the mirrored tips) of the sensing and reference optical fibers [Measures, 2001]. If there is a change in strain, the optical path length, nL, will change and there will be a corresponding shift in the cavity mode frequency [Measures, 2001].

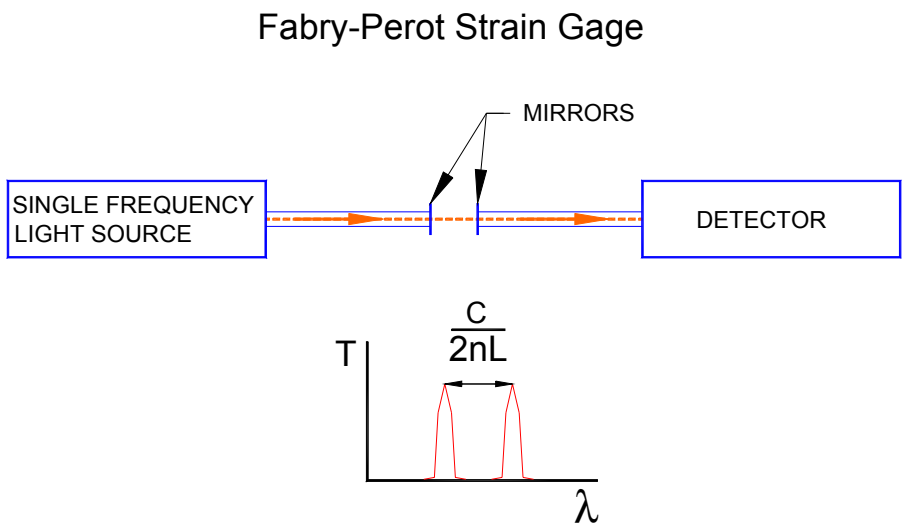

Figure 4.1. Fabry-Perot Fiber Optic Strain Gauge.

4.4.2 Bragg Grating Fiber Optic Strain Gauge

A Bragg grating fiber optic strain gauge has an impressed grating pattern written on its core by two interfering ultraviolet laser beams (Fig. 4.2) [Udd, 1995]. When broadband (white) light passes through the fiber, this grating pattern produces a specific reflected signal wavelength, typically referred to as the Bragg wavelength, λ_B. This Bragg wavelength is dependent upon the grating period, Λ, and the mean core index of refraction, n_o, as shown in Equation (4.1) [Measures, 2001]:

$$\lambda_B = 2n_o\Lambda \tag{4.1}$$

If the fiber experiences axial strain, the Bragg wavelength shifts. Changes measured in either reflected or transmitted light can be correlated to the fiber strain.

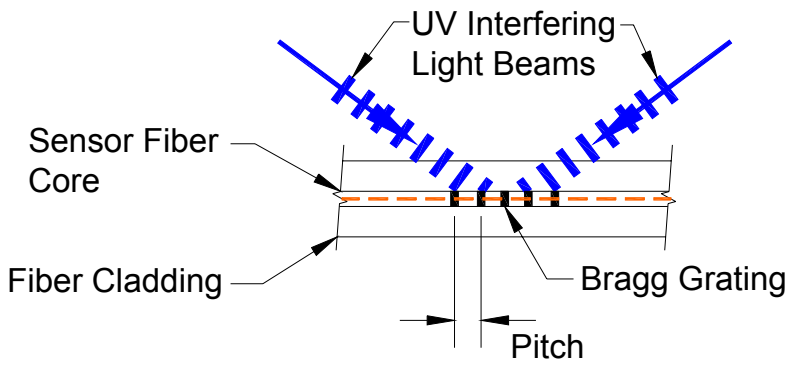

Figure 4.2. Fabrication of Bragg Grating Fiber Optic Strain Gauge.

4.4.2.1 Advantages of Bragg Grating Fiber Optics over Fabry-Perot Fiber Optics

There are many advantages to using Bragg grating fiber optic strain gauges over Fabry-Perot fiber optic strain gauges in instrumented structures. Bragg grating gauges provide a linear response because the Bragg wavelength is a linear function of the strain, whereas the Fabry-Perot sensors require quadrature detection and a suitable signal demodulation in order to achieve a linear response [Measures, 1995]. In addition, since there is a direct relationship between the Bragg wavelength and the strain, one can take absolute strain measurements. Other interferometers, such as the Fabry-Perot sensors, can only take incremental strain measurements, which then need to be demodulated by a specialized system in order to obtain absolute measurements. The Bragg grating system also can be multiplexed conveniently on a single fiber by impressing Bragg gratings with different wavelengths (Fig. 4.3). Multiplexing is difficult for Fabry-Perot sensors, except for large structures because time-division multiplexing can be used [Measures, 1995]. According to Measures [2001], Bragg grating sensors will probably dominate the world

of sensors because of their versatility, multiplexing capability, lower cost, and consistent manufacture in the long term.

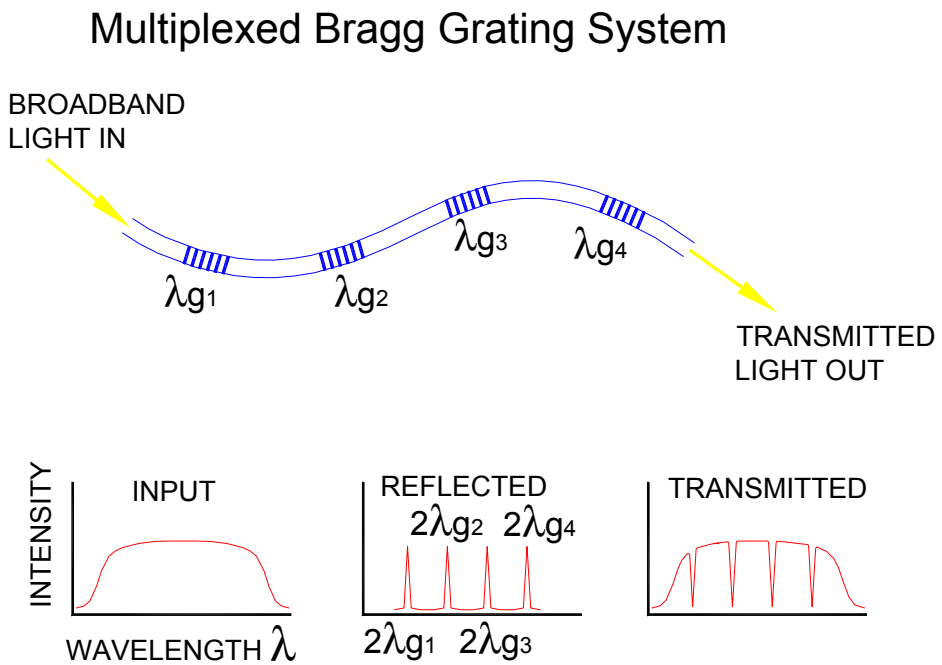

Figure 4.3. Multiplexed Bragg Grating System.

4.5 Typical Configurations

Fiber optic strain gauges can be installed by either surface mounting (Figs. 4.4, 4.5) or encasing them in a steel tube for concrete embedment (Figs. 4.6, 4.7). Typical configurations, particularly Fabry-Perot sensors, including their schematics are shown in the following figures:

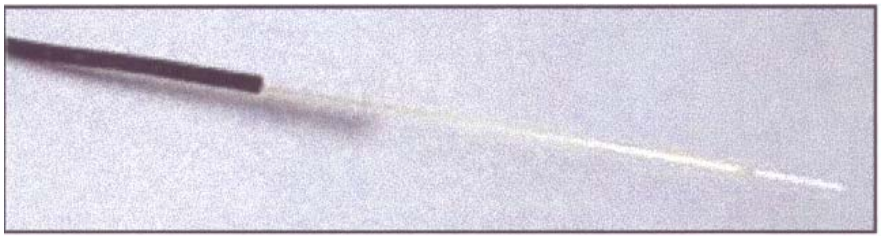

Figure 4.4. Bare FOS [www.roctest.com].

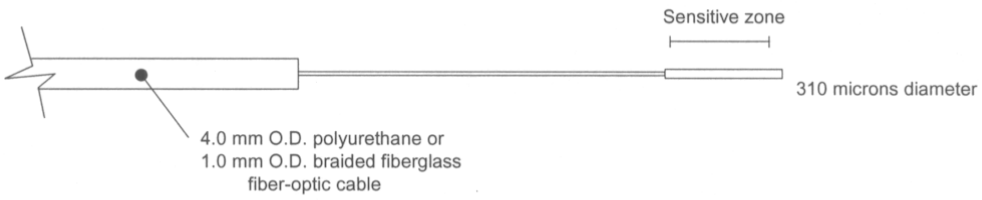

Figure 4.5. Bare FOS Schematic [www.roctest.com].

Figure 4.6. FOS for Embedment [www.roctest.com].

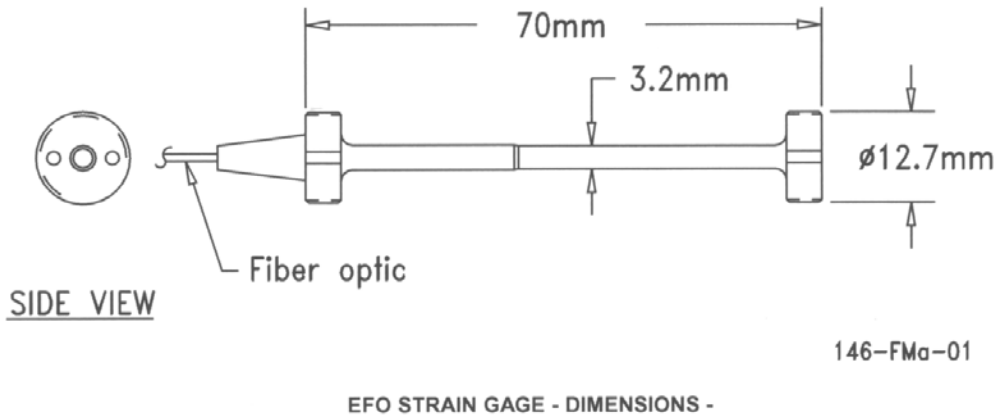

Figure 4.7. FOS for Embedment Schematic [www.roctest.com].

4.6 Fiber Optic Strain Gauge Systems Considered

Although the Bragg grating fiber optic strain gauges clearly have more advantages over the Fabry-Perot fiber optic strain gauges, one must also consider cost and availability when determining which system to purchase.

4.6.1 Fabry-Perot Fiber Optic System

The Fabry-Perot fiber optic strain gauge system consists of twelve fiber optic strain sensors that are approximately 0.394 in. (1 cm) gauge length. These strain sensors can be surface mounted on steel. They are non-compensated for temperature so one unattached strain sensor will be used to correct for temperature. They have a range of 1000 micro-strain and have compression or tension accuracy of 1 micro-strain. The readout data acquisition system is capable of supplying the light source and can monitor twelve fiber optic sensors simultaneously at 200 Hz.

4.6.2 Bragg Grating Fiber Optic System

The Bragg grating fiber optic strain gauge system also consists of twelve fiber optic strain sensors that are approximately 0.394 in. (1 cm) gauge length. They have a range of greater than 1000 micro-strain. At this time, Blue Road Research has a 4-channel 10MHz demodulation system, which has been used to acquire strains for dynamic tests. An affordable system that reads twelve channels in not available, but Blue Road Research is currently developing an 8-channel simultaneous unit prototype, which should be completed by late February 2003.

4.7 System Selected for Laboratory and Field Applications

The Roctest Fabry-Perot fiber optic strain gauges and data acquisition system was selected to be used in the initial laboratory and field applications. This is because, at the time of selection, the Roctest data acquisition system was the only system that could provide the rapid reading rate (200 Hz) of 12 channels simultaneously at an affordable price.

4.8 System Selected for Bridge Application

Subsequent to the field verification using Fabry-Perot gauges on the H-3 North Halawa Valley Viaduct, this system will be re-evaluated for use in the final Kealakaha Bridge instrumentation. If adequate data acquisition facilities are available for the Bragg grating fiber optics, they will also be evaluated for possible use in the final bridge application. The gauge length will be at least 6 inches (15.24 cm) so as to average the concrete strain over a representative concrete sample.

CHAPTER 5
TEST SET-UP AND PROCEDURES

5.1 Introduction

To verify the mathematical model discussed in the previous chapter, a series of experiments were performed on three beams in the Structures Laboratory at the University of Hawai`i at Manoa. These tests were performed on a simply-supported steel tube, a three-span steel tube, and a simply-supported prestressed concrete T-beam. The following sections describe the test set-up and the testing procedures for each of the specimens.

5.2 Electrical Resistance Strain Gauges

Initial model verification was performed using traditional electrical resistance strain gauges manufactured by the Micro-Measurements Division of Vishay Measurements Group, Inc. The gauges were LWK-06-W250B-350 weldable strain gauges with a gauge factor of 2.03. They were installed, including the surface preparation and the actual spot welding of the strain gauges, according to the procedures provided by Vishay Measurements Group, Inc (Fig. 5.1). Extension wires were soldered onto the lead wires for connection to the data acquisition system. Initially, the strains were measured using Vishay Measurements Group, Instrument Division, P-3500 Strain Indicators and SB-10 Switch and Balance Units (Fig. 5.2). All dynamic tests were recorded using a National Instruments Data Acquisition system LabVIEW 6.i (Fig.5.3), using four National Instrument SCXI-1520 conditioner cards in a SCXI-1001 12-slot chassis (Fig. 5.4). Later, static tests were recorded using both systems.

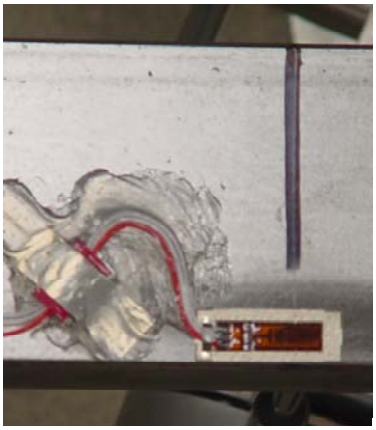

Figure 5.1. LWK-Series Weldable Strain Gauge.

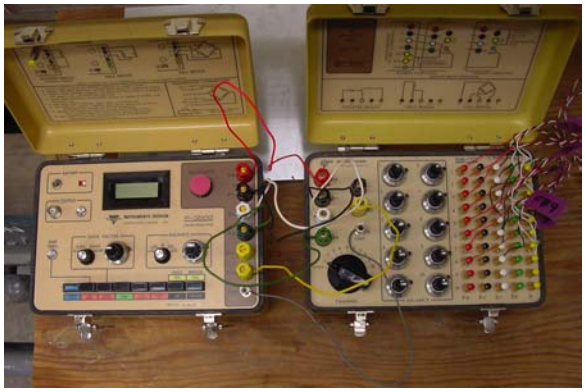

Figure 5.2. Vishay Measurement Group, Instrument Division, P-3500 Strain Indicator and SB-10 Switch and Balance Unit.

Figure 5.3. National Instruments Data Acquisition system.

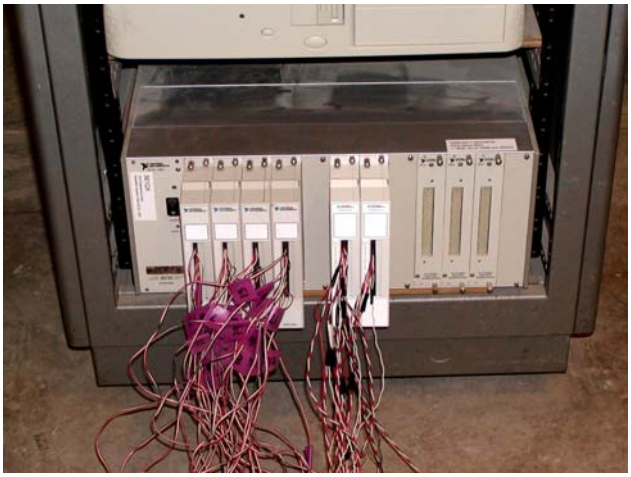

Figure 5.4. National Instrument SCXI-1520 Conditioner Cards in a SCXI-1001 12-slot Chassis.

5.3 Beam I: Simply-Supported Steel Tube

The first beam (Fig. 5.6) was a nominal 3 in (7.62 cm) by 6 in. (15.24 cm) rectangular steel tube subjected to four-point loading (see Fig. 5.5 for exact dimensions).

This beam was divided into three sections, their lengths being 34.16 in (86.77 cm), 29.28 in (74.37 cm), and 34.16 in (86.77 cm). Each section was then divided into three cells. Ideally, for a prismatic steel beam, the cells should be the same size with the strain gauges placed at the center of each cell because each strain gauge provides the average strain for the cell. In the case of Beam I, the electrical resistance strain gauges were installed at every tenth of the beam length along the top and the bottom of the tube. The end cell lengths were therefore adjusted so that the gauges were at, or close to, the center of each cell.

The beam was loaded with 4000 lbs. (17.19 kN), 2000 lbs. (8.896 kN) at each load point, and the strains were recorded from each of the 18 strain gauges. Because the beam was symmetric about the neutral axis, located at the mid-height of the section, only strain values from either the top face or bottom face of the beam were required. The top strain values were entered into the mathematical model described earlier to generate the numerical deformed shape. In addition, dial gauges were placed along one half of the beam in order to provide the "measured" deflection values to compare with the numerical deformed shape.

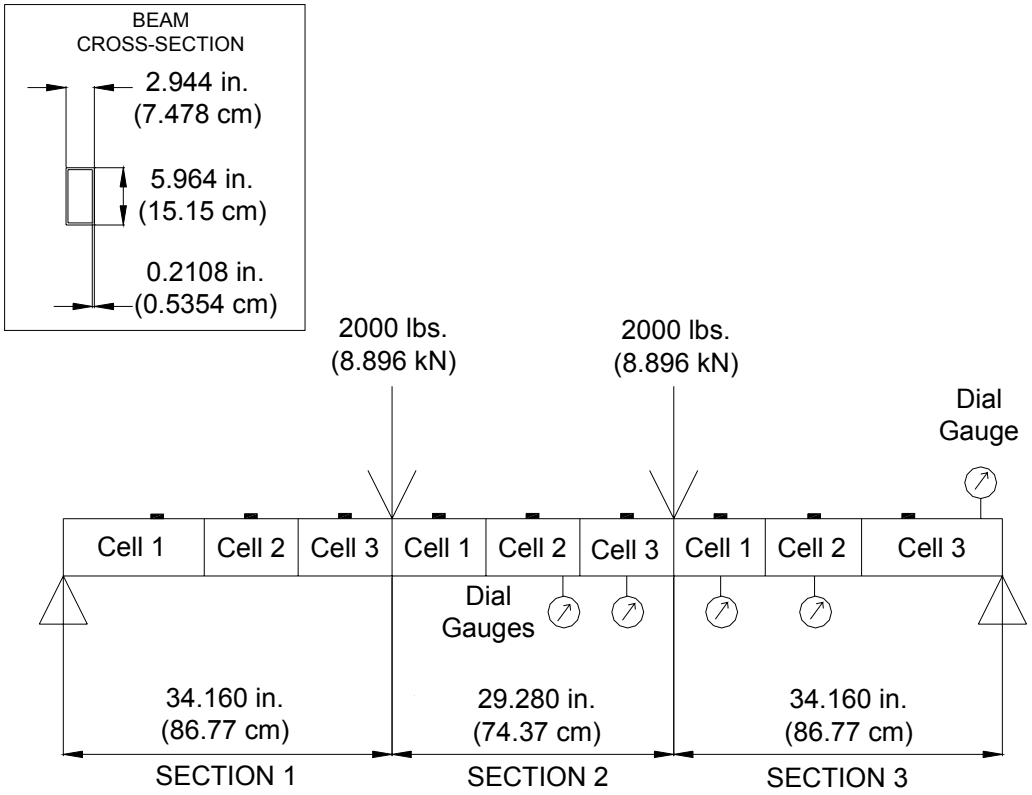

Figure 5.5. Beam I Layout.

Figure 5.6. Beam I Test Set-Up.

5.4 Beam II: Three-span Steel Tube

The second beam was a twenty-foot long rectangular steel tube with nominal cross-section dimensions of 2 in (5.080 cm) x 1.0 in (2.54 cm) x $^{1}/_{16}$ in (0.1588 cm) wall thickness (see Fig. 5.8 for exact dimensions). The beam rests on four pinned supports with a 1:2:1 length ratio for the three spans (Figs. 5.7 and 5.8). This beam approximates a 1/37-scale model of the Kealakaha Stream Bridge, but has a constant cross-section as opposed to the variable box girder section proposed for the bridge.

Figure 5.7. Beam II Test Set-Up.

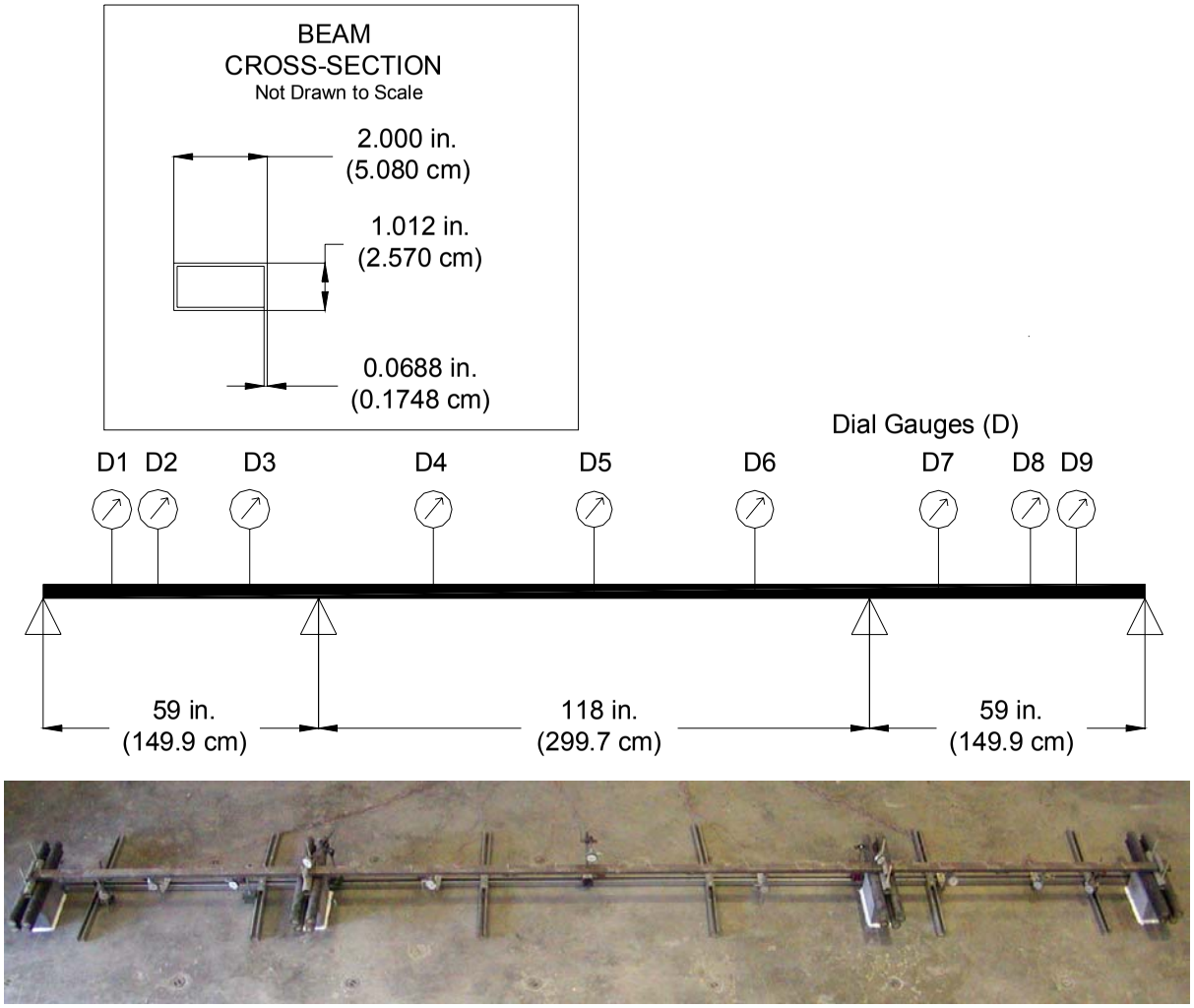

Figure 5.8. Beam II Layout.

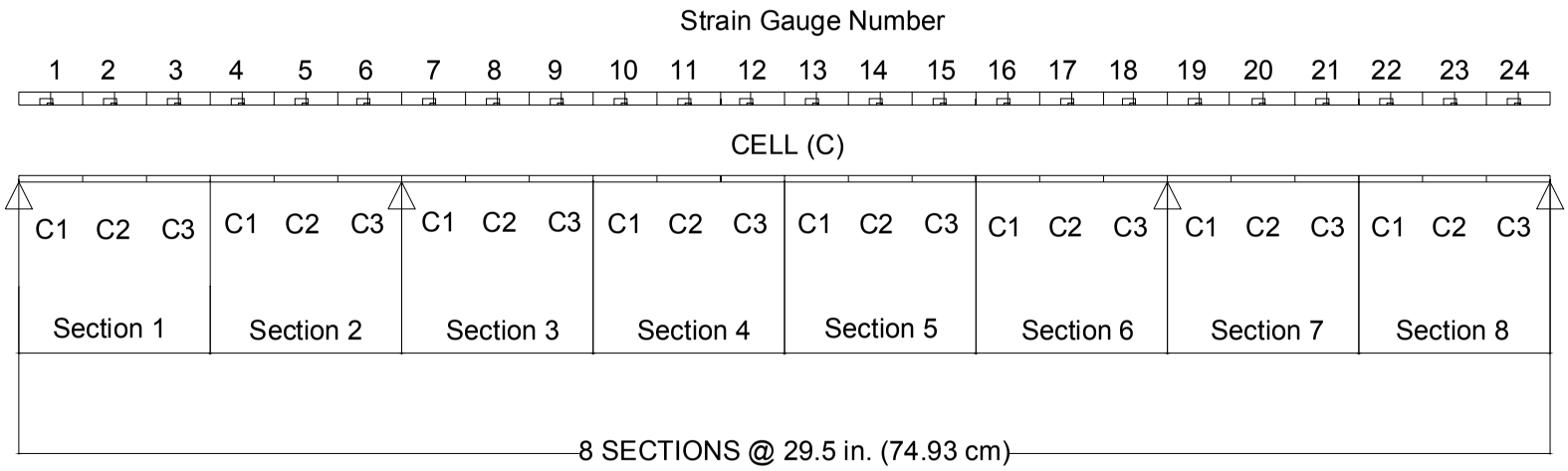

Figure 5.9. Beam II "Ideal 24" Strain Gauge System Layout.

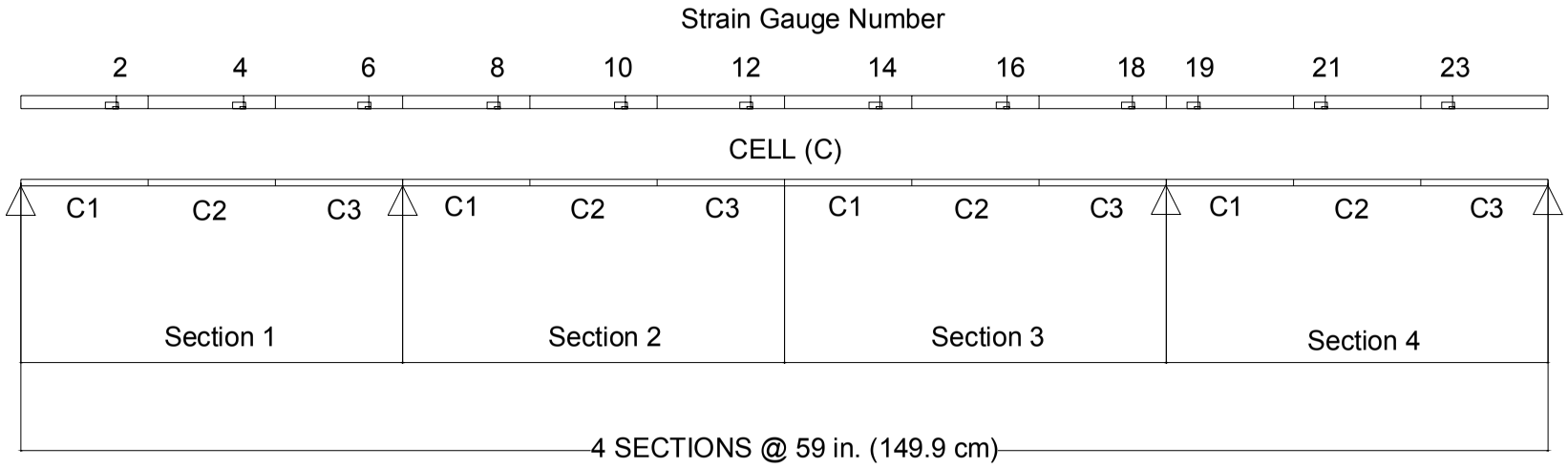

Figure 5.10. Beam II "Selected 12" Strain Gauge System Layout.

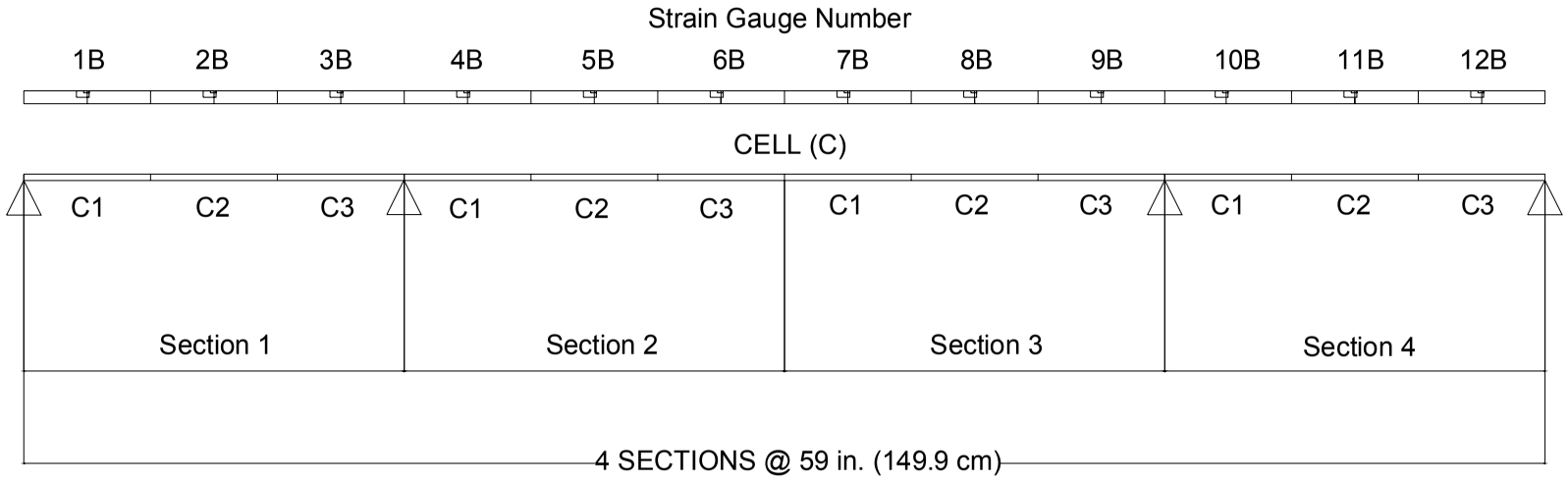

Figure 5.11. Beam II "Ideal 12" Strain Gauge System Layout.

The three-span beam was divided into eight sections, with each 29.5 in (74.93 cm) long section divided into three cells of equal length (Fig. 5.9). An electrical resistance strain gauge was placed on the top of the tube at the center of each cell, for a total of twenty-four strain gauges. This configuration is referred to as the "ideal 24" strain gauge layout. To evaluate the performance of a smaller number of strain gauges, twelve out of the twenty-four strain gauges were selected to represent a beam divided into four sections (Fig. 5.10). This configuration is referred to as the "selected 12" strain gauge layout. Since the laboratory results proved that twelve strain gauges were sufficient to provide an accurate deformed shape, the beam was later sub-divided into four sections. Each 59 in (149.9 cm) long section was divided into three cells, requiring a placement of twelve strain gauges, one at the center of each cell (Fig. 5.11). This configuration is referred to as the "ideal 12" strain gauge layout.

For both the twenty-four and twelve strain gauge configurations, nine dial gauges were placed throughout the length of the beam in order to provide a "measured" deflected shape (Fig. 5.8). Approximately twelve different loading conditions, including several support settlement conditions, were performed on this beam using the Vishay Measurements Group equipment and the dial gauges. The support blocks were fashioned such that the simple supports could be moved up and down to represent the settling of a support (Fig. 5.12). The settlement values did not have to be known in order to find the deflected shape of the beam.

As defined in Chapter 3, the mathematical model assumes that the end supports do not move. Therefore, when the end support was displaced vertically in the end settlement test, the mathematical method produced a deformed shape but not its rigid-

body displacements in space [Vurpillot, 1998]. The resulting numerical deflected shape reflects the true deformation of the beam although the kinematic rotation of this shape is not captured. If the end support settlement is known, the kinematic rotation can be superimposed on the numerical deformed shape for comparison with the "measured" deflection.

Figure 5.12. Beam II Support System.

Twelve Linear Variable Displacement Transducers (LVDTs) were purchased in the later part of this project. These LVDTs were to serve as the "measured" deflected values, previously recorded by the dial gauges. Nine LVDTs were placed at the locations of the original dial gauges (Fig. 5.8). Two more were placed at support 2 and support 3, the interior supports. In addition, it was now possible to measure all thirty-six strain gauges simultaneously for static loads. Thirty-two strain gauges were recorded using the LabVIEW data acquisition system (Fig. 5.3, 5.4) and the remaining 4 strain gauges were measured using the Vishay Measurements Group Strain Indicator and Switch and Balance Unit (Fig. 5.2). The "ideal 24" electrical resistance strain gauge system could

then be compared to the "ideal 12" electrical resistance strain gauge system. Several more verification tests were performed using the LabVIEW equipment and the LVDTs.

5.5 Concrete Electrical Resistance Strain Gauges

The model verification on a concrete specimen was performed using traditional electrical resistance strain gauges manufactured by the Micro-Measurements Division of Vishay Measurements Group, Inc. The gauges were EA-06-20CBW-120 epoxy-bonded strain gauges with a 2 in. (50 cm) gauge length (Fig. 5.13). They were installed according to the procedures provided by Vishay Measurements Group, Inc. Extension wires were soldered onto the lead wires for connection to the data acquisition system. The test was recorded using the National Instruments Data Acquisition system used in the previous verification tests.

Figure 5.13. Electrical Resistance Strain Gauge on Concrete T-Beam.

5.6 Beam III: Simply-Supported Pre-stressed Concrete T-Beam

Beam III was a pre-stressed pre-cast concrete twenty-four-foot (7.315 m) girder taken from the Ala Moana Shopping Center parking structure (Figs. 5.14, 5.17). A 4.5 in (11.43 cm) reinforced concrete slab was added to the girder in order to recreate the original composite T-beam configuration (Fig. 5.15). The beam was to be tested under four-point loading to determine the flexural capacity of the beam (Fig. 5.16).

Figure 5.14. Girder from Ala Moana Shopping Center Parking Structure.

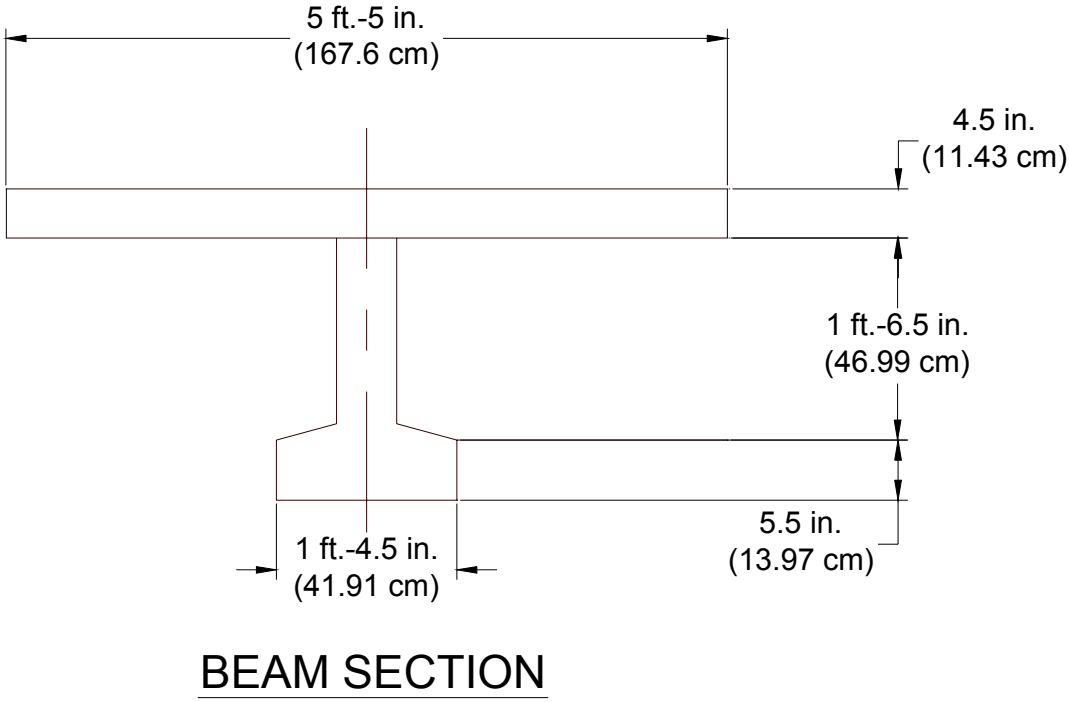

Figure 5.15. Pre-stressed Concrete T-Beam Cross-Section.

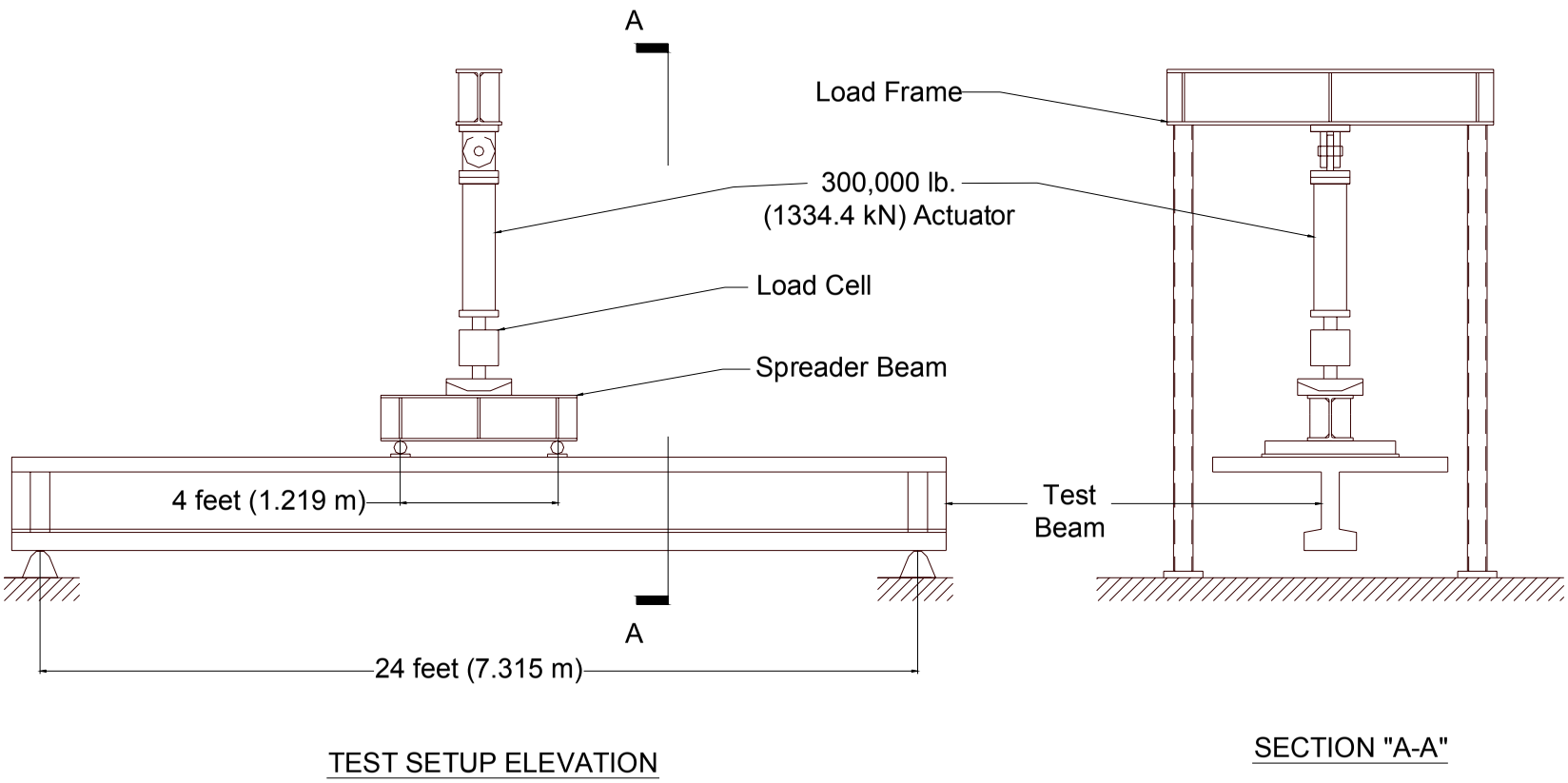

Figure 5.16. Beam III Test Set-Up.

Figure 5.17. Pre-stressed Concrete T-Beam Set-Up.

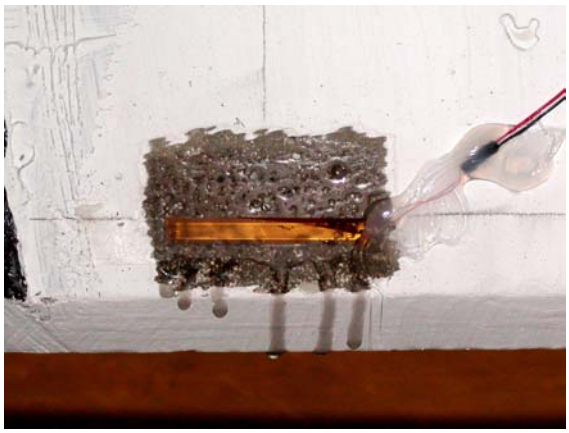

Figure 5.18. Concrete Strain Gauge Installed on the Bottom Bulb of the T-Beam.

Electrical resistance strain gauges were placed on the top of the slab and on the web of the pre-cast girder near the bottom (Fig. 5.18). The vertical distances between the top and bottom strain gauges were measured as well as the horizontal locations of the strain gauges along the length of the girder. Because the exact cross-section and the

effect of reinforcement in the beam and the flanges was not known precisely, both top and bottom readings were used to calculate the curvature of the beam. The T-beam was loaded with two point loads, which were four feet apart, to produce a region of constant moment at midspan (Fig. 5.16).

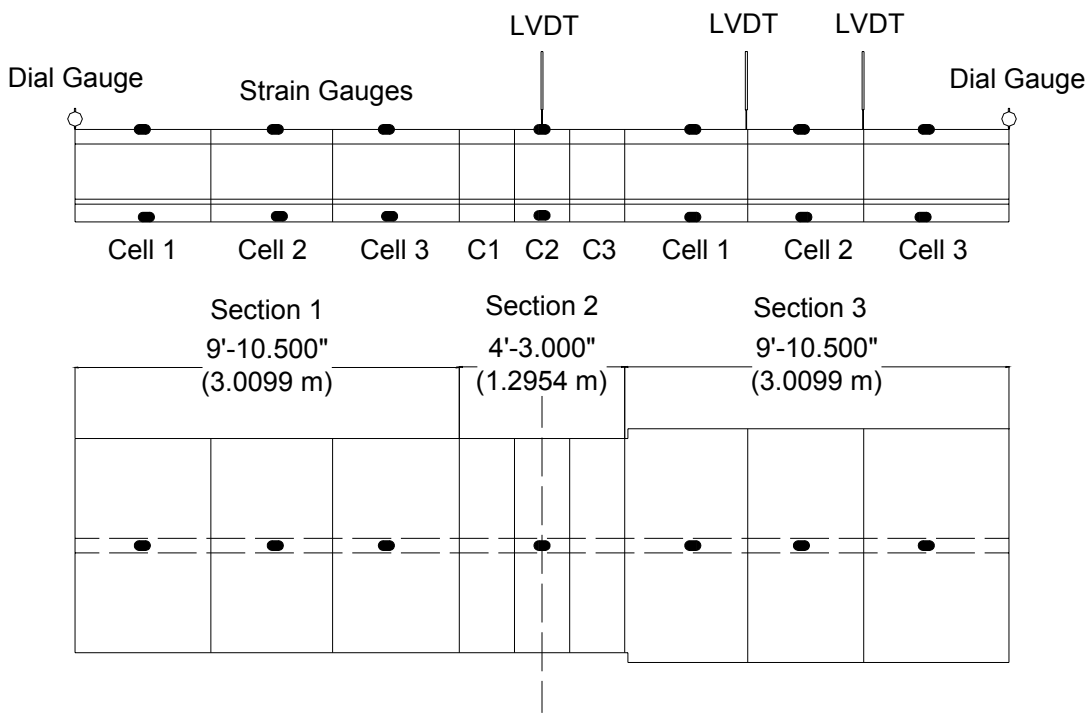

Figure 5.19. Beam III Schematic.

To limit the number of strain gauges required, the T-beam was divided into only three sections, each section having three cells (Fig. 5.19). In theory, the bending moment in the middle section of the T-beam should have a constant value; therefore, the curvature would be constant. Using this assumption, only one pair of strain gauges was placed at the top and bottom of the beam at midspan. The readings obtained from these strain gauges were used to represent the strains in all three cells in the middle section. As will

be shown in the Chapter 6, this assumption is not accurate because the beam deformation was not symmetric about midspan.

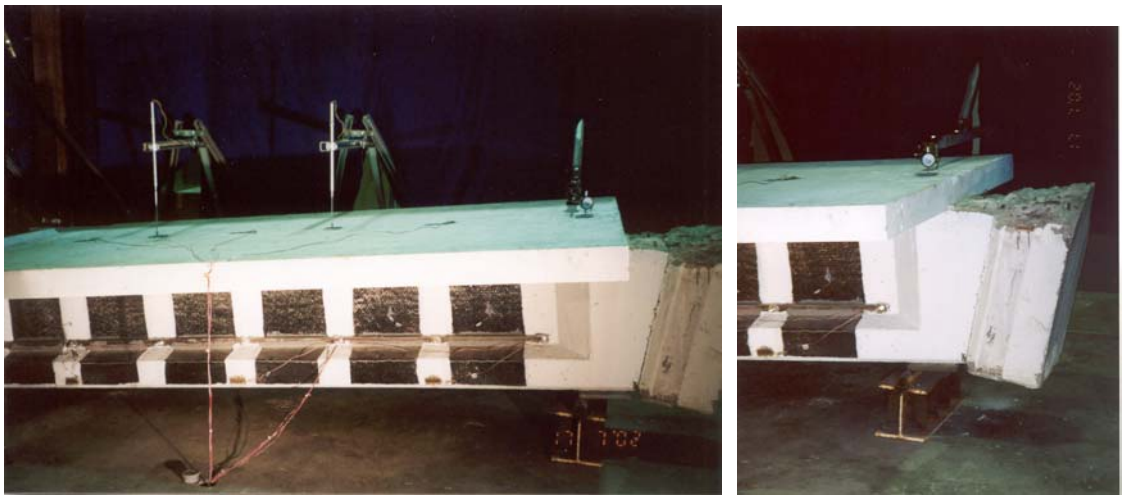

Figure 5.20. Linear Variable Displacement Transducers (LVDTs) on RHS of T-Beam (left); Dial Gauge at RHS support (right).
Note: Photographs show the Pre-stressed Concrete T-Beam after failure.

Linear variable displacement transducers (LVDTs) were placed on the right hand side of the T-beam (Fig. 5.20). Their readings were mirrored to the left side, assuming symmetric deformation, which is not accurate. The measurements from the LVDTs were taken as the "measured" deflections. Dial gauges were also located at each end support to determine if there was any vertical movement at the roller supports (Fig. 5.20). Because the supports moved slightly during testing, the dial gauge readings were used to correct the LVDT measurements to reflect the relative deflection of the beam assuming zero support displacement.

Figure 5.21. Pre-stressed Concrete T-Beam after Failure.

The T-beam was loaded under displacement control until failure due to flexure at mid-span (Fig. 5.21). The strain values were of relevance to this project up until initiation of concrete cracking. After cracking, the strain gauge readings no longer represent the average strain in a cell. This is because the gauge lengths of the strain gauges were very small compared to the lengths of the cells. To ensure that the strain gauges to represent the average strain in the cell, a longer gauge length or smaller cells are necessary. It is likely that micro-cracking will also affect the results, but since micro-cracking cannot be detected with the naked eye, the data was deemed viable up until there were visible cracks in the beam.

CHAPTER 6
RESULTS

6.1 Static Laboratory Verification

6.1.1 Beam I: Simply-Supported Steel Tube

Beam I could only be subjected to a specific loading pattern due to the testing apparatus configuration. The beam was subjected to a total load of 4000 lbs. (17.79 kN), resulting in two point loads of 2000 lbs. (8.896 kN) each.

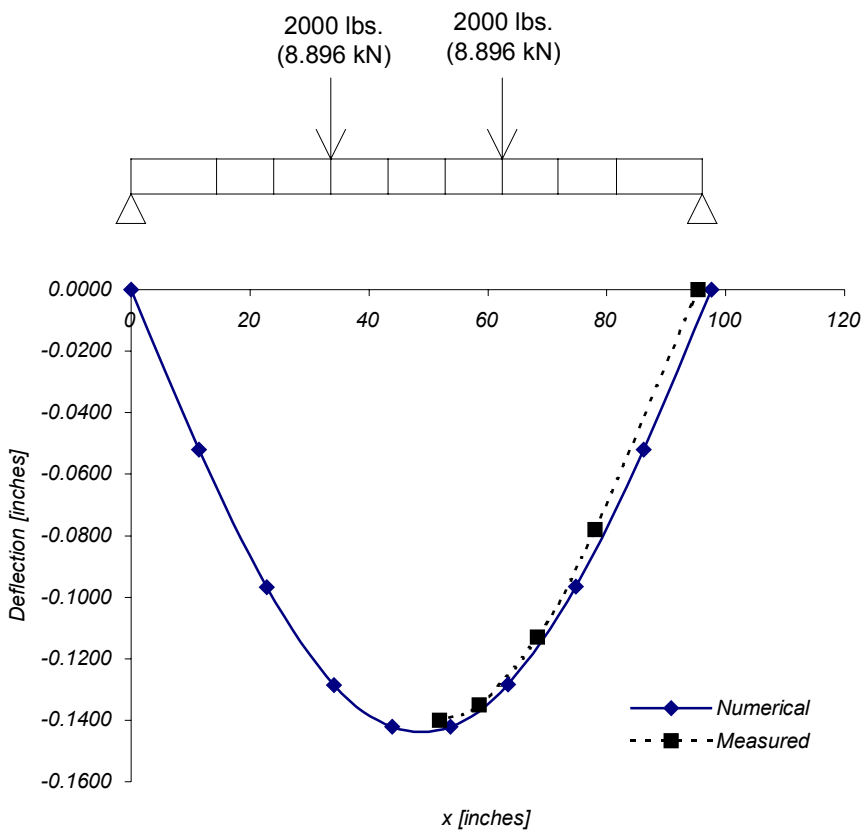

Figure 6.1. Beam I Test.

The "numerical" values obtained from the mathematical model produced a deformed shape very similar to the "measured" values given by the dial gauges placed along the right side of the beam (Fig. 6.1). Note that the dial gauge at the extreme right

in Figure 6.1 is not exactly at the support. This is because the dial gauges were placed beneath the beam and therefore, this particular dial gauge could not be at the support. Nevertheless, since the dial gauge was very close to the support and its value showed movement of the support, the value at this gauge was zeroed and the other dial gauge readings were adjusted by this value.

6.1.2 Beam II: Three-Span Steel Tube

6.1.2.1 "Ideal 24" Electrical Resistance Strain Gauge System

Beam II was subjected to seven different loading conditions and three support settlement conditions. Strains were obtained using the twenty-four electrical resistance strain gauge system described earlier. To evaluate the effect of using only twelve strain gauges, the results from the twenty-four gauges at "ideal" locations were compared with the deflections obtained from twelve gauges selected from the twenty-four as described in Chapter 5.

The various loading patterns and support settlement conditions were modeled in SAP2000 [CSI, 2000]. The beam was represented by frame elements (Fig. 6.2) with the exact tube dimensions input as a user-defined cross-section. The steel elastic modulus was input as 29,000 psi (199.9 MPa). For loading conditions, all four supports were modeled as pinned. For the settlement conditions, the vertical displacement values were equivalent to the support displacements that were induced on the real beam.

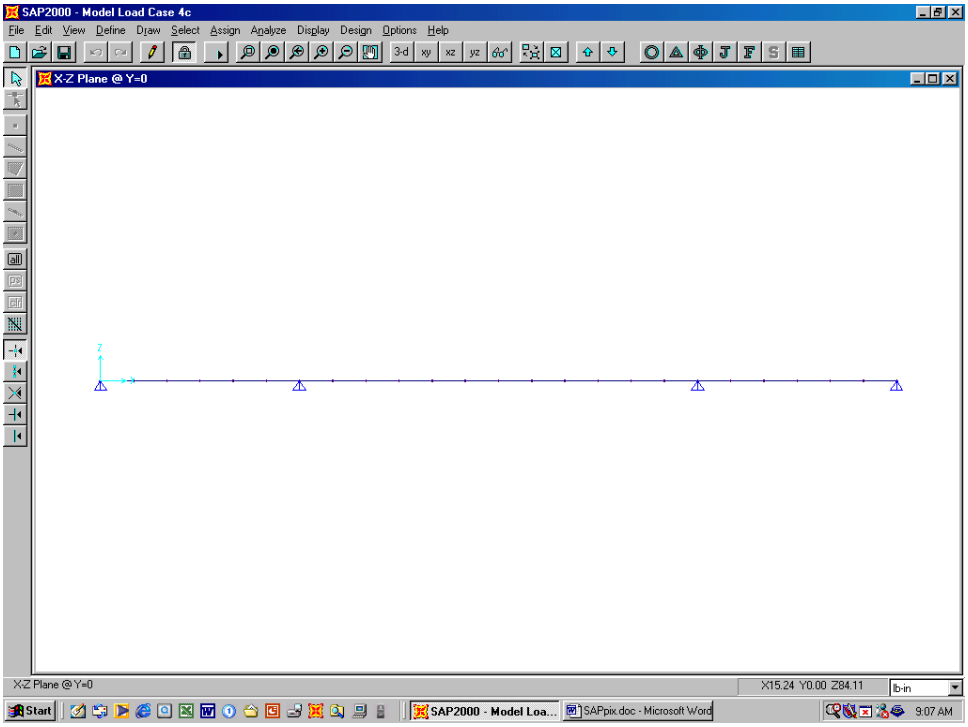

Figure 6.2. SAP2000 Model of Beam II.

The deformed shapes produced by the mathematical model were also compared with the SAP2000 deformed shapes. Table 6.1 provides a brief description of each of the loading conditions.

TABLE 6.1. Loading Conditions for "Ideal 24" and "Selected 12" Strain Gauge Systems.

Loading Patterns		
Test 1	(Fig. 6.3)	Midpoint of central span loaded with 14.2 lbs. (63.16 N)
Test 2	(Fig. A.1)*	Midpoint of central span loaded with 14.2 lbs. (63.16 N), two quarter points of central span loaded with 12.9 lbs. (57.38 N) and 11.6 lbs. (51.60 N), respectively
Test 3	(Fig. A.2)*	Midpoint of each of the outer spans loaded with 12.9 lbs. (57.38 N) and 11.6 lbs. (51.60 N), respectively
Test 4	(Fig. 6.4)	Midpoint of each of the outer spans loaded with 27.1 lbs. (120.5 N) and 11.6 lbs. (51.60 N), respectively
Test 5	(Fig. 6.5)	Midpoint of outer left-hand side span loaded with 27.1 lbs. (120.5 N) and midpoint of central span loaded with 11.6 lbs. (51.60 N)
Test 6	(Fig. 6.6)	Midpoint of span 1 (LHS span) loaded with 14.2 lbs (63.16 N); quarter points and midpoint of span 2 (central span) loaded with 12.9 lbs. (57.38 N), 14.2 lbs. (63.16 N), and 11.6 lbs. (51.60 N), respectively; midpoint of span 3 (RHS span) loaded with 14.2 lbs. (63.16 N)
Test 7	(Fig. A.3)*	Midpoints of outer spans loaded with 23.8 lbs. (105.9 N) and 25.2 lbs. (112.1 N), respectively
Settlement Patterns		
Test 8	(Fig. A.4)*	Support 3 lowered by 0.872 inches (2.215 cm)
Test 9	(Fig. 6.7)	Support 2 raised by 0.328 inches (0.8331 cm) and Support 3 lowered by 0.885 inches (2.248 cm)
Test 10	(Fig. 6.8)	Support 4 lowered by 0.63 inches (1.600 cm)

***See Appendix A for results of these loading conditions.**

Figure 6.3 shows the loading configuration and resulting deflected shape for Beam II Test 1. As for all output plots for the different loading conditions, this figure includes the deflections from the mathematical model using the "ideal 24" strain gauge system and the "selected 12" strain gauge system, along with the measured deflected shapes from the dial gauge readings, and the theoretical deflection obtained from the SAP2000 model. The output plot for loading conditions utilizes a constant (magnified) vertical scale, ranging from –0.25 to 0.15 inches, to allow direct comparison between plots. Also, it should be noted that the mathematical model assumed zero displacement at the end supports, while the "measured" shape and SAP2000 model assume zero displacements at all supports since they were modeled as pinned supports.

The "numerical" deformed shape using the "ideal 24" strain gauge system agrees exactly with both the measured and SAP2000 predicted deflected shapes (Fig. 6.3). The "selected 12" strain gauge system deviates slightly from the other plots, but a subsequent experiment with the "ideal 12" strain gauge layout produced improved results (Fig. 6.9). This could be due to the fact that the "selected 12" strain gauges are not located at the center of each cell as they were for the "ideal 12". Therefore, they are less likely to represent the average strain in each cell. Figures 6.4 to 6.6 show similar deflection plots for three other loading conditions. There were some discrepancies at the interior supports, which may have been the result of slight movement of the supports. In general, the agreement between numerical and measured deflected shapes is very good.

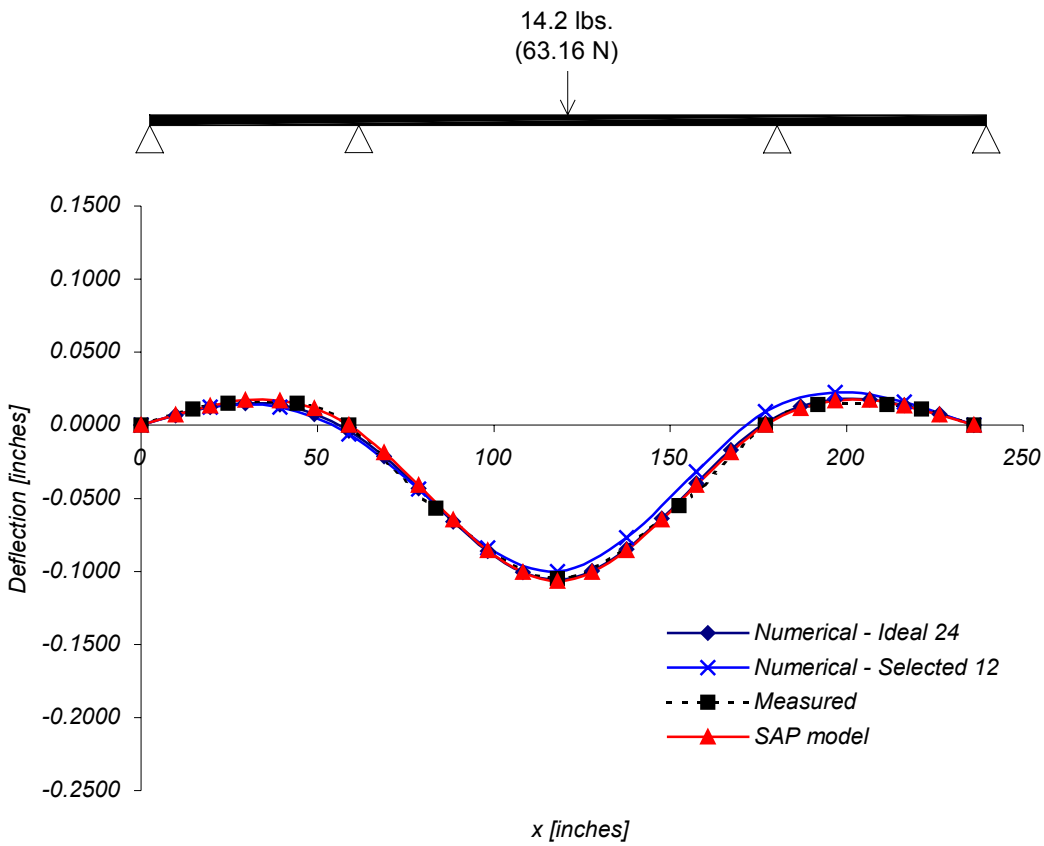

Figure 6.3. Beam II Test 1, Center Span Load.

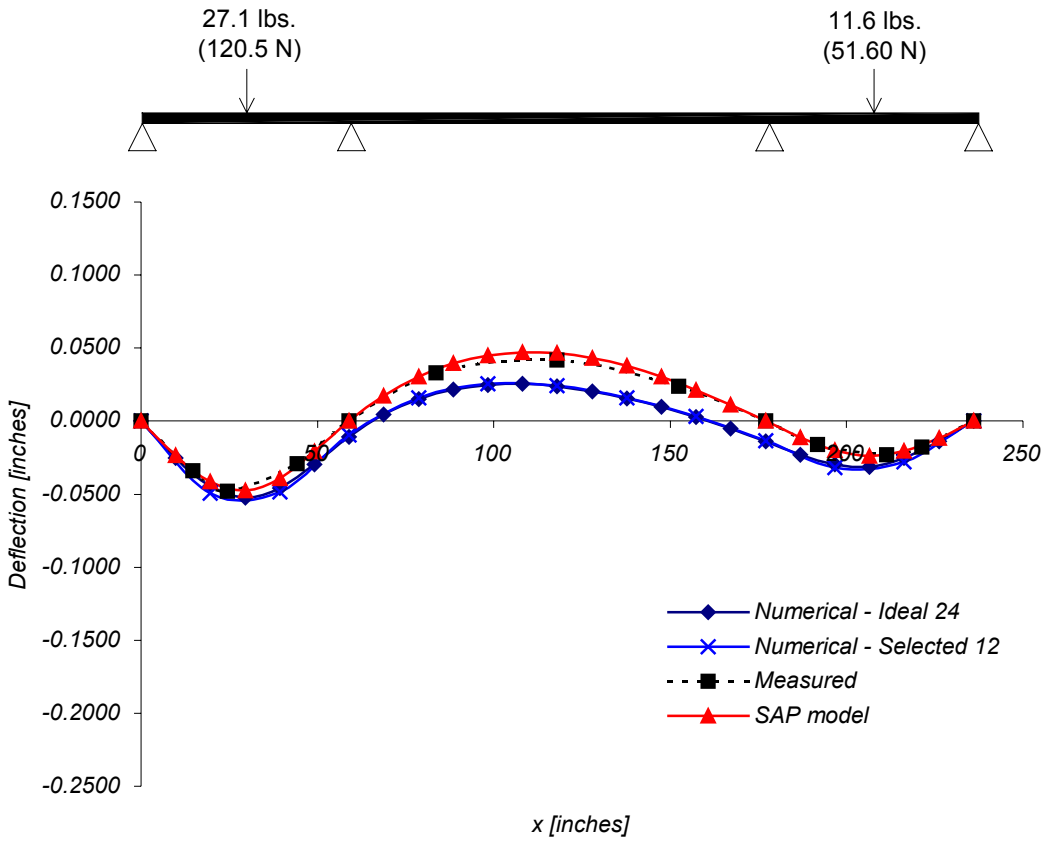

Figure 6.4. Beam II Test 4, End Span Loads.

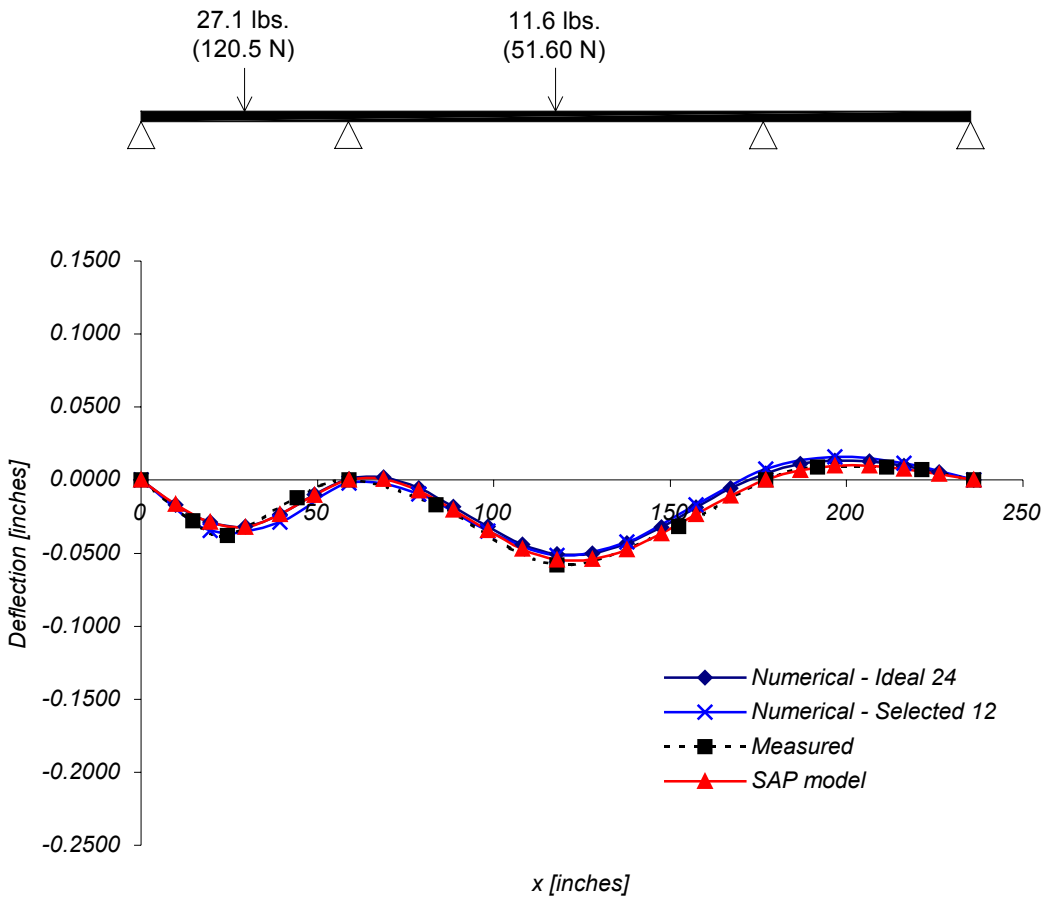

Figure 6.5. Beam II Test 5, Adjacent Span Loading.

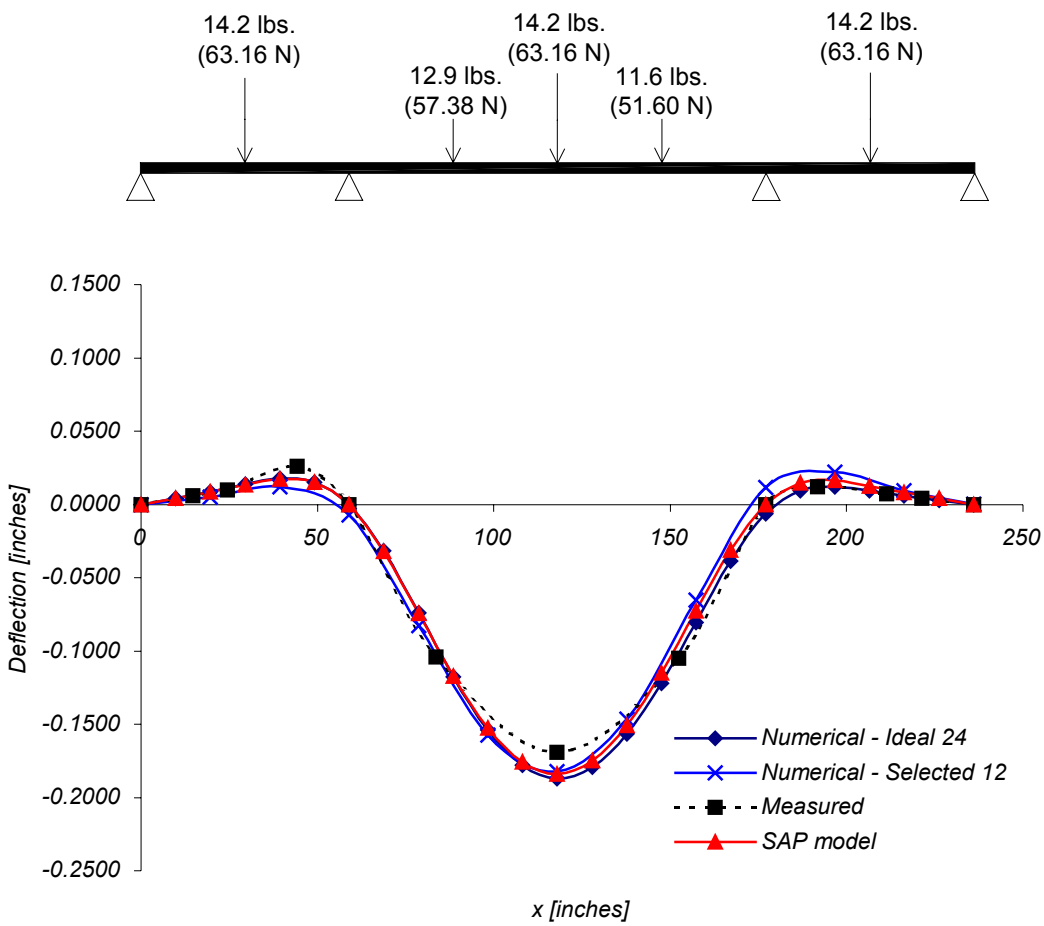

Figure 6.6. Beam II Test 6, Multiple Loading.

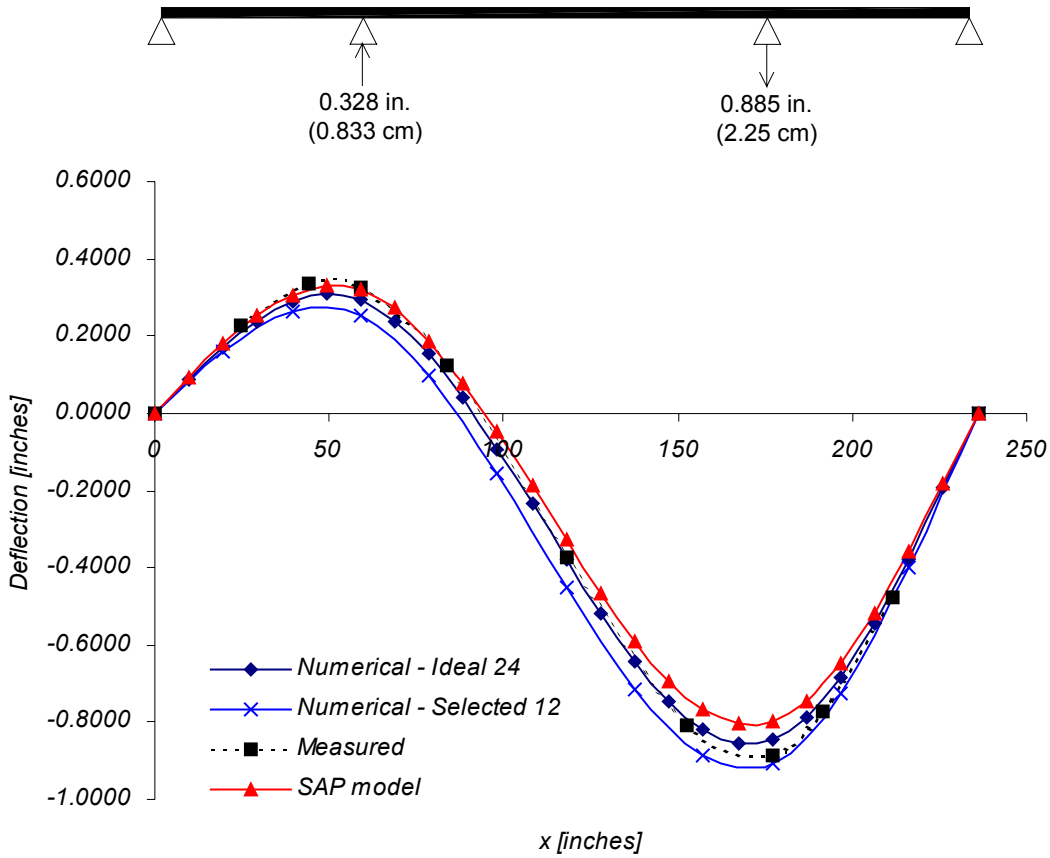

Figure 6.7. Beam II Test 9, Support Movement.

From the plots, one can conclude that the mathematical model produced deflected shapes with considerable accuracy. The percent error was below 15% in the majority of the loading cases (refer to Table 6.4). Most of the shapes produced using the mathematical model agree well with the measured deformation and the SAP2000 model predictions. The largest deviations between the "numerical" deformed shape and the "measured" deformed shape were observed in the tests where only the midpoints of the outer spans were loaded, as in Test 4 (Fig. 6.4). A likely source of error is movement of the supports as the beam is loaded. Both interior and exterior support deflections were

assumed to be zero in both the "measured" deflected shape and the SAP2000 model when in reality, the supports may have moved. This problem was corrected before the dynamic tests were performed on Beam II. The concrete blocks below each support were shimmed and then attached to the laboratory floor using silicone.

Figure 6.7 shows a support movement involving raising support 2 and lowering support 3. The results show good agreement between the "numerical," "measured," and SAP2000 deformed shapes.

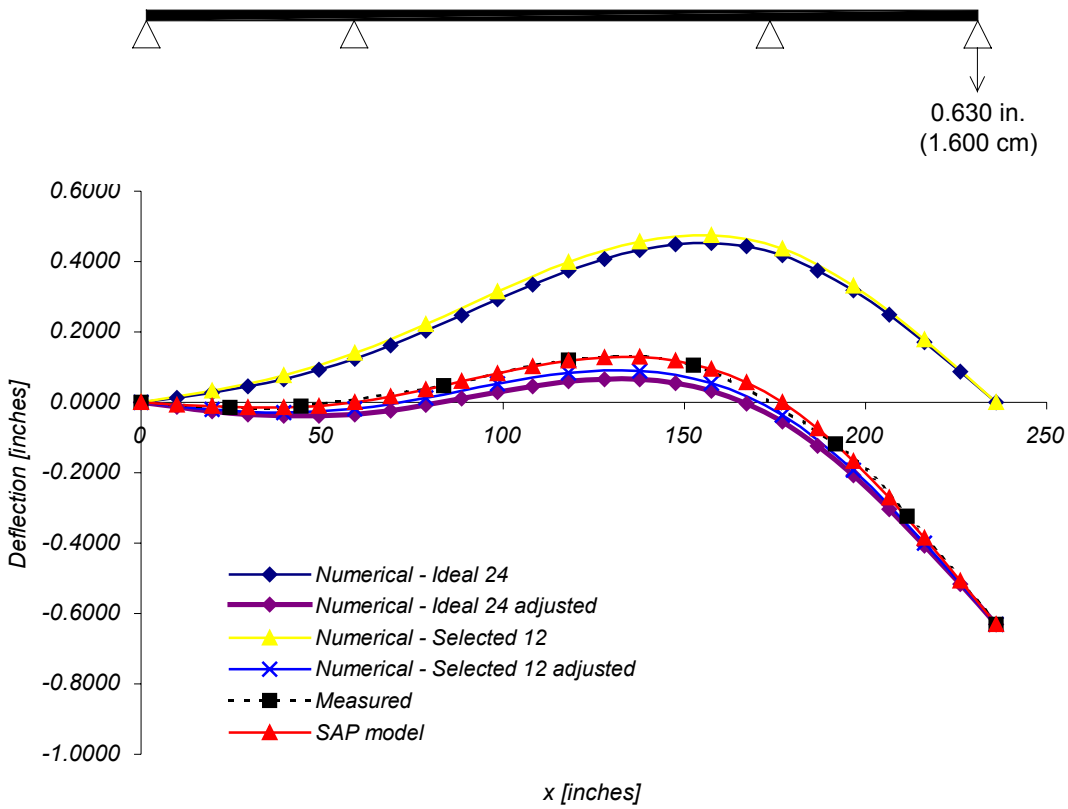

Figure 6.8. Beam II Test 10, End Support Settlement.

Figure 6.8 shows the results for Test 10, the case of settlement of an end support. The mathematical model assumes that the end supports do not move. The mathematical

model produces the correct deformed shape for the beam except for the rigid body rotation caused by the support settlement ("Ideal 24" and "Selected 12" plots in Fig. 6.8). To compare these deformed shapes with the measured deflection, the deflected shapes produced by the mathematical model were adjusted by moving the right hand support to its actual settled location. Then, each value was proportionally adjusted ("Adjusted" plots in Fig. 6.8). Again, the agreement between "numerical," "measured," and SAP2000 deformed shapes is very good.

6.1.2.1.1 "Ideal 24" Strain Gauge System versus "Selected 12" Strain Gauge System

Optimizing the number of strain gauges necessary to create accurate deformed shapes is important in minimizing costs for the Kealakaha Stream Bridge project. Twelve strain gauges were selected from the twenty-four strain gauge system in order to investigate the use of a minimum number of strain gauges. Beam II was reconfigured into four sections with 12 strain gauges as described in Section 5.4 and Figure 5.10. The strain gauges were not located at the center of each cell because they were selected from the original twenty-four strain gauge system. However, the deformed shapes produced from the "selected 12" gauges were in good agreement with the shapes produced by the original "ideal 24" as shown in Figures 6.3 to 6.8. The percent error for the "ideal 24" versus "selected 12" were within a few percent of each other (Refer to Table 6.4). Based on this result, twelve more strain gauges were installed on Beam II in the ideal locations. The next section discusses the results of deflection tests using this "ideal 12" strain gauge system.

6.1.2.2 "Ideal 12" Electrical Resistance Strain Gauge System

Two static loading tests were performed using the "ideal 12" strain gauge system. Table 6.2 lists the loading conditions.

TABLE 6.2. Loading Conditions for "Ideal 12" Strain Gauge System.

Loading Patterns		
Test 11	(Fig. 6.9)	Midpoint of central span loaded with 18.71 lbs. (83.22 N)
Test 12	(Fig. 6.10)	18.71 lbs. (83.22 N) at 78.67in. (199.8 cm), 9.6325 lbs. (42.85 N) at midpoint of central span, and 14.69 lbs. (65.34 N) at 157.3 in. (399.6 cm)

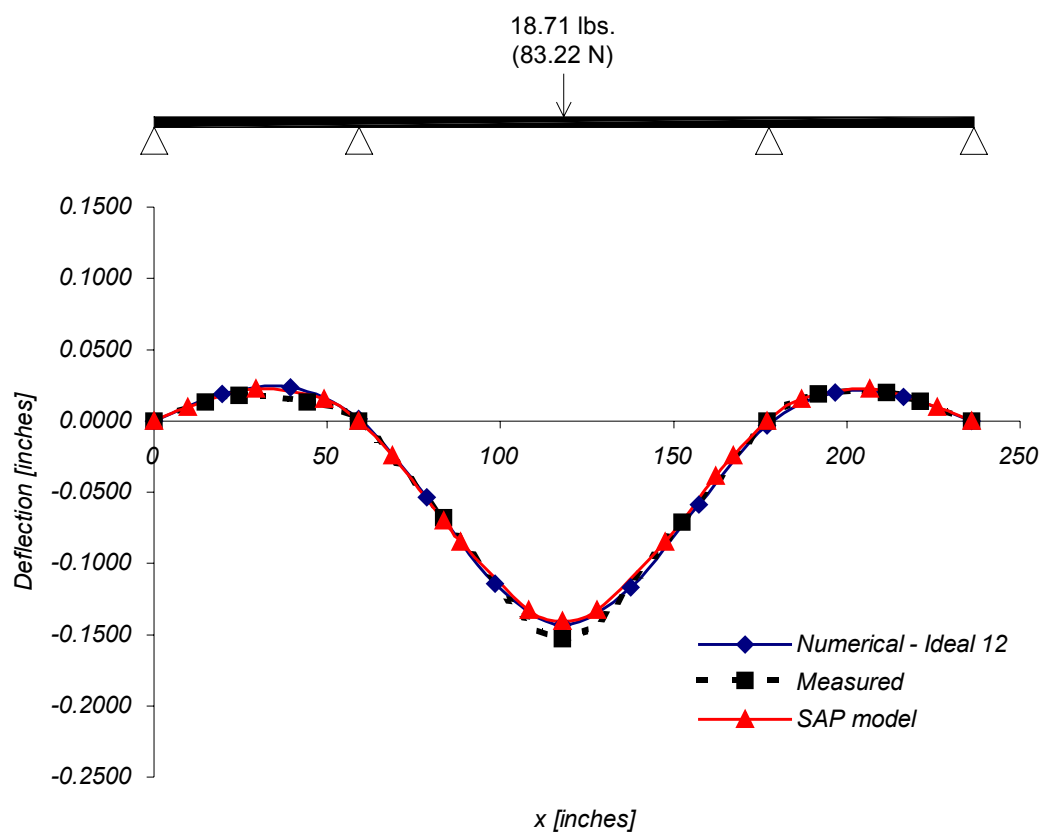

Figure 6.9. Beam II Test 11, Center Span Loading.

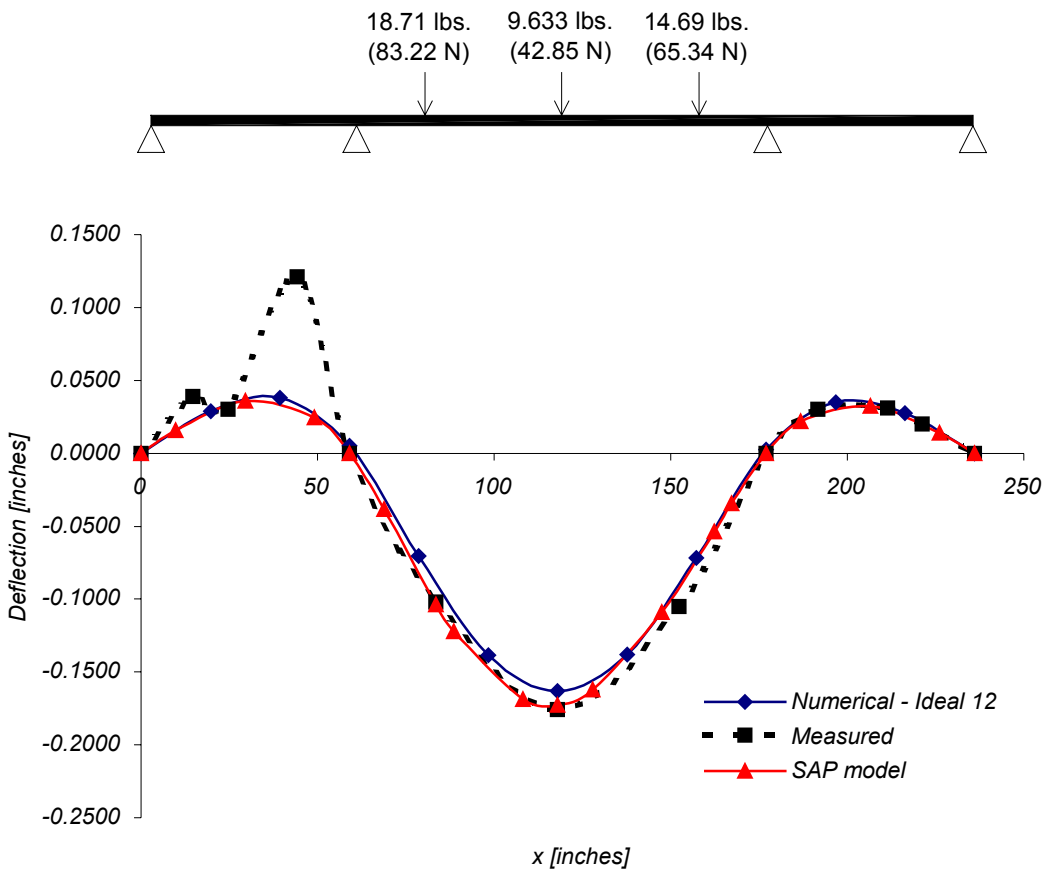

Figure 6.10. Beam II Test 12, Multiple Center Span Loadings.

The results of the tests performed using the "ideal 12" strain gauge system are very good, the percent error was less than 10%. The "numerical," "measured," and SAP deflected shapes correspond almost exactly, especially in Test 11 (Fig. 6.9). In Test 12, the "measured" deflected shape traces the SAP shape except for a few deviations due to apparent reading errors. The "numerical" shape also agrees well with the "measured" and SAP deflected shapes.

In the development of the mathematical model, Vurpillot *et al*. [1998] assumed that the loads had to be applied at the section boundaries. In Test 12 (Fig. 6.10) and

many of the "selected 12" strain gauge system tests, the loads were not located at the boundaries of the sections, however, the mathematical model still provided accurate deflections for the beam. It was therefore concluded that this system could be applied to more general loading conditions, including moving loads as experienced by a bridge during ambient traffic flow.

6.1.2.3 "Ideal 24" versus "Ideal 12" Electrical Resistance Strain Gauge Systems

Beam II was subjected to four different loading conditions and four different support settlement conditions. Strains obtained using both the "ideal 24" and the "ideal 12" strain gauge systems were used to determine the "numerical" deformed shapes. This allowed for direct comparison between the two ideal systems. The various loading patterns and support settlement conditions were also modeled in SAP2000 as they were in the previous tests [CSI, 2000]. Table 6.3 lists a description of each test performed. They include some of the same loading patterns used in previous tests and also some settlement conditions.

TABLE 6.3. Loading Conditions for "Ideal 24" and "Ideal 12" Strain Gauge Systems

Loading Patterns		
Test 13	(Fig. A.5)*	Midpoint of each of the outer spans loaded with 14.92 lbs. (66.38 N) and 14.23 lbs. (63.31 N), respectively
Test 14	(Fig. 6.11)	Midpoint of left-hand side span loaded with 14.92 lbs. (66.38 N) and midpoint of central span loaded with 14.23 lbs. (63.31 N)
Test 15	(Fig. 6.12)	Left-hand side span loaded with 14.92 lbs. (66.38 N) at 39.335 inches (99.9 cm) and right-hand side span loaded with 14.23 lbs. (63.31 N) at 196.665 inches (499.5 cm)
Test 16	(Fig. 6.13)	Midpoint of central span loaded with 14.23 lbs. (63.31 N)
Settlement Patterns		
Test 17	(Fig. A.6)*	Support 2 lowered by 0.6226 inches (1.581 cm)
Test 18	(Fig. A.7)*	Support 2 lowered by 0.1862 inches (0.4729 cm)
Test 19	(Fig. 6.14)	Support 3 raised by 3 revolutions, approximately 0.188 inches (0.4775 cm). (Note: the LVDT at Support 3 was not working during this test. Therefore, the "measured" deflection could not be recorded.)
Test 20	(Fig. 6.15)	Support 3 lowered by 0.188 inches (0.4775 cm)

***See Appendix A for results of these loading conditions.**

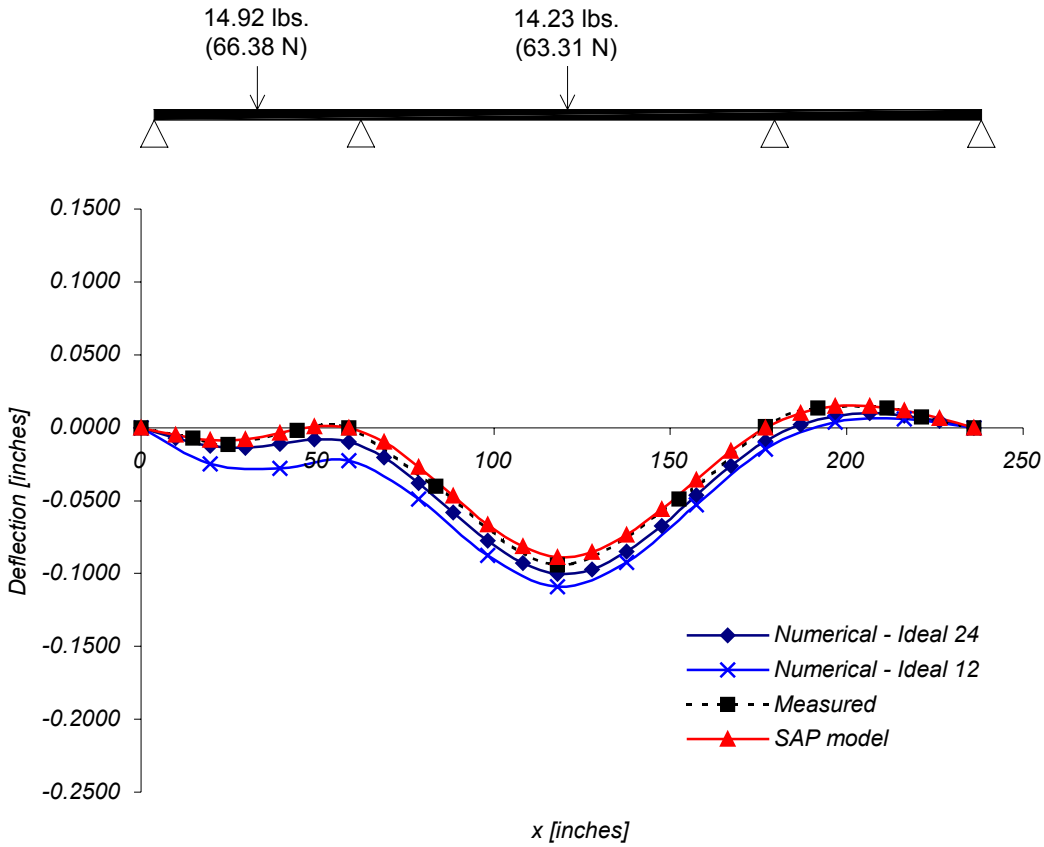

Figure 6.11. Beam II Test 14, Adjacent Span Loading.

All of the plots of the various loading conditions are presented in the same manner as discussed in Section 6.1.2.1. Figure 6.11 is the resulting plot of Beam II loaded at the midpoint of the left-hand side span and the midpoint of the center span. Note that the numerically produced deflected shape for the "ideal 12" deviates quite a bit, especially where the load is located on the left-hand side. This is because the load was placed directly on top of strain gauge 2B, which was one of the strain gauges in the "ideal 12" strain gauge layout (Fig. 5.11). The concentrated load distorted the strain gauge reading resulting in an inaccurate deflected shape. This is also shown in Figure A.5, where the loads were located directly on two strain gauges in the "ideal 12" strain gauge layout. This will not be a problem for the final bridge project because the strain gauges

will be embedded in the concrete or mounted on the surface of the concrete within the box girder, therefore, wheel loads will not be directly applied to the gauges.

Because of the discrepancy noted in Test 3 (Fig. A.2), another end span load verification test was performed on Beam II in Test 15, as shown in Figure 6.12. To avoid placing the load directly on a strain gauge, the loads were moved closer to the interior supports. LVDT's were used to measure any vertical movement at the interior supports, which had now been shimmed and siliconed to the laboratory floor. The original percent error of 38 - 51% was reduced to 17-25%. The mathematical model therefore works reasonably accurately for end span loading.

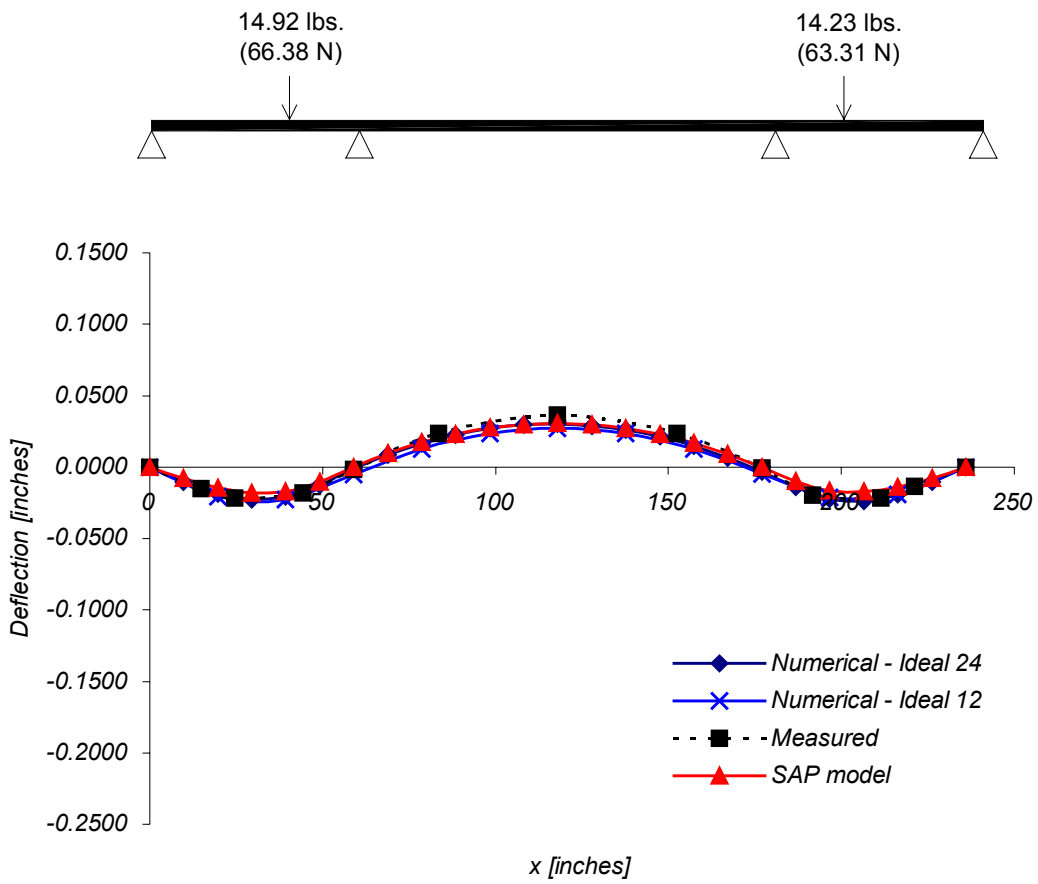

Figure 6.12. Beam II Test 15, End Span Loads.

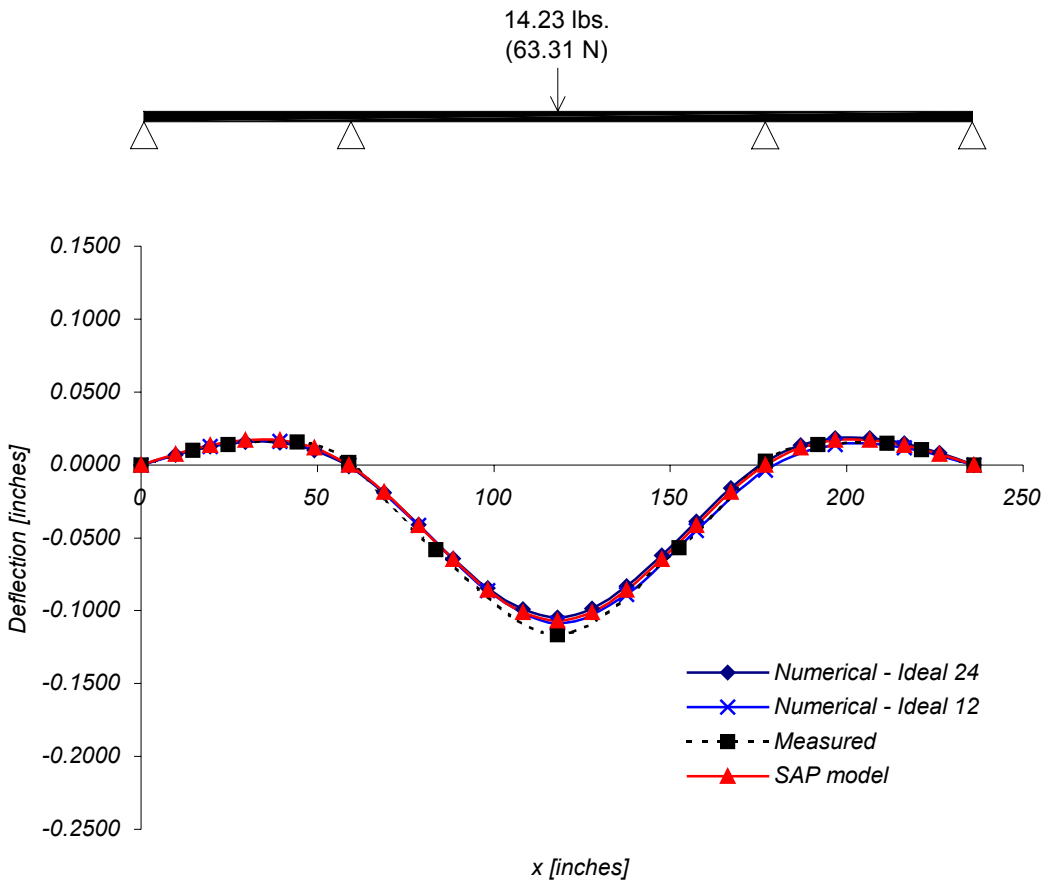

Figure 6.13. Beam II Test 16, Center Span Load.

For Test 16 shown in Figure 6.13, both "numerical" systems, the "ideal 24" and the "ideal 12", the "measured", and the theoretical deflected shapes also correspond excellently for loading in the center span. The percent error was 10% or less for both strain gauge systems.

Several settlement tests were performed on Beam II. It was shown in Test 19 (Fig. 6.14) that the LVDT at Support 3 was not working properly; it was doubling the value of the support movement. Therefore, the LVDT was replaced and another test considering the movement of Support 3 was performed (Fig. 6.15). Test 19 could not be

modeled in SAP2000 because the "measured" value of the vertical deflection of Support 3 could not be obtained.

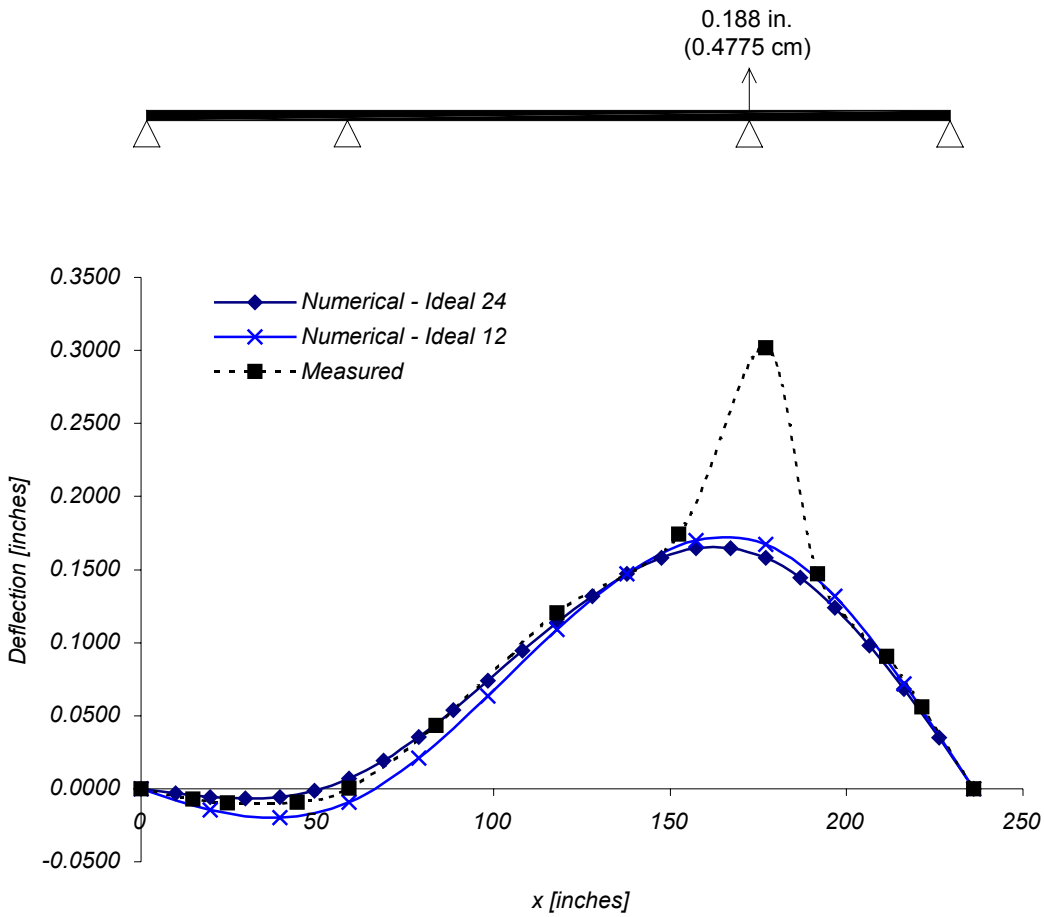

Figure 6.14. Beam II Test 19, Support Movement.

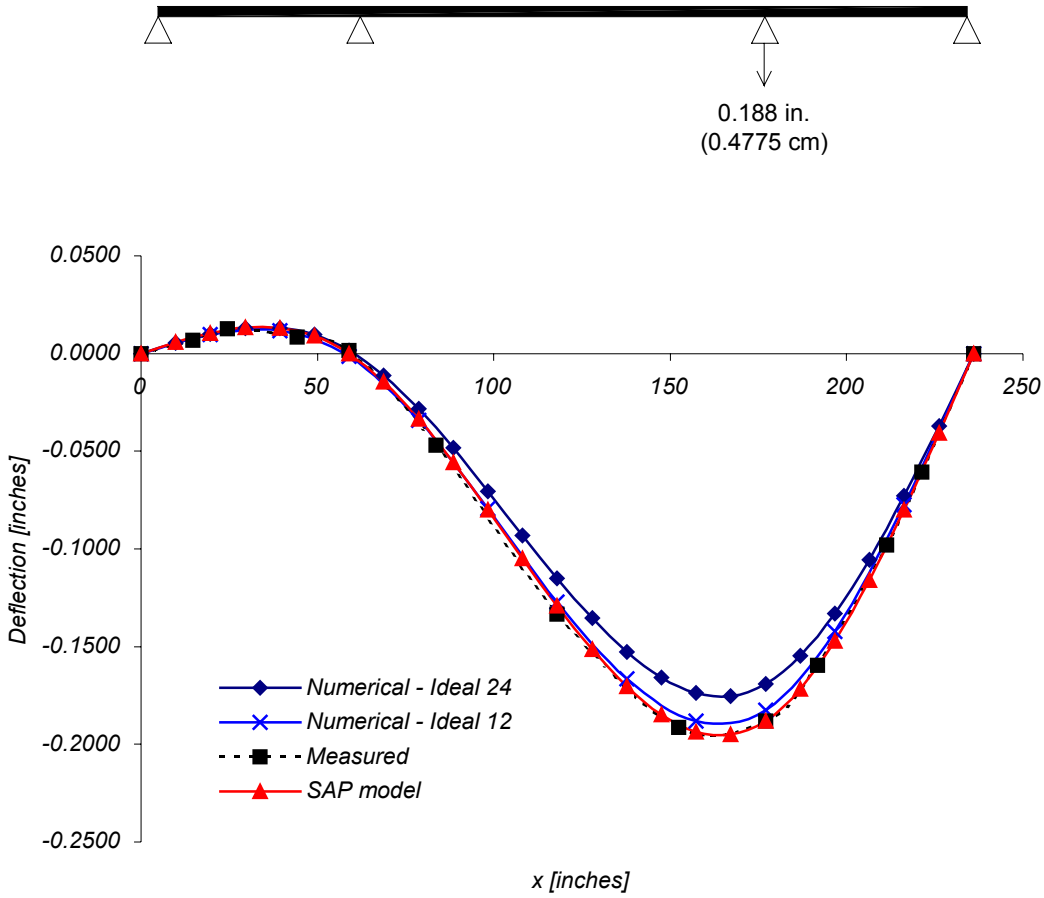

Figure 6.15. Beam II Test 20, Support Movement.

The "ideal 12," "measured," and theoretical deflected shapes correspond well. The "ideal 24" deviates at the support location, but not significantly.

The tests using both the "ideal 24" and the "ideal 12" strain gauge systems verified that the mathematical model works equally well for either strain gauge system.

6.1.3 SAP2000 Model Confirmation

The various loading patterns and support settlement conditions were modeled in SAP2000. The SAP2000 model was helpful in pointing out errors in dial gauge readings. Figure 6.10 shows two dial gauge readings that deviate from the SAP2000 deflection,

indicating that errors were made when taking these readings. The SAP2000 model also helped point out problem areas in the test set-up, such as the movement of supports. The SAP2000 model also confirmed that the results from the tests were reasonable.

6.1.4 Beam II: Discussion of Error

For the percent error calculations, the "measured" values, or the vertical deflections obtained from the dial gauges or the LVDTs, were used as the theoretical values and the "numerical" values, or the values obtained from the mathematical model, were used as the experimental values.

$$PercentError = \frac{Theoretical - Experimental}{Theoretical} * 100 \tag{6.1}$$

The percent error for the vertical displacement at the midpoint of the center span was calculated for each of the loading conditions. The results are found in Table 6.4. The percent error remained below 15% for the majority of the static loading tests. For the initial end span load tests, the percent error was as high as 51%.

Some possible sources of error include the movement of the interior supports, the placement of loads directly on strain gauges, and strain gauge, dial gauge, and LVDT precision. The end span load test error was reduced by more that 50% after the supports were secured with silicone and the loads were not placed directly on the strain gauges.

TABLE 6.4. Percent Error in Midspan Measurements for Various Loading Conditions.

Test #	Description of Loading Condition	Measured [in]	Ideal 24 [in]	% Error	Selected 12 [in]	% Error	Ideal 12 [in]	% Error
1	Center Span Load	-0.1050	-0.1059	-0.9	-0.1000	4.7		
2	Multiple Center Span Loadings	-0.2260	-0.2104	6.9	-0.2122	6.1		
3	End Span Loads *	0.0380	0.0522	-37.4	0.0542	-42.6		
4	End Span Loads *	0.0420	0.0236	43.7	0.0242	42.5		
5	Adjacent Span Loading	-0.0580	-0.0508	12.4	-0.0516	11.1		
6	Multiple Loading	-0.1690	-0.1872	-10.8	-0.1825	-8.0		
7	End Span Loads *	0.0470	0.0692	-47.2	0.0710	-51.0		
11	Center Span Load	-0.1530					-0.1433	6.3
12	Multiple Center Span Loadings	-0.1760					-0.1630	7.4
13	End Span Loads *	0.0363	0.0338	6.9			0.0257	29.3
14	Adjacent Span Loading	-0.0942	-0.1003	-6.4			-0.1089	-15.6
15	End Span Loads *	0.0363	0.0300	17.3			0.0274	24.6
16	Center Span Load	-0.1164	-0.1046	10.1			-0.1084	6.8

6.1.5 Beam III: Simply-Supported Pre-stressed Concrete T-Beam

The data from the testing of the old Ala Moana Shopping Mall Parking Structure T-beam were useful until the beam cracked, which was at a displacement of about 0.43 in (1.092 cm), because the lengths of the strain gauges were not sufficient to provide the average strain in each cell. Depending on the strain gauge length, the data may also not be useful after micro-cracking occurs, but this is not detectable visually. Therefore, some error in the "numerical" deflected shapes can be attributed to micro-cracking. When the beam cracks, the strain gauges cannot provide the mean strain in each cell if the gauge lengths are not the full length of the cell.

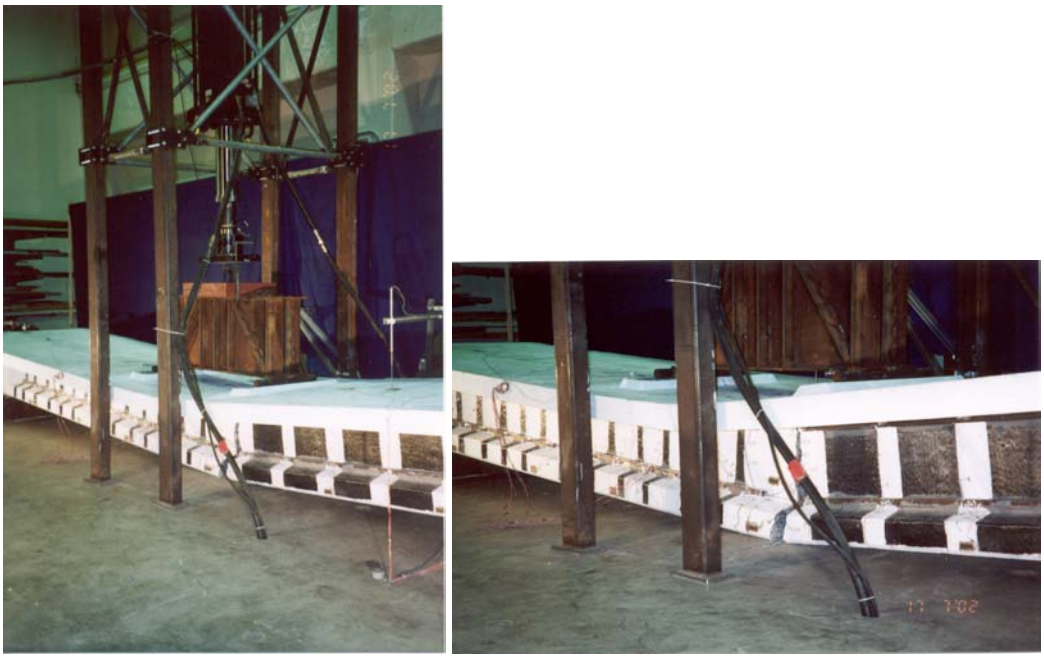

Figure 6.16. Pre-stressed Concrete T-Beam Failure in Bending.

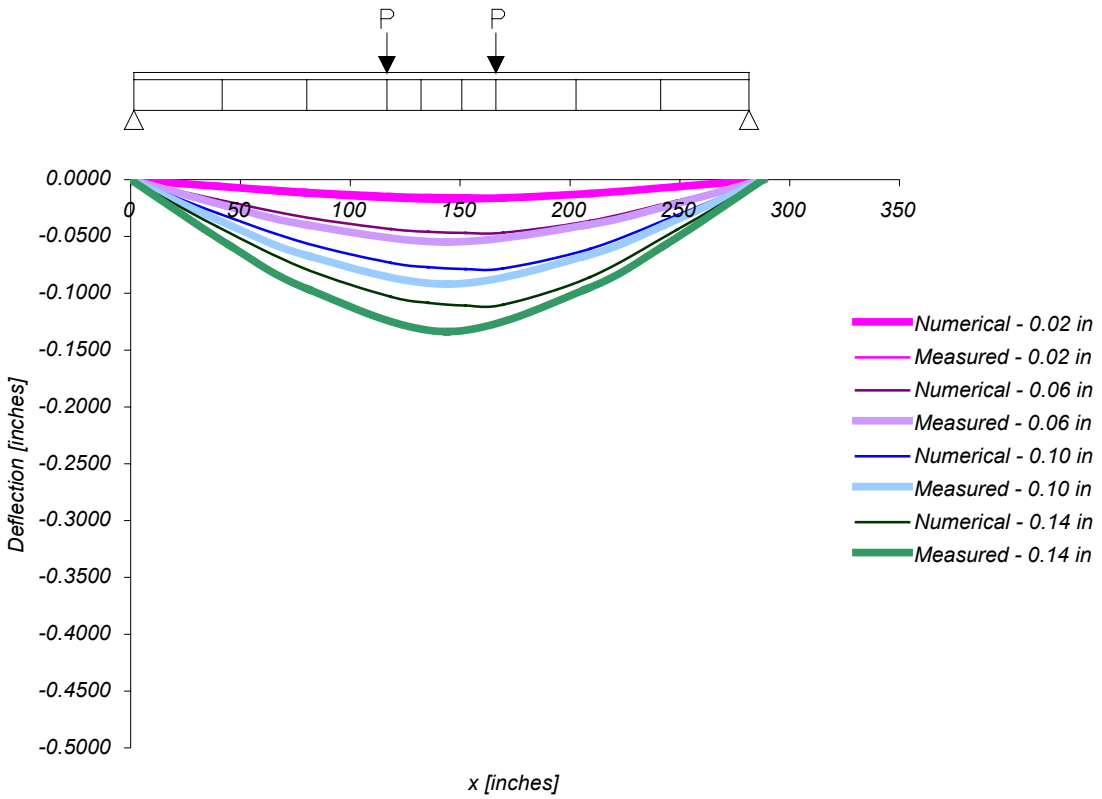

Figure 6.17. Plot of Pre-stressed Concrete T-Beam for Small Deflections.

Figure 6.17 shows the "numerical" deflected shapes produced by the mathematical model and the "measured" deflected shapes produced by the LVDT-dial gauge system for the first four displacement steps. The "numerical" solution provides reasonably accurate deflections for small loads, but starts to deviate from the measured results as the load increases, which could be due to micro-cracking. This is particularly evident around the midspan of the beam, where three cells used the same strain value obtained from the set of strain gauges located at the middle cell. The percent error for each displacement step is around 22 to 26 % (Refer to Table 6.4). Ideally, one should not assume that the strain is the same in each of the midspan cells even though in theory, the moment should be constant in this region (i.e. the strain should be constant).

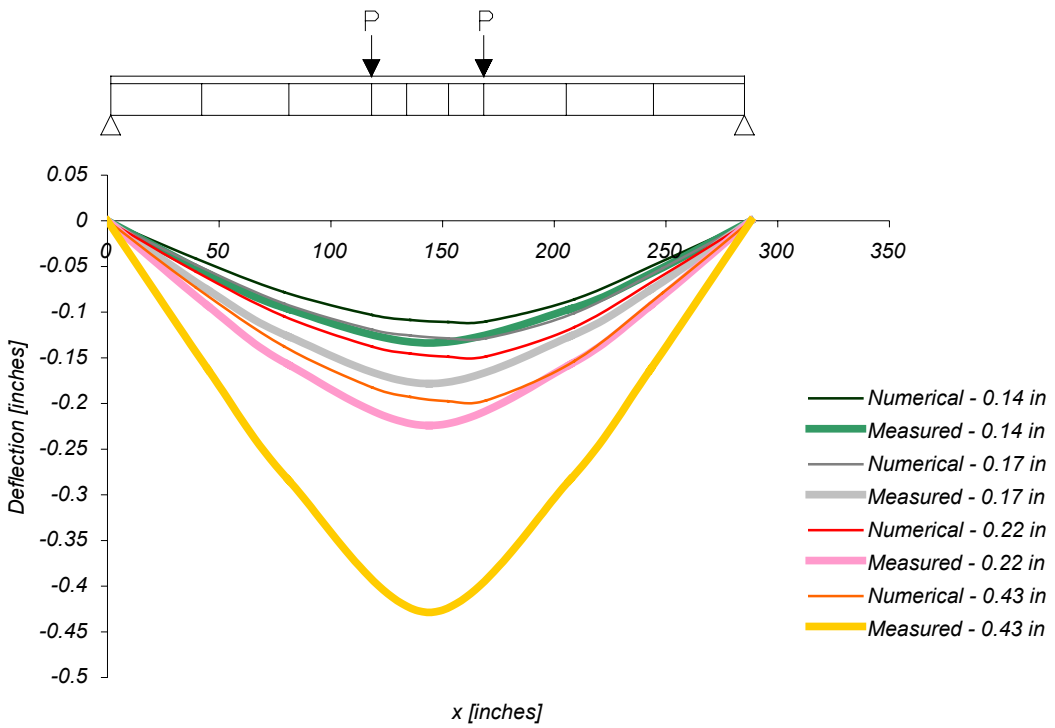

Figure 6.18. Plot of Pre-stressed Concrete T-Beam After Cracking.

Figure 6.18 shows the plots of "numerical" and "measured" deflected shapes after the beam started to crack. For Figure 6.18, the error increases about 10% from the first displacement step (0.14 in), which has 25.2 % error, to the second displacement step (0.17 in), which has 34.9 % error (Refer to Table 6.4). From the plots, one can conclude that the mathematical model does not hold after the beam cracks because the strain values measured by the 2 in. long gauges no longer represent the average strain for each cell.

TABLE 6.5. Percent Error in Midspan Displacements for Beam III.

Displacement Step [in]	Measured [in]	Numerical [in]	% Error
0.02	-0.019	-0.014	25.6
0.06	-0.055	-0.042	23.1
0.1	-0.092	-0.071	22.7
0.14	-0.134	-0.100	25.2
0.17	-0.178	-0.116	34.9
0.22	-0.224	-0.134	40.2
0.43	-0.429	-0.177	58.8

6.2 Dynamic Laboratory Verification

6.2.1 Beam II: Three-Span Steel Tube

6.2.1.1 "Ideal 12" Strain Gauge System

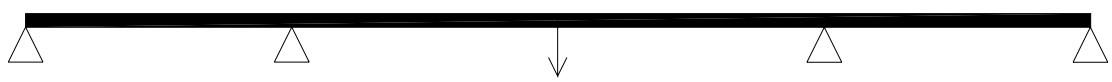

Figure 6.19. Beam II Dynamic Test Load Condition.

Dynamic tests were performed on Beam II using the "ideal 12" electrical strain gauge system. The mid-point of the center span was pulled down by weights attached to the beam by a piece of string (Fig. 6.19). The string was then cut and the beam was allowed to vibrate freely. After a few cycles, the free vibration approximated the fundamental mode shape for the beam. SAP2000 estimated the theoretical natural period of the first mode of vibration at 0.0684 seconds. Several dynamic tests were run on Beam II using this procedure. The strain gauges were scanned sequentially by a high-speed data acquisition system at a frequency of 8200 Hz. Each gauge was therefore scanned approximately 680 times/second. Assuming a natural period of 0.0684 seconds, there were approximately 48 readings/cycle. It should be noted that the data-acquisition

system used could not read the whole set of twelve strain gauges simultaneously. Therefore, there was a fraction-of-a-second lag between each reading. This will not be an issue when the fiber optic strain gauge data acquisition units are used.

When the first mode of vibration is induced, the maximum strains occur in gauges 6B and 7B, which are near the middle of the central span. The strain measured from Strain Gauge 6B is plotted versus time in Fig. 6.20. After a few initial cycles, the free vibration becomes repetitive. One representative free vibration cycle of data was processed to produce 48 separate deflected shapes as shown in Figure 6.21. From the representative cycle of data, it was calculated that the natural period from the dynamic test data was 0.07 seconds.

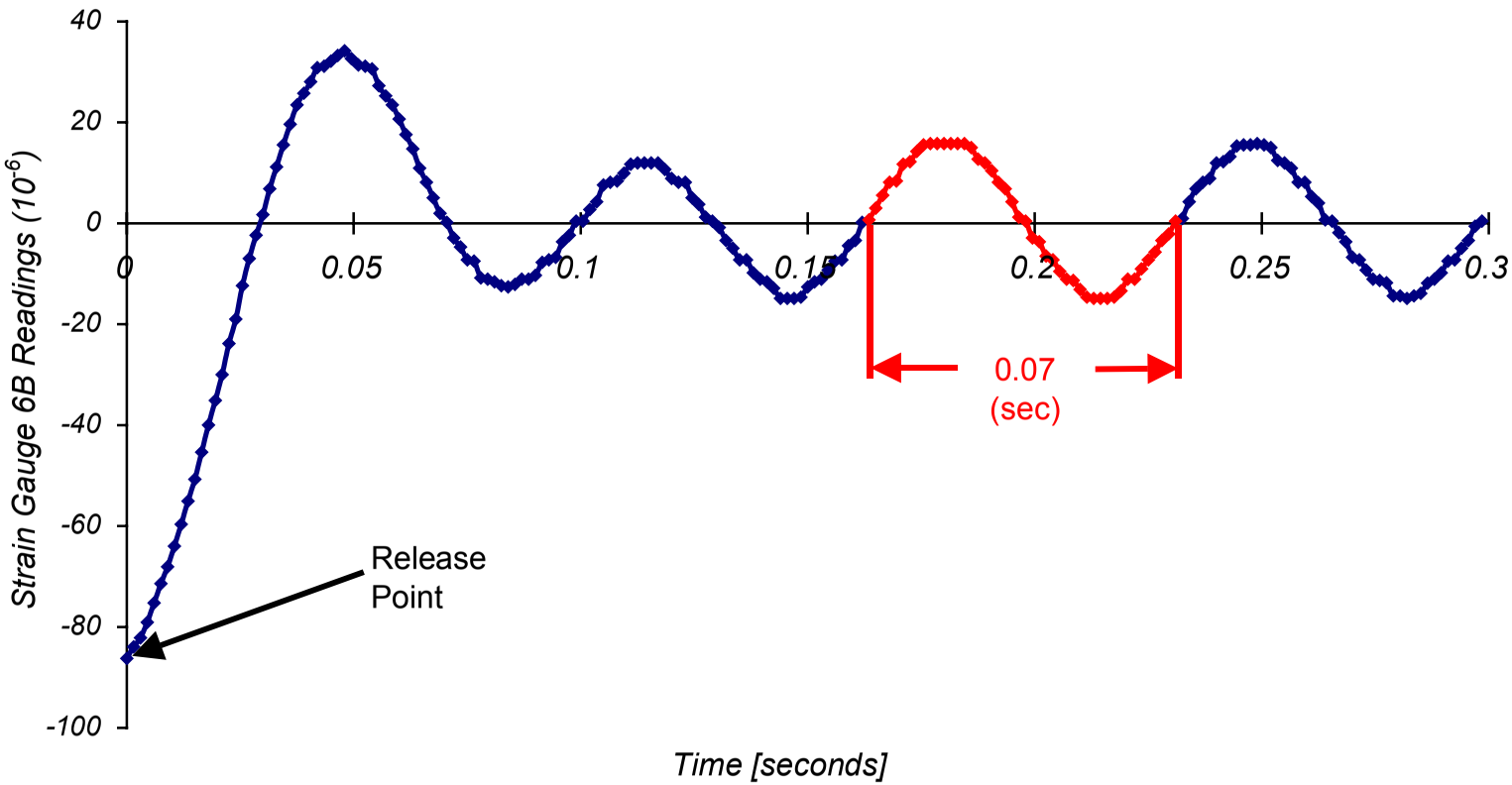

Figure 6.20. Vibration Trace of Strains in Strain Gauge 6B.

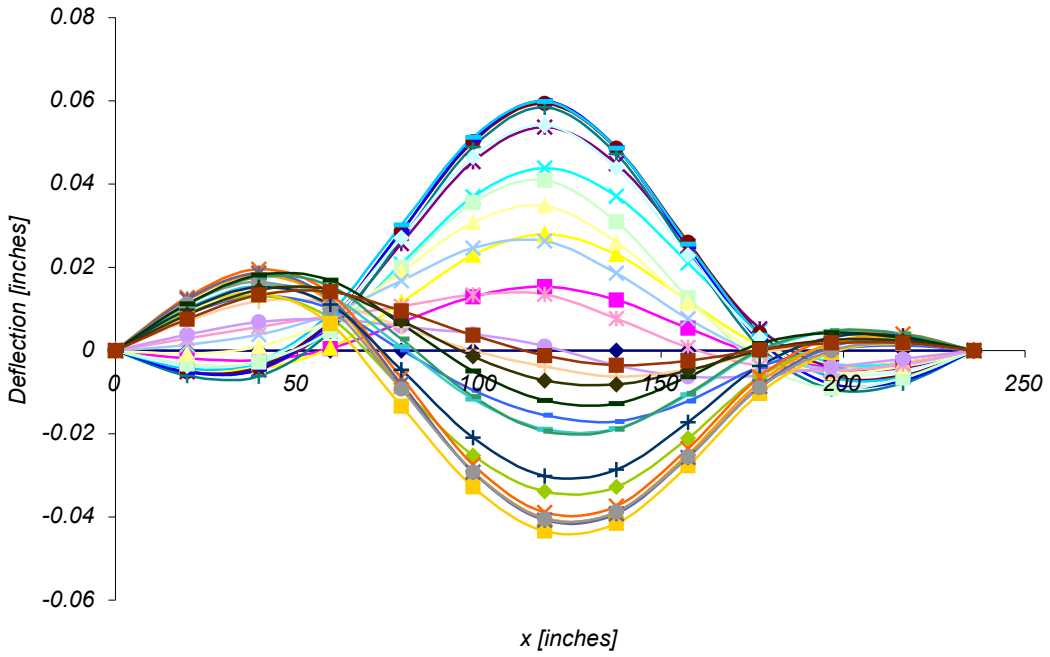

Figure 6.21. Beam II Test 4L-D.

After the first test, the data showed that the supports were moving and the movement was in a non-symmetrical manner as evident in the results of Test 4L-D (Fig. 6.21). To correct this problem, shims were placed under the supports to create a level surface for them to rest on and silicone was applied around the supports to help keep them in place. Note that the movement of the supports could have affected the previous static laboratory verification tests as mentioned earlier.

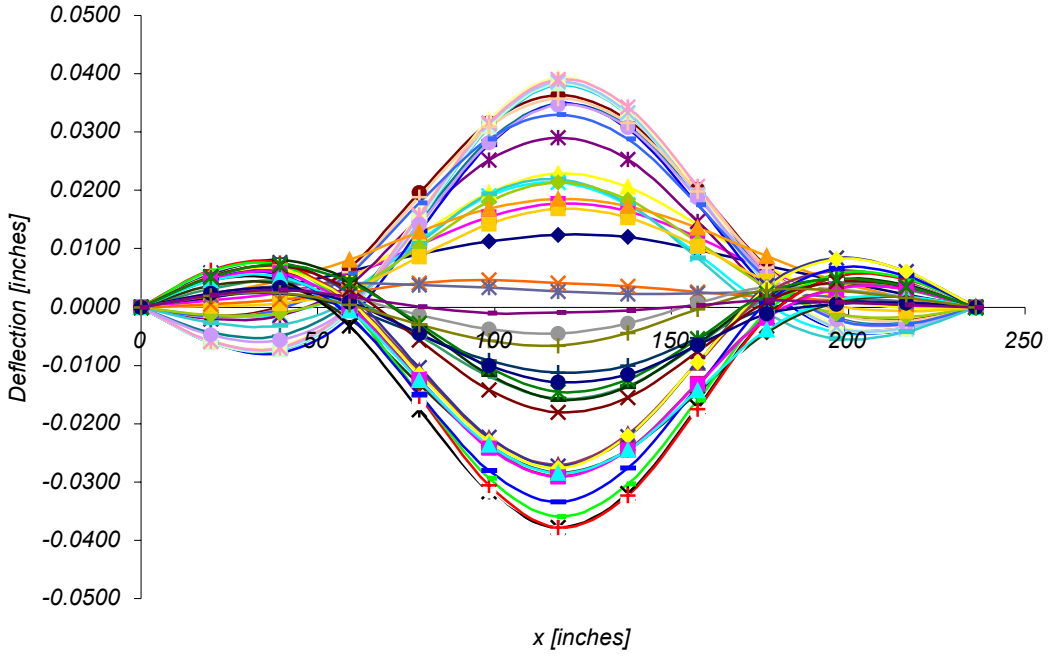

Figure 6.22. Beam II Test 7L-D.

In Test 7L-D (Fig. 6.22), the supports still moved up and down despite the effort previously mentioned to eliminate movement at the supports. Although the supports moved, they did so in a symmetric manner. Note that the movement of the supports was about ± 0.005 in (0.0127 cm). Also, it should be noted that the support arrangement does not provide perfect-pinned supports.

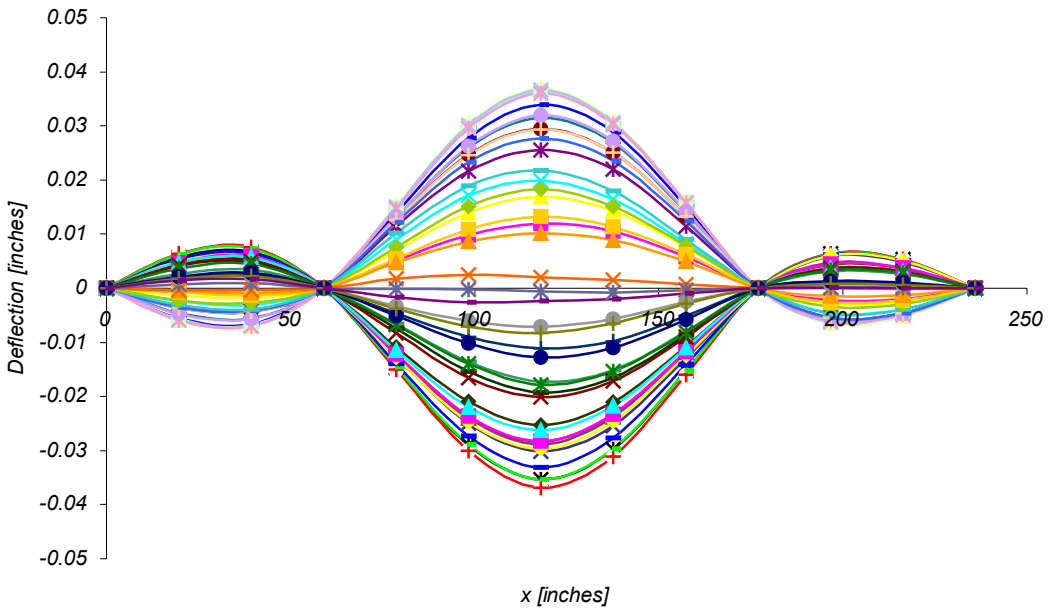

Figure 6.23. Beam II Test 7L-D Normalized.

To compare the numerical deflection with the analytical mode shape obtained from SAP2000, the deformed shapes were normalized, assuming that the interior supports did not move. At the time of the testing, a "measured" value of the deflections could not be obtained. Therefore, the deflected shape produced by the data could not be verified. The natural period from the dynamic test data was 0.07 seconds. This is very close to the natural period from the SAP2000 model of Beam II, which was 0.0684 seconds. Note that the data acquisition equipment could not record the time steps to more than three digits of accuracy, which could be a source of error for the period obtained.

The dynamic test performed on Beam II induced the first mode shape of the beam. This mode shape was compared to the first mode shape obtained from SAP2000, scaled to match the peak midspan deflection. The shapes were very similar (Fig. 6.24).

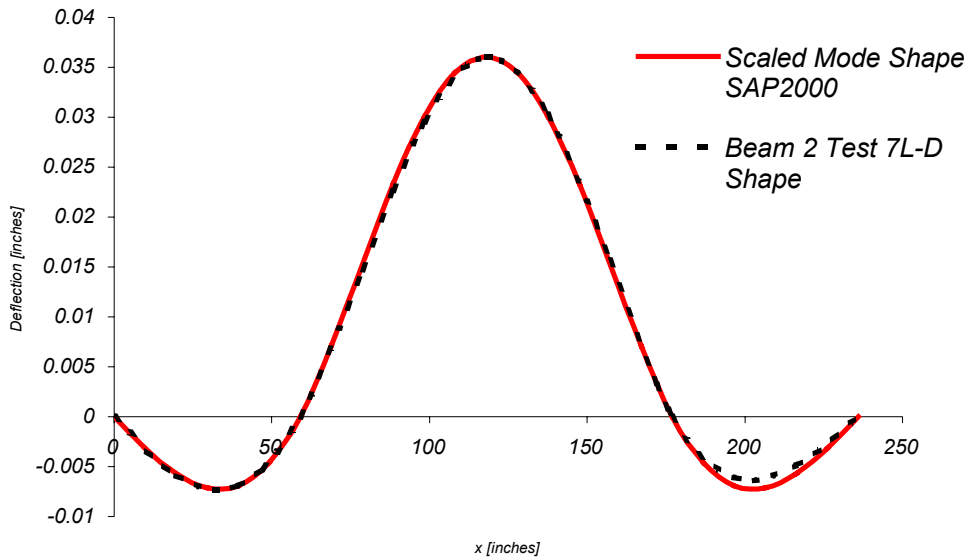

Figure 6.24. Mode Shape Comparison for Test 7L-D.

6.2.1.2 "Ideal 12" Strain Gauge System and Linear Variable Displacement Transducers (LVDTs)

After the Linear Variable Displacement Transducers (LVDTs) were purchased, additional dynamic tests were performed. The LVDTs provided the "measured" deflection values that could be compared to the values obtained using the mathematical model. The numerically produced deformed shapes are shown in Figure 6.25 and the "measured" deformed shapes are shown in Figure 6.26.

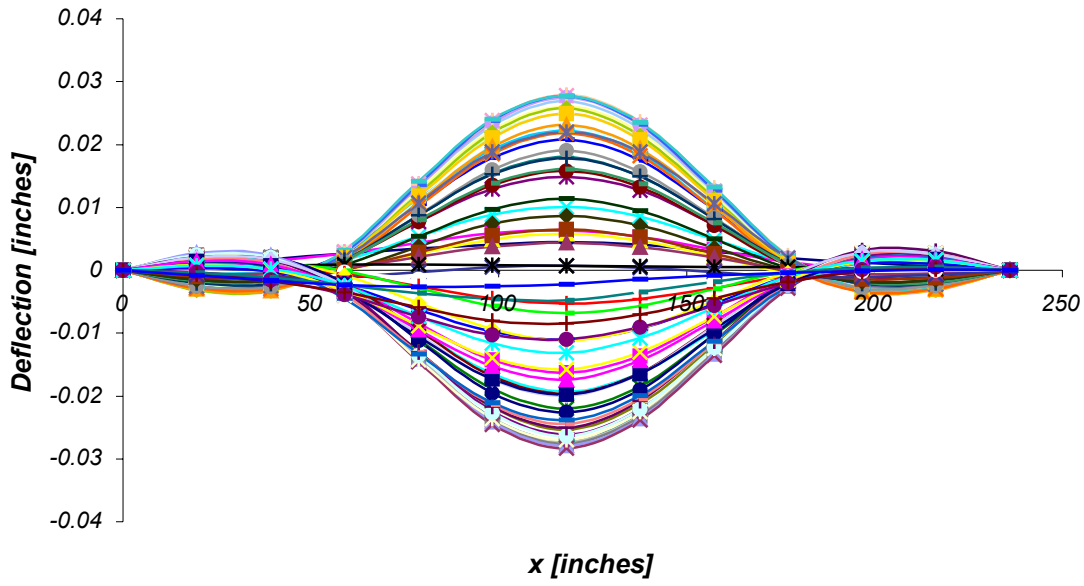

Figure 6.25. Beam II Test 9L-D "Ideal 12" Strain Gauge System Results.

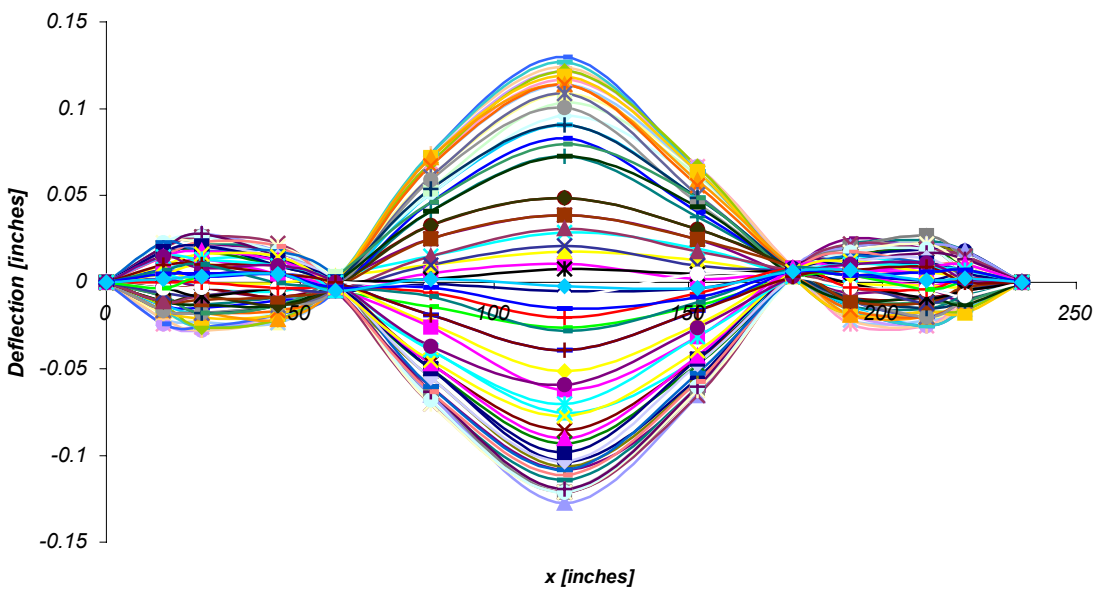

Figure 6.26. Beam II Test 9L-D "Measured" Deflections.

Although the deformed shapes in both Figures 6.25 and 6.26 look similar, the deflections calculated using the mathematical model are about 1/4th the value of the

“measured” deflections. There was also a slight phase shift between the LVDT measured response and the strain gauge response. Consequently, the cycle of data used in the mathematical model to generate Figure 6.25 was slightly delayed compared with the cycle of data used as the “measured” deflections. This was unexpected because the cycles should occur simultaneously. From these observations, it was deduced that the weldable electrical resistance strain gauges are not capable of registering the correct strain experienced by the steel beam. This is because the substrate to which the strain gauges are attached cannot transfer the strains experienced in the beam to the gauge at this extremely high frequency. Vishay Measurements Group, Inc. technical support confirmed that the weldable strain gauges do not work well for dynamic loads. These strain gauges experience a shear lag, meaning there will not be a full transfer of strain from the beam to the strain gauge under rapid loading conditions. This problem should not be a factor when the fiber optic strain gauges are epoxy-bonded directly to the steel tube. In addition, the weldable strain gauges are not as accurate as the epoxy-installed strain gauges. Their gauge factor could vary 5-10% from the specified value. The supports had slight movement as shown in both Figures 6.25 and 6.26, but this was less significant then in previous tests.

The data acquisition program was edited after the previous dynamic tests, which enabled the time to be recorded with four digits of accuracy. From the recorded data, there were approximately 63 cycles/second and the natural period was calculated to be 0.069 seconds, which corresponds to the value obtained previously (0.07 seconds) and the theoretical value obtained from the SAP2000 model (0.0684 seconds).

6.2.2 Animation of Dynamic Deflections

The cycle of 48 deformed shapes from Test 7L-D was animated using a Digital Visual Fortran code [Digital Equipment Corporation, 1998], which was used to prepare the data, and Tecplot 8.0 [Amtec Engineering, Inc., 1999], which was used to animate the plots. The cycle of 63 deformed shapes from Test 9L-D was also animated. Ultimately, it would be beneficial to produce real-time animated deformed shapes for the Kealakaha Stream Bridge.

CHAPTER 7
FIELD APPLICATIONS

7.1 Kealakaha Stream Bridge

The mathematical model provided good deflection predictions for the steel beam applications and reasonable results for the pre-stressed concrete T-beam application. The concrete T-beam results show discrepancies due to cracking of the concrete. The Kealakaha Stream Bridge will be a pre-stressed concrete box girder designed for zero concrete tension. In other words, the concrete throughout the box girder will always be in compression under working conditions. Therefore, there should be no cracking in the concrete. The mathematical model should work for this bridge under working and low to moderate earthquake conditions.

The proposed fiber optic strain gauge system to be used in the bridge is composed of 12 cells along the span of the bridge (Fig. 7.1). At the center of each cell is a set of four strain gauges with one gauge at each of the four corners of the box girder. By monitoring the vertical deflection at each side of the base girder, it is anticipated that this will provide the data needed to calculate the twist of the bridge as well as the average vertical deflection. The next phase of this project will evaluate whether a quadratic polynomial adequately describes the curvature diagram for this bridge using a finite element analysis. If a higher order polynomial is necessary to accurately describe the curvature, then more cells, and thus more strain gauges, will be required.

The fiber optic strain sensors to be used for this installation will have a gauge length of at least six inches (15.24 cm). The need for a longer gauge length will be determined after preliminary field verification of the FOS system on the H-3 North

Halawa Valley Viaduct as part of a future project. This project will also investigate the two different fiber optic strain gauge systems, the Fabry-Perot fiber optic strain gauge system and the Bragg grating fiber optic strain gauge system, in laboratory and field verification tests to determine which is most suited for this bridge application.

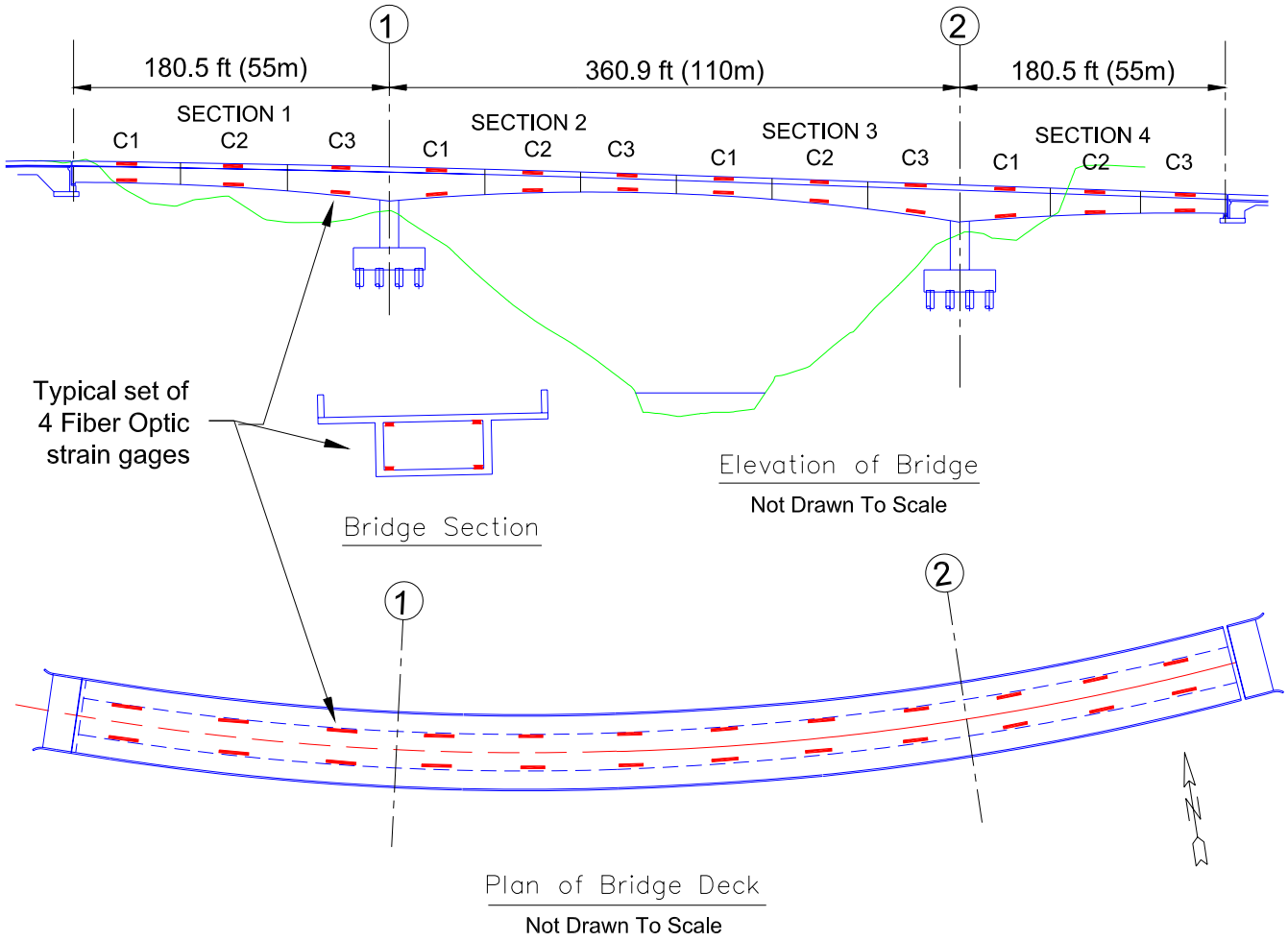

Figure 7.1. Kealakaha Stream Bridge.

CHAPTER 8
SUMMARY AND CONCLUSIONS

8.1 Summary

A mathematical model is introduced for determination of deflected beam shapes based on strain gauge measurements. Strain values are measured at discrete points along the beam, and are used to calculate the curvature for those points. Curve fitting is used to develop a set of curvature equations for the beam, which is then used to determine deflection equations by double integration. Boundary conditions, which are known or assumed, are used to solve the constants of integration.

Numerous laboratory verification tests, including static and dynamic loads, were performed on three beam specimens, two steel tube specimens and one pre-stressed concrete girder, at the Structures Laboratory at the University of Hawai`i at Manoa. These tests involved various loading and settlement conditions, similar to what may be expected for the Kealakaha Stream Bridge. The results from the mathematical model agreed well with the measured deflections from the dial gauges or Linear Variable Displacement Transducers (LVDTs) and with the results from SAP2000 analyses of the various loading conditions. The percent error in center span midpoint deflection was less than 15% for the majority of the loading conditions.

To develop an accurate yet economical fiber optic strain gauge system for use in the Kealakaha Stream Bridge Project, several strain gauge systems were tested on a 1/37th scale model of the bridge. First the "ideal 24" strain gauge system was analyzed, producing results that agreed well with the measured and theoretical deflections. To reduce costs, a 12-gauge system was investigated. Thus, 12 gauges were selected out of

the “ideal 24” to produce the “selected 12” strain gauge system. Although the selected 12 strain gauges were not located in ideal positions within the cells, the results were almost as accurate as the “ideal 24” strain gauge system. Therefore, an “ideal 12” strain gauge system was installed and tested. The results agreed well with the measured values and the SAP2000 model results. Finally, the “ideal 24” and the “ideal 12” strain gauge systems were compared and agreed well with each other and with the “measured” values recorded using Linear Variable Displacement Transducers (LVDTs) and the theoretical values obtained from the SAP2000 model.

The “ideal 12” strain gauge system was then used under dynamic loading conditions. Several dynamic tests were performed on Beam II. The initial tests, such as Test 7L-D, produced a series of deflected beam shapes that matched the first mode shape for free vibration. The magnitude of the deflections could not be verified using the dial gauges. Once high-speed LVDTs were installed, several more dynamic tests were performed. The deflected shapes and values produced by the mathematical model for Test 9L-D were very similar to those produced in Test 7L-D, but the deflected magnitudes did not agree with the LVDT “measured” values. According to Vishay Measurement Group, the weldable strain gauges used in the tests are not suitable for such high-speed frequencies due to the incomplete transfer of strain from the steel beam through the substrate to the strain gauge. This will be corrected when the fiber optic strain gauges are used as they will be epoxied directly to the surface of the beam.

8.2 Conclusions

The mathematical model was verified by a series of static laboratory verification tests. The "ideal 24" strain gauge system performed extremely well. To reduce costs, tests were performed using the "ideal 12" strain gauge system. This system performed also provided accurate deflection measurements. Subsequent to field verification tests, the "ideal 12" strain gauge system will be implemented in the Kealakaha Stream Bridge and should provide enough information to produce accurate vertical deflection values.

The results of the dynamic tests illustrate the importance of using fiber optic strain gauges capable of high frequency monitoring rather than the weldable electrical resistance strain gauges. The Fabry-Perot strain gauges and data acquisition system were selected as the fiber optic strain gauge system to be used in future laboratory and field experiments. The Bragg grating fiber optic strain gauge system will also be investigated if a suitable data acquisition system becomes available. The results from these tests will determine the final gauge layout and system to be installed in the Kealakaha Stream Bridge.

APPENDIX A
DEFLECTED SHAPE PLOTS FOR BEAM II

"Ideal 24" and "Selected 12" Strain Gauge System Variable Loading Patterns:

Beam II Test 2

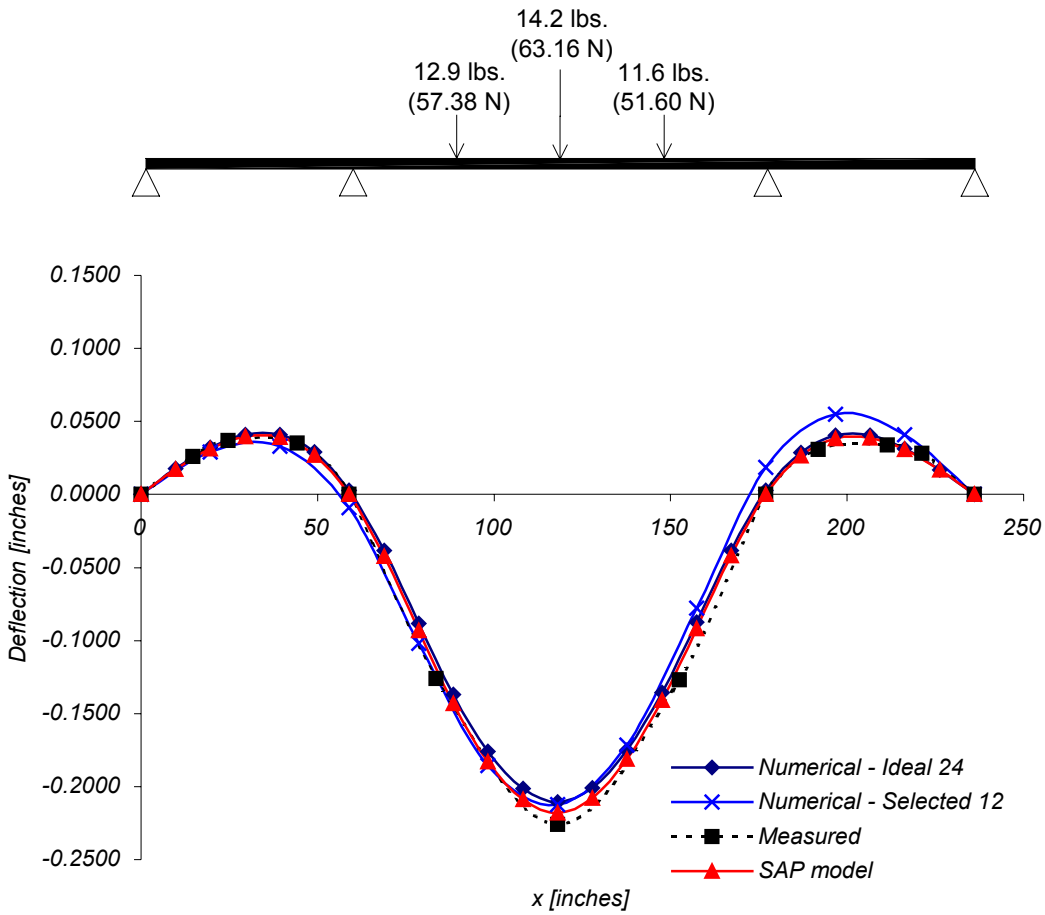

Figure A.1. Beam II Test 2, Multiple Center Span Loadings.

Beam II Test 3

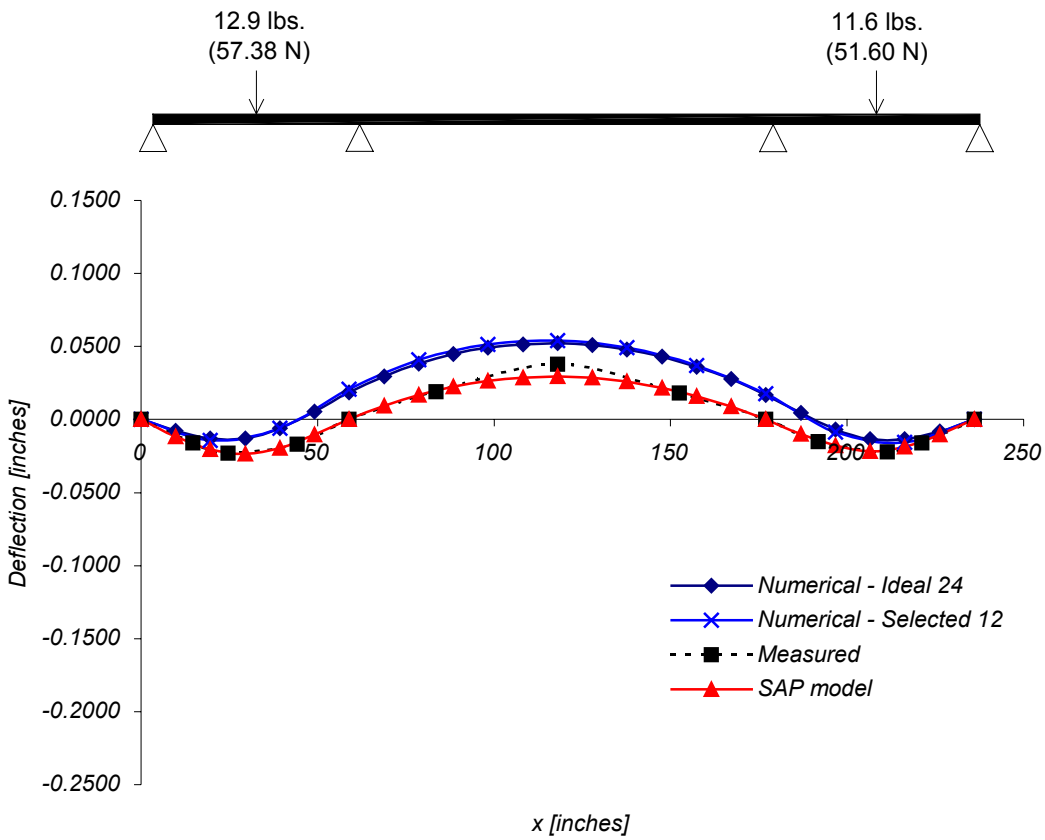

Figure A.2. Beam II Test 3, End Span Loads.

Beam II Test 7

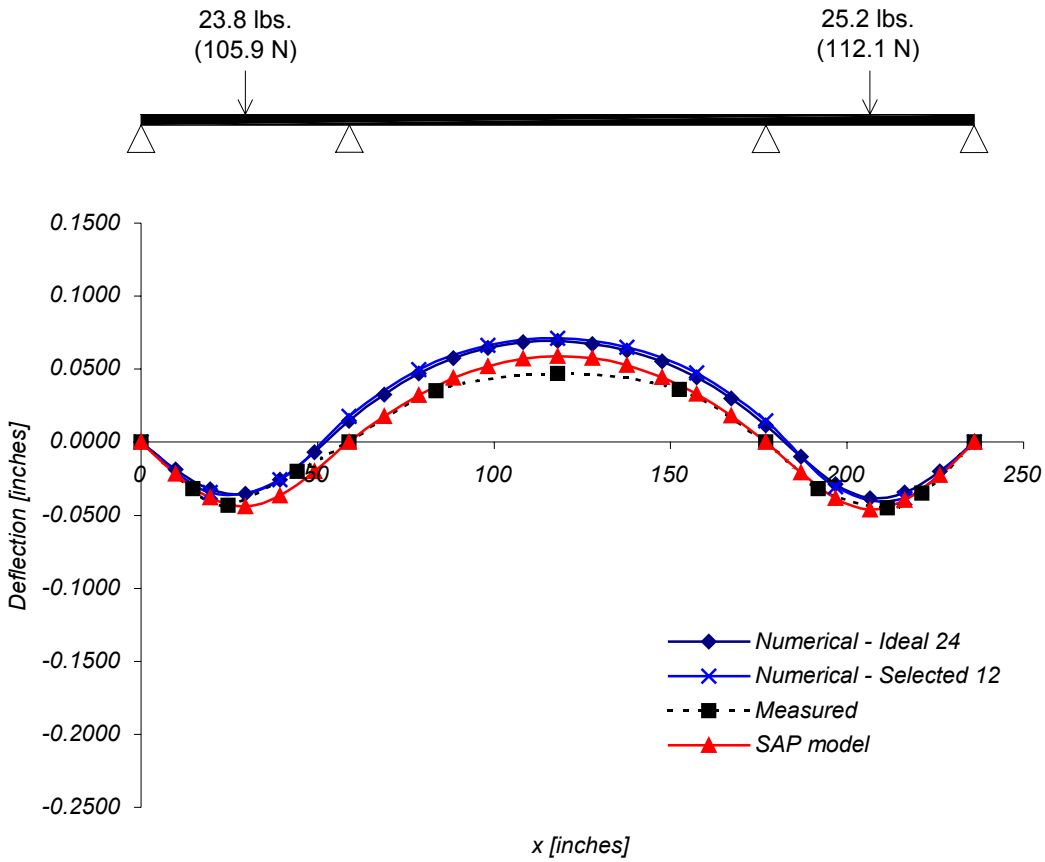

Figure A.3. Beam II Test 7, End Span Loads.

"Ideal 24" and "Selected 12" Strain Gauge System
Variable Settlement Patterns:
Beam II Test 8

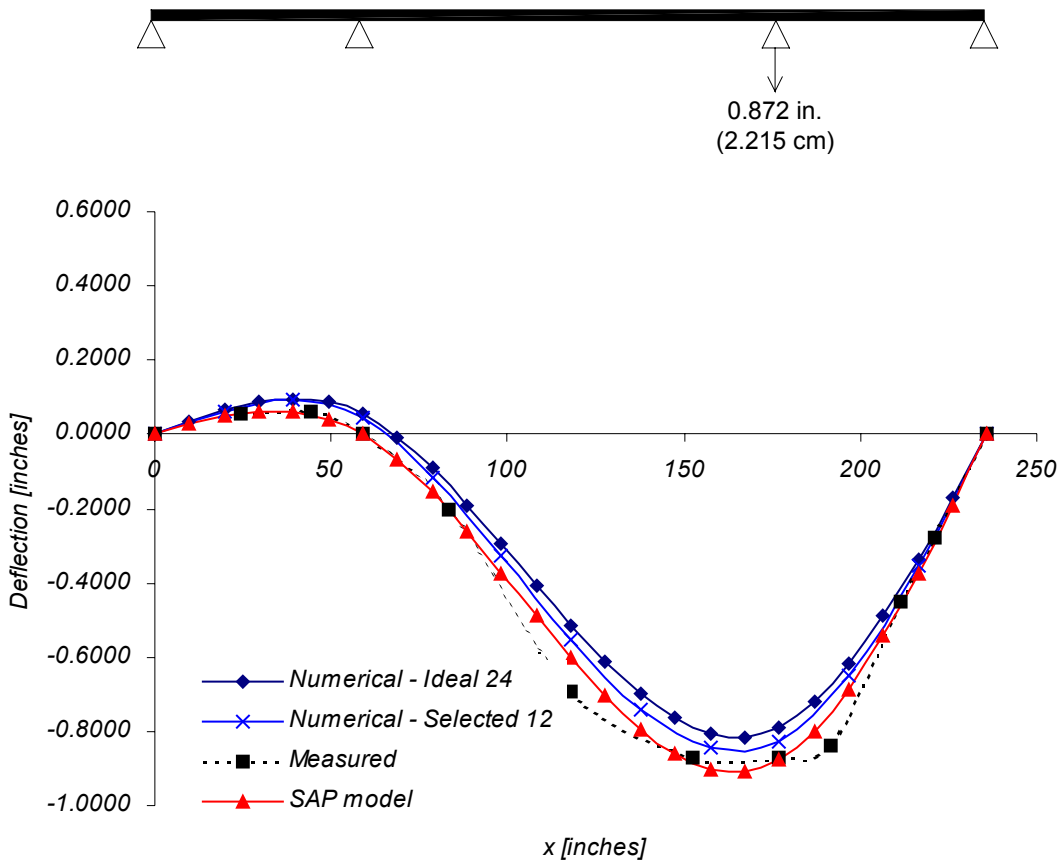

Figure A.4. Beam II Test 8, Support Movement.

"Ideal 24" and "Ideal 12" Strain Gauge System Variable Loading Patterns:

Beam II Test 13

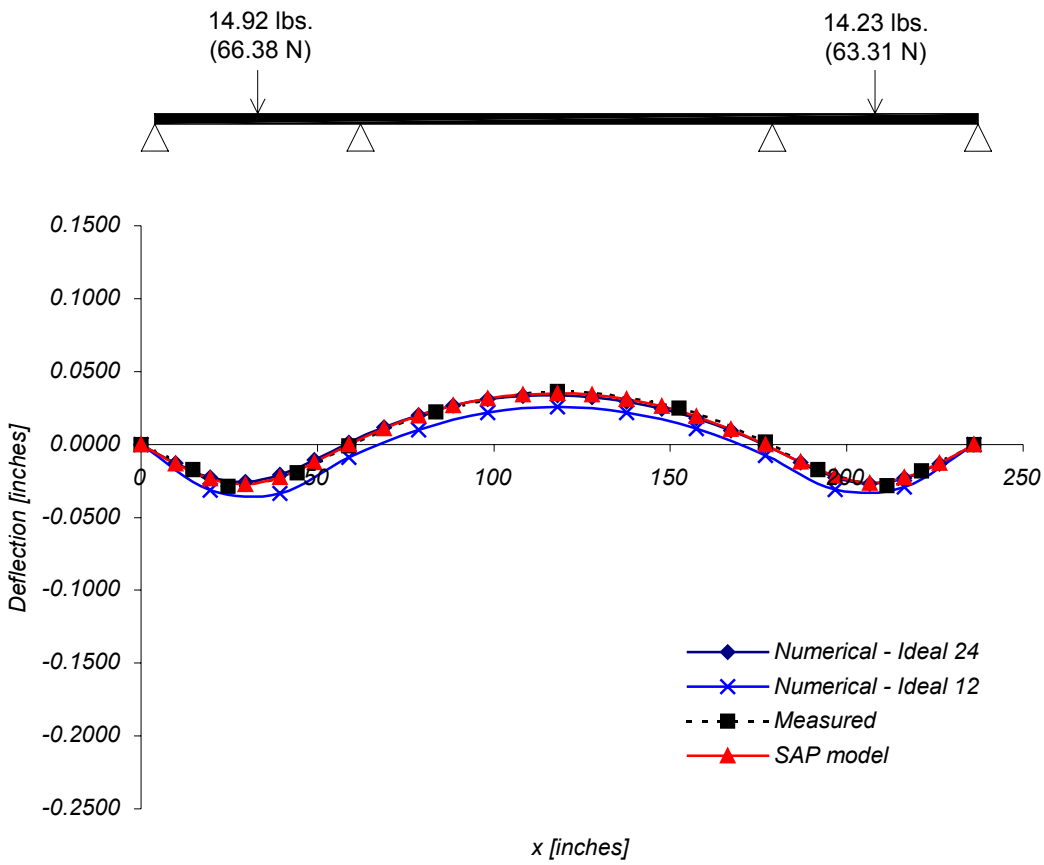

Figure A.5. Beam II Test 13, End Span Loads.

"Ideal 24" and "Ideal 12" Strain Gauge System Variable Settlement Patterns:

Beam II Test 17

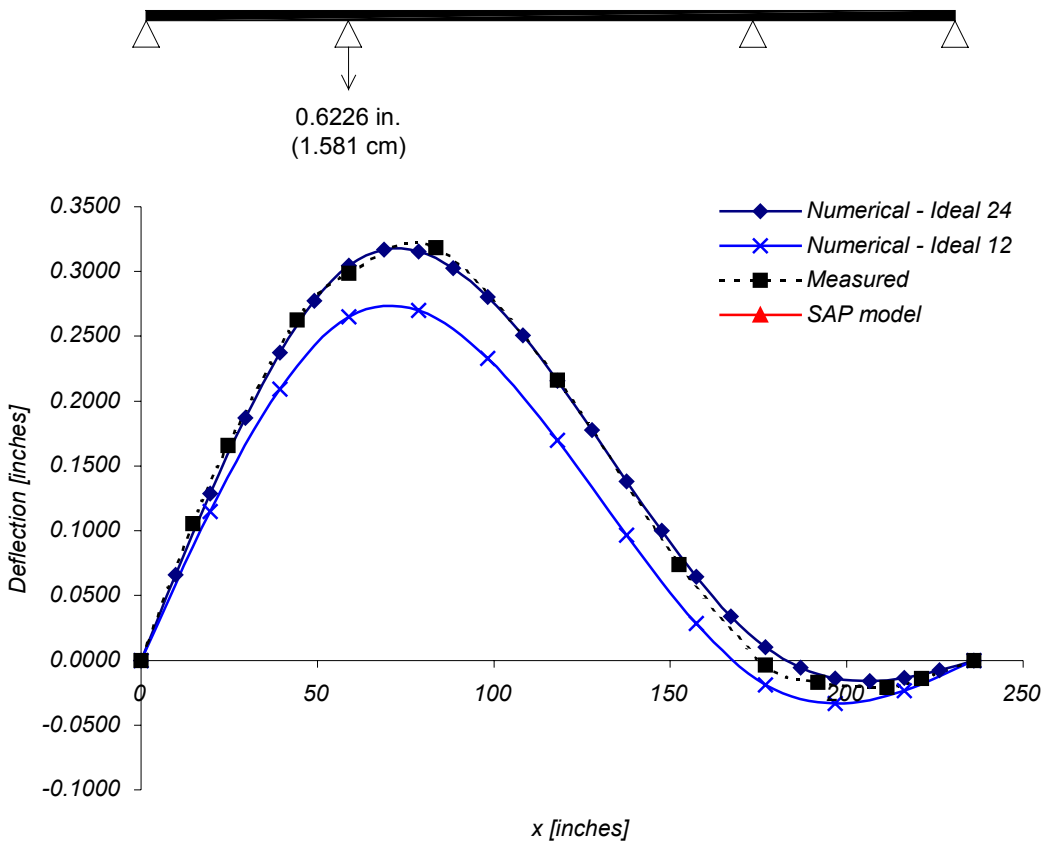

Figure A.6. Beam II Test 17, Support Movement.

Beam II Test 18

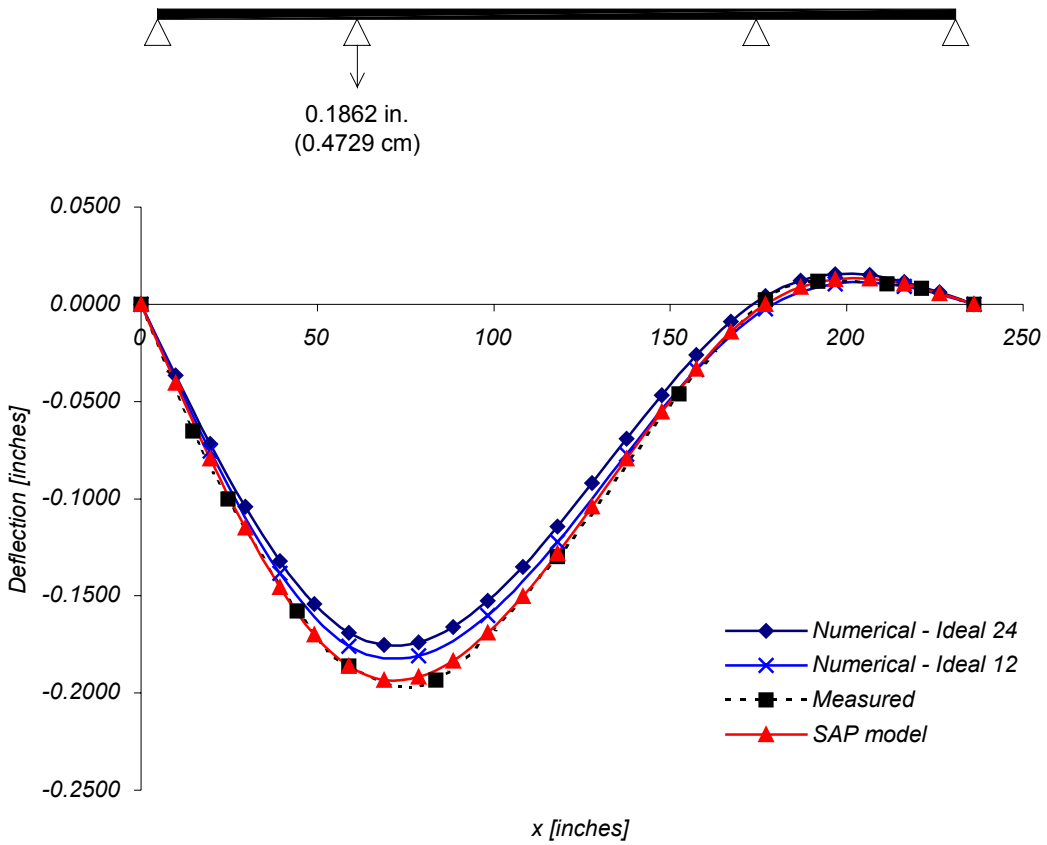

Figure A.7. Beam II Test 18, Support Movement.

APPENDIX B
VISUAL BASIC CODE FOR SPREADSHEET
By: Dr. Marcus Aberle

```
VERSION 1.0 CLASS
BEGIN
  MultiUse = -1  'True
END
Attribute VB_Name = "Sheet2"
Attribute VB_GlobalNameSpace = False
Attribute VB_Creatable = False
Attribute VB_PredeclaredId = True
Attribute VB_Exposed = True

Sub Accept()
Worksheets("Input").Activate
End Sub

Sub ABC()
Worksheets("a,b,c").Activate
End Sub
Sub Alpha()
Worksheets("alpha-beta").Activate
End Sub
Sub Measurements()
Worksheets("Measurements").Activate
End Sub
Sub Plot()
Worksheets("Plot").Activate
End Sub
Sub Inp()
Worksheets("Input").Activate
End Sub
Sub Graph()
Worksheets("Input").Rows(34).Activate
End Sub
Sub Up()
Worksheets("Input").Rows(1).Activate
End Sub
Sub Data()

'       Declares variables

Dim Cell As Integer
Dim Section As Integer
```

```
'       Clears cells from previous analysis

Sheet2.Range("A4:H50").ClearContents
Sheet3.Range("A4:H50").ClearContents
Sheet5.Range("A4:H50").ClearContents
Sheet6.Range("A4:H50").ClearContents

'       Input Data

Section = Sheet1.Cells(5, 13)
Cell = 3 * Section

Sheet2.Cells(4, 2) = "xA [inches]"
Sheet2.Cells(4, 3) = "xB [inches]"
Sheet2.Cells(4, 4) = "Strain"
Sheet2.Cells(4, 5) = "Curvature"

Sheet3.Cells(4, 2) = "a"
Sheet3.Cells(4, 3) = "b"
Sheet3.Cells(4, 4) = "c"

Sheet5.Cells(4, 2) = "alpha"
Sheet5.Cells(4, 3) = "beta"

Sheet6.Cells(4, 1) = "x [inches]"
Sheet6.Cells(4, 2) = "Deflection [inches]"

For i = 1 To Cell
   Sheet2.Cells(4 + i, 1) = "Cell" & " " & i
Next i

For i = 1 To Section
   Sheet3.Cells(4 + i, 1) = "Section" & " " & i
   Sheet5.Cells(4 + i, 1) = "Section" & " " & i
Next i

Worksheets("Measurements").Activate

End Sub

Sub GaussJ()

'       Declaration of variables
```

```
Dim i As Integer
Dim j As Integer
Dim k As Integer
Dim L As Integer
Dim ll As Integer
Dim n As Integer
Dim m As Integer
Dim s As Integer
Dim irow As Integer
Dim icol As Integer

Dim ipiv() As Integer
Dim indxr() As Integer
Dim indxc() As Integer
Dim Cell As Integer
Dim Section As Integer

Dim big As Double
Dim dum As Double
Dim one As Double
Dim zero As Double
Dim a() As Double
Dim b() As Double


'       Input Data

Section = Sheet1.Cells(5, 13)
Cell = 3 * Section

'-------------------------------------------------------------
'       Calculation to obtain a, b, and c for each section
'       based on a quadratic curvature polynomial over section
'-------------------------------------------------------------

n = 3

ReDim ipiv(n) As Integer
ReDim indxr(n) As Integer
ReDim indxc(n) As Integer
ReDim a(n, n) As Double
ReDim b(n, 1) As Double

m = 1
one = 1#
```

```
zero = 0#

For s = 1 To Section
a(1, 1) = 1 / 3 * ((Sheet2.Cells(3 * s + 2, 3)) ^ 3 - (Sheet2.Cells(3 * s + 2)) ^ 3)
a(1, 2) = 1 / 2 * ((Sheet2.Cells(3 * s + 2, 3)) ^ 2 - (Sheet2.Cells(3 * s + 2, 2)) ^ 2)
a(1, 3) = (Sheet2.Cells(3 * s + 2, 3)) - (Sheet2.Cells(3 * s + 2, 2))
a(2, 1) = 1 / 3 * ((Sheet2.Cells(3 * s + 3, 3)) ^ 3 - (Sheet2.Cells(3 * s + 3, 2)) ^ 3)
a(2, 2) = 1 / 2 * ((Sheet2.Cells(3 * s + 3, 3)) ^ 2 - (Sheet2.Cells(3 * s + 3, 2)) ^ 2)
a(2, 3) = (Sheet2.Cells(3 * s + 3, 3)) - (Sheet2.Cells(3 * s + 3, 2))
a(3, 1) = 1 / 3 * ((Sheet2.Cells(3 * s + 4, 3)) ^ 3 - (Sheet2.Cells(3 * s + 4, 2)) ^ 3)
a(3, 2) = 1 / 2 * ((Sheet2.Cells(3 * s + 4, 3)) ^ 2 - (Sheet2.Cells(3 * s + 4, 2)) ^ 2)
a(3, 3) = (Sheet2.Cells(3 * s + 4, 3)) - (Sheet2.Cells(3 * s + 4, 2))

b(1, 1) = ((Sheet2.Cells(3 * s + 2, 3)) - (Sheet2.Cells(3 * s + 2, 2))) * (Sheet2.Cells(3 * s
+ 2, 5))
b(2, 1) = ((Sheet2.Cells(3 * s + 3, 3)) - (Sheet2.Cells(3 * s + 3, 2))) * (Sheet2.Cells(3 * s
+ 3, 5))
b(3, 1) = ((Sheet2.Cells(3 * s + 4, 3)) - (Sheet2.Cells(3 * s + 4, 2))) * (Sheet2.Cells(3 * s
+ 4, 5))

'------------------------
'Gauss-Jordan Elimination
'------------------------

'  Gauss-Jordan solution of linear equations in double precision.
'  Adapted from the routine GAUSSJ in the Numerical Recipes package.
'  A is an NxN double-precision matrix, declared as double-precision
'  A(:,:).
'  B contains M right-hand side vectors, where M = 1 in many cases,
'  and is declared as double-precision B(:,:).
'  On output, A has been overwritten by its inverse, and B has been
'  replaced with the solutions.

For i = 1 To n
   ipiv(i) = 0
Next i

For i = 1 To n
  big = 0#
  For j = 1 To n
    If ipiv(j) <> 1 Then
      For k = 1 To n
        If ipiv(k) = 0 Then
          If Abs(a(j, k)) >= big Then
            big = Abs(a(j, k))
```

```
          irow = j
          icol = k
        End If
      ElseIf ipiv(k) > 1 Then
        MsgBox ("Singular matrix")
      End If
    Next k
  End If
Next j
ipiv(icol) = ipiv(icol) + 1

'      Pivot has been selected.   Interchange rows, if necessary, to
'      put the element on the diagonal.

If irow <> icol Then
  For L = 1 To n
    dum = a(irow, L)
    a(irow, L) = a(icol, L)
    a(icol, L) = dum
  Next L
  For L = 1 To m
    dum = b(irow, L)
    b(irow, L) = b(icol, L)
    b(icol, L) = dum
  Next L
End If
indxr(i) = irow
indxc(i) = icol

'      Now do the pivoting

If a(icol, icol) = 0# Then
  MsgBox ("Singular Matrix")
End If
pivinv = one / a(icol, icol)
a(icol, icol) = one
For L = 1 To n
  a(icol, L) = a(icol, L) * pivinv
Next L
For L = 1 To m
  b(icol, L) = b(icol, L) * pivinv
Next L
For ll = 1 To n
  If ll <> icol Then
  dum = a(ll, icol)
```

```
    a(ll, icol) = zero
    For L = 1 To n
      a(ll, L) = a(ll, L) - a(icol, L) * dum
    Next L
    For L = 1 To m
      b(ll, L) = b(ll, L) - b(icol, L) * dum
    Next L
    End If
  Next ll
Next i

'      Finally unscramble A by re-arranging the columns

For L = n To 1 - 1
  If indxr(L) <> indxc(L) Then
    For k = 1 To n
      dum = a(k, indxr(L))
      a(k, indxr(L)) = a(k, indxc(L))
      a(k, indxc(L)) = dum
    Next k
  End If
Next L

'      Writes a, b, and c for each section

Sheet3.Cells(4 + s, 2) = b(1, 1)
Sheet3.Cells(4 + s, 3) = b(2, 1)
Sheet3.Cells(4 + s, 4) = b(3, 1)

Next s

'-----------------------------------------------
'      Calculations to obtain alpha's and beta's
'            from boundary conditions
'-----------------------------------------------

n = 2 * Section

ReDim ipiv(n) As Integer
ReDim indxr(n) As Integer
ReDim indxc(n) As Integer
ReDim a(n, n) As Double
ReDim b(n, 1) As Double

'      Set all values in matrix A to zero
```

```
For i = 1 To n
   For j = 1 To n
      a(i, j) = 0#
   Next j
Next i

'     Set all values in vector B to zero

For i = 1 To n
   b(i, 1) = 0#
Next i

'     Correct matix A and vector B

For i = 1 To n
   For j = 1 To n

      If i = 1 Then
         If j = 2 Then
            a(i, j) = 1#
         End If
      End If

      If i > 1 And i < n Then
         If i = 2 Or i = 4 Or i = 6 Or i = 8 Or i = 10 Or i = 12 Or i = 14 Or i = 16 Or i = 18
Then
            s = i / 2
            b(i, 1) = -((Sheet3.Cells(4 + s, 2)) / 12 * (Sheet2.Cells(3 * s + 4, 3)) ^ 4 +
(Sheet3.Cells(4 + s, 3)) / 6 * (Sheet2.Cells(3 * s + 4, 3)) ^ 3 + 0.5 * (Sheet3.Cells(4 + s,
4)) * (Sheet2.Cells(3 * s + 4, 3)) ^ 2)
               If j = i - 1 Then
                  a(i, j) = Sheet2.Cells(3 * s + 4, 3)
               End If
               If j = i Then
                  a(i, j) = 1#
               End If
               If j = i + 2 Then
                  a(i, j) = -1#
               End If

         Else
            s = (i - 1) / 2
```

```
            b(i, 1) = -((Sheet3.Cells(4 + s, 2)) / 3 * (Sheet2.Cells(3 * s + 4, 3)) ^ 3 +
(Sheet3.Cells(4 + s, 3)) / 2 * (Sheet2.Cells(3 * s + 4, 3)) ^ 2 + (Sheet3.Cells(4 + s, 4)) *
(Sheet2.Cells(3 * s + 4, 3)))
                If j = i - 2 Then
                   a(i, j) = 1#
                End If
                If j = i Then
                   a(i, j) = -1#
                End If
          End If
       End If

       If i = n Then
          s = i / 2
          b(i, 1) = -((Sheet3.Cells(4 + s, 2)) / 12 * (Sheet2.Cells(3 * s + 4, 3)) ^ 4 +
(Sheet3.Cells(4 + s, 3)) / 6 * (Sheet2.Cells(3 * s + 4, 3)) ^ 3 + 0.5 * (Sheet3.Cells(4 + s,
4)) * (Sheet2.Cells(3 * s + 4, 3)) ^ 2)
          If j = i - 1 Then
             a(i, j) = Sheet2.Cells(3 * s + 4, 3)
          End If
          If j = i Then
             a(i, j) = 1#
          End If
       End If

    Next j
Next i

'      Writes matrix A

'For i = 1 To n
'    For j = 1 To n
'        Sheet5.Cells(20 + i, j) = a(i, j)
'    Next j
'Next i

'      Writes vector B

'For i = 1 To n
'    Sheet5.Cells(20 + i, n + 2) = b(i, 1)
'Next i

'-----------------------------------------------------
'      Start of Gauss-Elimination for alpha and beta
'-----------------------------------------------------
```

```
For i = 1 To n
   ipiv(i) = 0
Next i

For i = 1 To n
  big = 0#
  For j = 1 To n
    If ipiv(j) <> 1 Then
      For k = 1 To n
        If ipiv(k) = 0 Then
          If Abs(a(j, k)) >= big Then
            big = Abs(a(j, k))
            irow = j
            icol = k
          End If
        ElseIf ipiv(k) > 1 Then
          MsgBox ("Singular matrix")
        End If
      Next k
    End If
  Next j
  ipiv(icol) = ipiv(icol) + 1

'      Pivot has been selected.   Interchange rows, if necessary, to
'      put the element on the diagonal.

  If irow <> icol Then
    For L = 1 To n
      dum = a(irow, L)
      a(irow, L) = a(icol, L)
      a(icol, L) = dum
    Next L
    For L = 1 To m
      dum = b(irow, L)
      b(irow, L) = b(icol, L)
      b(icol, L) = dum
    Next L
  End If
  indxr(i) = irow
  indxc(i) = icol

'      Now do the pivoting

  If a(icol, icol) = 0# Then
```

```
    MsgBox ("Singular Matrix")
  End If
  pivinv = one / a(icol, icol)
  a(icol, icol) = one
  For L = 1 To n
    a(icol, L) = a(icol, L) * pivinv
  Next L
  For L = 1 To m
    b(icol, L) = b(icol, L) * pivinv
  Next L
  For ll = 1 To n
    If ll <> icol Then
    dum = a(ll, icol)
    a(ll, icol) = zero
    For L = 1 To n
      a(ll, L) = a(ll, L) - a(icol, L) * dum
    Next L
    For L = 1 To m
      b(ll, L) = b(ll, L) - b(icol, L) * dum
    Next L
    End If
  Next ll
Next i

'      Finally unscramble A by re-arranging the columns

For L = n To 1 - 1
  If indxr(L) <> indxc(L) Then
    For k = 1 To n
      dum = a(k, indxr(L))
      a(k, indxr(L)) = a(k, indxc(L))
      a(k, indxc(L)) = dum
    Next k
  End If
Next L

'      Writes alpha's and beta's for each section

For i = 1 To Section
    Sheet5.Cells(4 + i, 2) = b(2 * i - 1, 1)
    Sheet5.Cells(4 + i, 3) = b(2 * i, 1)
Next i

'-------------------------------
'      Plot of Deflection
```

```
'-------------------------------

Dim Step As Double
Dim x As Double

x = 0#
Sheet6.Cells(5, 1) = 0
Sheet6.Cells(5, 2) = 0

For i = 1 To Section
   Step = (Sheet2.Cells(3 * i + 4, 3)) / 3
   Sheet6.Cells(3 * i + 3, 1) = x + Step
   Sheet6.Cells(3 * i + 3, 2) = -1 * (Sheet3.Cells(4 + i, 2) * (Step) ^ 4 / 12 +
Sheet3.Cells(4 + i, 3) * (Step) ^ 3 / 6 + Sheet3.Cells(4 + i, 4) * (Step) ^ 2 / 2 +
Sheet5.Cells(4 + i, 2) * (Step) + Sheet5.Cells(4 + i, 3))
   Sheet6.Cells(3 * i + 4, 1) = x + 2 * Step
   Sheet6.Cells(3 * i + 4, 2) = -1 * (Sheet3.Cells(4 + i, 2) * (2 * Step) ^ 4 / 12 +
Sheet3.Cells(4 + i, 3) * (2 * Step) ^ 3 / 6 + Sheet3.Cells(4 + i, 4) * (2 * Step) ^ 2 / 2 +
Sheet5.Cells(4 + i, 2) * (2 * Step) + Sheet5.Cells(4 + i, 3))
   Sheet6.Cells(3 * i + 5, 1) = x + 3 * Step
   Sheet6.Cells(3 * i + 5, 2) = -1 * (Sheet3.Cells(4 + i, 2) * (3 * Step) ^ 4 / 12 +
Sheet3.Cells(4 + i, 3) * (3 * Step) ^ 3 / 6 + Sheet3.Cells(4 + i, 4) * (3 * Step) ^ 2 / 2 +
Sheet5.Cells(4 + i, 2) * (3 * Step) + Sheet5.Cells(4 + i, 3))
   x = x + 3 * Step
Next i


End Sub
```

APPENDIX C
DIGITAL VISUAL FORTRAN CODE
FOR THE ANIMATION OF DEFLECTED SHAPES
FOR TEST 7L-D

```
module commondata
!
implicit none
save
!
!  Defines the kind parameters
!
INTEGER, parameter :: double = SELECTED_REAL_KIND(p=13,r=200)
!
INTEGER :: filein=7, fileres=8, fileout=9, maxiteration = 100
REAL(KIND=DOUBLE), parameter :: zero=0.0_double, one=1.0_double,
two=2.0_double, &
                        bignumber = 1.0e20_double, TOL = 1.0e-12_double
REAL(KIND=DOUBLE) :: pi, onevector(3)
end module commondata
!
program animation
!
USE commondata
implicit none
!
REAL(KIND=DOUBLE) :: factor
REAL(KIND=DOUBLE), ALLOCATABLE, DIMENSION(:) :: x
REAL(KIND=DOUBLE), ALLOCATABLE, DIMENSION(:,:) :: deflection

INTEGER :: nodata, i, j, k, noframepc, nocycle, frameno
!
open(unit=7,file='input.inp',status='unknown')
open(unit=8,file='tecplot.dat',status='unknown')
!
noframepc = 29
nocycle = 5
pi = 4.0_double*atan(one)
!
read(7,*) nodata
allocate (x(nodata),deflection(nodata,noframepc))
do i = 1, nodata
  read(7,*) x(i), (deflection(i,j), j = 1, noframepc)
end do
!
```

```
do i = 1, nocycle
  do j = 1, noframepc
    write(8,100) noframepc*(i-1) + j, nodata
100 format('TITLE="Deflected Shape"'/ &
          'VARIABLES="X" "Y"'/ &
          'ZONE T="FRAME',i4,'", I=',i4,', F=POINT')
    do k = 1, nodata
            write(8,200) x(k), deflection(k,j)
200 format(2e15.7)
          end do
  end do
end do
!
deallocate(x,deflection)
!
end program
```

Bibliography

Amtec Engineering, Inc., Tecplot 8.0-0-6, 1999.

Çelebi, M., Sanli, A., "GPS in Pioneering Dynamic Monitoring of Long-Period Structures." Earthquake Spectra, V. 18, No. 1, 2002, pp. 47-61.

Computers and Structures, Inc., SAP2000 NonLinear Version 7.40, Berkeley, CA, 2000.

Digital Equipment Corporation, DIGITAL Visual Fortran Version 6.0, 1998.

Fung, S., Aberle, M., Robertson, I., "Bridge Deflection Measurements during Earthquake Ground-shaking", Proceedings of the IABSE Symposium "Towards a Better Built Environment", IABSE Volume 86, Melbourne, Australia, 2002.

Inaudi, D., Casanova, N, Vurpillot, S., "Bridge Deformation Monitoring with Fiber Optic Sensors", Proceedings of the IABSE Symposium "Structures for the Future-The Search for Quality", Rio de Janeiro, Brazil, 1999.

Inaudi, D., Casanova, N, Vurpillot, S., Glisic, B., Kronenberg, P., Lloret, S., "Lessons learned in the use of fiber optic sensor for civil structural monitoring", Proceedings of "The present and the future in health monitoring", Weimar, Germany, 2000.

Inaudi, D., Casanova, N, Vurpillot, S., "Monitoring of Concrete Bridges with Long-Gage Fiber Optic Sensors", Journal of Intelligent Material Systems and Structures, V.10, April 1999, pp. 280-292.

Lee, A., Robertson, I., "Instrumentation and Long-Term Monitoring of the North Halawa Valley Viaduct", Research Report UHM/CE/95-08, University of Hawaii, Honolulu, HI, September 1995, pp.149.

McKinley, B., Aarnes, K., Boswell, L., "Bridge Monitoring Using an Optical Fibre Sensor System", Proceedings of the IABSE Symposium "Towards a Better Built Environment", IABSE Volume 86, Melbourne, Australia, 2002.

Measures, R. M., "Fiber Optic Smart Structures." Fiber Optic Smart Structures. Ed. E Udd. John Wiley & Sons, Inc., New York, NY, 1995.

Measures, R. M., "Structural Monitoring with Fiber Optic Technology." Academic Press, San Diego, CA, 2001.

Schultz, W., Conte, J., Udd, E., "Long Gage Fiber Optic Bragg Grating Strain Sensors to Monitor Civil Structures", www.bluerr.com/2.pdf, June 12, 2002.

Udd. E., “Fiber Optic Sensor Overview.” Fiber Optic Smart Structures. Ed. E. Udd. John Wiley & Sons, Inc., New York, N.Y., 1995.

Vurpillot, S., Krueger, G., Benouaich, D., Clement, D., and Inaudi, D., “Vertical Deflection of a Pre-Stressed Concrete Bridge Obtained Using Deformation Sensors and Inclinometer Measurements”, ACI Structural Journal, Vol. 95, No. 5, September-October 1998.

Vurpillot, S., Inaudi, D., Scano, A., “Mathematical model for the determination of the vertical displacement from internal horizontal measurements of a bridge”, Proceedings of "SPIE Smart Structures and Materials", San Diego, USA, 1996.

Yu, F., Yang, X., “Introduction to Optical Engineering.” Cambridge University Press, New York, NY, 1997.